CANADIAN THESES

THÈSES CANADIENNES

NOTICE

The quality of this microfiche is heavily dependent upon the quality of the original thesis submitted for microfilming. Every effort has been made to ensure the highest quality of reproduction possible.

If pages are missing, contact the university which granted the degree.

Some pages may have indistinct print especially if the original pages were typed with a poor typewriter ribbon or if the university sent us an inferior photocopy.

Previously copyrighted materials (journal articles, published tests, etc.) are not filmed.

Reproduction in full or in part of this film is governed by the Canadian Copyright Act, R.S.C. 1970, c. C-30.

AVIS

La qualité de cette microfiche dépend grandement de la qualité de la thèse soumise au microfilmage. Nous avons tout fait pour assurer une qualité supérieure de reproduction.

S'il manque des pages, veuillez communiquer avec l'université qui a conféré le grade.

La qualité d'impression de certaines pages peut laisser à désirer, surtout si les pages originales ont été dactylographiées à l'aide d'un ruban usé ou si l'université nous a fait parvenir une photocopie de qualité inférieure.

Les documents qui font déjà l'objet d'un droit d'auteur (articles de revue, examens publiés, etc.) ne sont pas microfilmés.

La reproduction, même partielle, de ce microfilm est soumise à la Loi canadienne sur le droit d'auteur, SRC 1970, c. C-30.

THIS DISSERTATION HAS BEEN MICROFILMED EXACTLY AS RECEIVED

LA THÈSE A ÉTÉ MICROFILMÉE TELLE QUE NOUS L'AVONS REÇUE

PRACTICAL AND THEORETICAL EVALUATION OF A TRANSMISSION SYSTEM USING THE CPFSK DIGITAL MODULATION SCHEME

by

AHMAD TALAL AHDAB

A THESIS PRESENTED TO THE SCHOOL OF GRADUATE STUDIES AND RESEARCH AT THE UNIVERSITY OF OTTAWA IN PARTIAL FULFILLMENT OF THE REQUIREMENTS FOR THE DEGREE OF MASTER OF APPLIED SCIENCE IN ELECTRICAL ENGINEERING

OTTAWA, ONTARIO, 1986

ISBN 0-315-36465-3

UNIVERSITÉ D'OTTAWA
UNIVERSITY OF OTTAWA

IN THE NAME OF GOD, MOST GRACIOUS, MOST MERCIFUL

...but say, "O my LORD! advance me in Knowledge"

(Qur'an, 20:114)

"Seek knoweledge from the Cradle to the Grave"

"If anybody proceeds on his way in search of knowledge, God will make easy for him the way to Paradise"

"The superiority of the learned over the mere pious is like the superiority of the moon when it is full over all other stars"

The Prophet Muhammad

(Peace and Blessings of God be upon him)

The University of Ottawa requires the signatures of all persons using or photocopying this thesis. Please sign below, and give address and date.

ABSTRACT

A new method for generating h = 1/b, bandwidth efficient binary CPFSK modulated signals with one single circuit, is introduced. The h = 1/b binary CPFSK signal is first represented by its preenvelope r(t). A baseband processor generates the real part I(t) and the imaginary part Q(t) of the CPFSK complex preenvelope r(t). The two baseband signals are filtered before being combined with quadrature phase modulation scheme. The transmit filter is a fourth order Butterworth low pass filter approximating an $\alpha = 0.5$ raised cosine channel. Experimental results of eye patterns, state space diagrams, and envelope fluctuations of CPFSK are presented. The spectral characteristics of CPFSK signals are derived using an N-state (N = 4b) Markov chain model. The results are presented and the case of h = 1/4 is shown to be of interest. The probability of error performance of CPFSK in an additive white Gaussian noise (AWGN) single channel environment, is analyzed and compared to that of M-ary PSK and MSK. Further, it is shown that the probability of error of h = 1/b CPFSK is comparable to that of the differentially encoded and coherently detected M-ary PSK with M = b. For a constant envelope modulation scheme, h = 1/4

should be considered since it is shown to be worse than DE-MSK by only 0.95 dB at a P(e) of 10^{-4}, in term of E_b/N_0, yet with almost half the bandwidth. A block diagram of the demodulator is proposed. Moreover, for h = 1/2 CPFSK generated as proposed, it is shown that the quadrature demodulator (MSK demodulator) can still be used with slight modifications. For future research, h = 1/4 CPFSK is suggested as a bandwidth efficient CPFSK scheme. To attain even higher spectral efficiency, a duo-binary and modified duo-binary h = 1/4 CPFSK is suggested. The effects of ACI and CCI on the probability of error may be an interesting topic for future study. These desirable performance characteristics, combined with the simple hardware implementation that is proposed in this thesis may lead to numerous satellite and terrestrial radio system applications.

ACKNOWLEDGMENTS

The author would like to express grateful thanks to his supervisor, Dr. Willem Steenaart for introducing him to the field of digital signal processing and strengthening his knowledge in communications; and for his encouragement and constructive criticism throughout this work and during the final phase of this thesis, without which this thesis would not have been possible.

The author's appreciation is also extended to the IC Product and the IC Design Engineering Groups at the Semiconductor Division of Mitel Corporation, for their continuous encouragement.

Many thanks are furthermore extended to all of his close friends and colleagues for their continuous encouragement and their way of maintaining the author's positive attitude.

Finally, the author would like to express his deep appreciation to every member in his family for the love they always covered him with and for their constant understanding and encouragement.

CONTENTS

LIST OF FIGURES

LIST OF SYMBOLS AND ABBREVIATIONS

a	numerator of the modulation index h = a/b
a(t)	amplitude of the received signal corrupted by noise
A	amplitude of the transmitted signal
A_y	amplitude of the received signal at sampling instants
A/D, ADC	analog to digital converter
AM	amplitude modulation
AM/AM	amplitude modulation to amplitude modulation conversion
AM/PM	amplitude modulation to phase modulation conversion
b	denominator of the modulation index h = a/b
BER	bit error rate
BPF	band pass filter
bps,b/s	bits per second
BPSK	binary phase shift keying
b/s/Hz	efficiency
C	carrier
$C_1..C_m$	coefficients of the scrambler/descrambler

C(t)	$\cos\pi t/2T_b$
CORPSK	correlative PSK
$\cos\omega_c t$	sinusoidal carrier
CPFSK	continuous phase FSK
CPSK	coherent M-ary PSK
C/N	carrier to noise ratio in dB
D/A	digital to analog converter
dB	decibel
dBm	decibel relative to 1 milliwatt
DE	differentially encoding
demod	demodulator
DE-MPSK	differentially encoded and coherently detected M-ary PSK
D_i	input data to be scrambled
DOC	Department of Communications
E[.]	expectation of [.]
E_b/N_o	energy per bit to noise density ratio
erf(x)	error function $(2/(\pi)^{1/2})\int\exp(-t^2)dt \leq 1$
erfc(x)	complementary error function 2(1 - erf(x))

f	frequency in Hz
f_c	carrier frequency in Hz
FCC	Federal Communications Commission
f_d	peak deviation frequency in Hz
$F(\beta)$	probability distribution function of the phase of the complex Gaussian random variable
$F_i(f)$	Fourier transform of $r_i(t)$
FM	frequency modulation
FSK	frequency shift keying
g(t)	baseband pulse
$G_s(f)$	power spectral density of s(t)
h	modulation index
H	the set of h such that $a = 1,2, b \in N^+$ and $a \leq b$
h(t)	impulse response
H(f)	network transfer function
HPA	high power amplifier
Hz	hertz
i(t),I(t)	the I-channel
IF	intermediate frequency

IJF-QPSK	intersymbol interference & jitter free QPSK
ISI	intersymbol interference
j	$(-1)^{1/2}$ imaginary number
K	$\log_2(M)$
LPF	low pass filter
L_n	delay factor in the I and Q channels
m(t)	pulse shape
m(t)	pulse of unit hight
mod	modulator
modem	modulator - demodulator
M-ary PSK	multi phase shift keying
MSK	minimum shift keying
MAMSK	multi amplitude MSK
MUX	multiplexer
n	accumulated number of clock cycles
n_c	zero mean Gaussian low pass random process
n_s	zero mean Gaussian low pass random process
N	noise power
NLSF	non-linear switched filter

N_o	noise density
N+	the set of all positive integers
NB	noise bandwidth
NRZ	non return to zero
OQPSK	offset QPSK
p_e,p(e)	probability of error
P	transition probability matrix
P_1	probability of event #1
P_2	probability of event #2
P_3	probability of event #3
$P_\theta(e)$	probability of making an incorrect decision on $\theta_n(nT_b)$
p_i	stationary (initial) probability
p_{ik}	probability of the transition from state i to state k
p^{ℓ}_{ik}	probability that the elementary signal r(t) is transmitted l signaling intervals after the occurrence of r(t)
$p_{ik}(z)$	$\Sigma p^{\ell}_{ik} z^{\ell}$
$P_{x_n}(e)$	probability of making an incorrect decision on x_n
PRBS	pseudo random binary sequence

PM	phase modulation
q(t),Q(t)	the Q channel
QPSK	quadrature PSK
r(t),r_i(t)	preenvelope of the CPFSK signal
r(t)	received signal
R	bit rate
R_i	output of scrambler
R(t,τ)	autocorrelation function of r(t)
Re	real part
RF	radio frequency
ROM	read only memory
s(t)	the modulated signal
S(t)	sinπt/2T_b
SFSK	sinusoidal FSK
sinω_ct	sinusoidal carrier
t	time variable
T,T_b	bit interval
T_s	symbol interval
b-aryPSK	multi phase PSK where M=b

TFM	tamed frequency modulation
TSI	two symbol interval
TWT	travelling wave tube
Q	the set of all p/q
u(t)	unit step function
VCO	voltage controlled oscillator
x(t) $\{x_n\}$	the incoming binary data stream
y(t), y_n	output of the detector filter
z(t), z_n	output of the detector filter
$\theta_n(t)$	transmitted phase
$\phi(t)$	phase
$\phi_n(t)$	received phase corrupted by noise
δ	phase dviation from the ideal
$\delta(t)$	dirac delta function
ω	angular frequency in radian/sec
ω_c	carrier angular frequency
π	ratio of the circumference of a circle to its diameter 22/7
Σ	summation over i
Σ	power combiner or linear adder
$\|(.)\|$	absolute value of (.)

$\eta_i(t)$	phase of the CPFSK preenvelope
α	roll-off factor of a raised cosine channel
$\beta(t)$, β_n	phase noise contributed by the AWGN
ACI	adjacent channel interference
CCI	cochannel interference

CHAPTER ONE

INTRODUCTION

Most inventions arise from the need to solve problems and, paradoxically, most inventions lead in turn to the discovery of new and hitherto unsuspected problems. The growing demand for communications, particularly between widely separated areas has resulted in an ever-increasing proliferation, by planners, users and manufacturers, of the transmission of information in digital form. As an interesting observation reinforcing the view that very little in technology is genuinely novel, we shall recall that the earliest modulation systems of the spark transmitter type were digital. The invention of the amplifying TRIODE then shifted emphasis onto analogue modulation systems for over half a century; the present interest in digital modulation might be regarded as a rebirth of the concept at a higher level of technology and expertise. In modern digital communications systems, the crowded conditions prevailing in many regions of the radio spectrum have created a need for improved spectrum and power utilization techniques. In recent years, a wide variety of techniques for solving the problem of spectral congestion, have been investigated. Various filtering

and baseband signal processing techniques have been studied. One of the proposed solutions was to better manage the existing allocations at high frequencies by means of spectrally efficient modulation techniques, in which, the primary objective was to maximize the bandwidth efficiency, defined as the ratio of the data rate to channel bandwidth (in units of bit/sec/Hz), at a prescribed average bit error rate with minimum expenditure of signal power. Communications systems using certain types of non-linear channels may force other constraints on the modulations techniques, namely, a constant envelope of the modulated signal to avoid AM to PM conversion due to the non-linearity. In summary, to attain high spectral efficiency, the power spectrum of the signal should have a narrow main lobe and a fast spectral roll-off. To attain high power efficiency, the transmit high power amplifier (HPA) should be operated in a saturated (non-linear) mode. Quadrature-phase-shift-keying (QPSK), Offset QPSK (OQPSK), and Minimum-shift-keying (MSK) modulation techniques are widely used because of their simple hardware implementation and good P(e) performance in a linearily amplified channel. Since both FSK and PSK type signals exhibit sidelobes that may interfere with adjacent channels, filtering is necessary at the transmitter so as

to conform with out of band spectral emission standards (DOC, FCC or CCITT): In the case of QPSK, the bandlimiting operation on the modulated signal, results in a great amount of envelope fluctuation in the signal (a result of filtering the phase shifts in the carrier) which leads to spectrum spreading due to the AM/AM and AM/PM conversion resulting from the transmit or satellite transponder's high power amplifiers (HPA). Thus, when the bandlimited signal is hardlimited, the spectral sidelobes are restored to their original level prior to filtering. These regrown sidebands introduce out of band radiation on the satellite down link, causing significant interference into the adjacent channels, and degrade the probability of error performance. In OQPSK, the HPA's non-linearities affect less the signal envelope and cause smaller overall envelope fluctuations (a maximum of 3 dB) than those of conventional QPSK. In MSK, the phase transitions are linear and continuous, resulting in a constant envelope modulated signal. Therefore, the MSK signal is affected much less by bandlimiting/hardlimiting operation, and the degree of regeneration of the previously filtered sidelobes is less than the case of either OQPSK or M-ary PSK. The normalized bandwidth [21], i.e., bandwidth in which 99% of the

power is contained, divided by the bit rate, is 8.65 for QPSK and OQPSK with rectangular shaping, and only 1.15 for MSK [21,22,37]. The MSK spectrum, however, has a wider main lobe than QPSK or OQPSK and thus, it may not be the preferred method for narrow-band satellite links. Multi-interval pulse overlapping techniques have been introduced to achieve higher spectral efficiency compared to the conventional QPSK, OQPSK and MSK signals. A class of intersymbol interference and jitter-free (IJF) OQPSK schemes studied by Feher et al [12,46,47] also retains a compact main lobe and low spectral spreading after non-linear amplification. Further spectral economy is achieved in MSK, by using multilevel pulses, known as multiple amplitude MSK (MAMSK) [37]. More recently, another version of MSK with phase correlation over a three bit interval duration, known as tamed frequency modulation (TFM), was introduced, resulting in a spectrum in which the power radiated into the adjacent channel is 60 dB (in $1/T_b$ Hz) lower than the power radiated into the desired channel. MSK or continuous phase FSK, with half the bit rate as separation between the two transmitted frequencies, may be generalized to include other values of the frequency deviation f_d ($f_d = 0.71/2T_b$); however, the

circuits involved are complex and the benefits reported do not seem to favor these schemes over the simple yet relatively efficient MSK modulation. Hence, generating CPFSK signals with narrower main lobe and with different peak frequency deviation values, exhibiting smooth phase transitions and therefore constant envelope, are called for.

In this thesis, a general method for generation of constant envelope bandlimited CPFSK signals is introduced. In particular, a low cost CPFSK modulation scheme, with and without spectrum lines, is designed, analyzed and implemented. The CPFSK modulated signal, having no envelope fluctuations when passed through a channel with a high degree of AM/AM and AM/PM non-linearity, has a greatly reduced spectral spreading as well as equal or narrower main lobe than that of MSK with low out of band energy and good P(e) performance. To compute the modulated signal's mean power spectral properties, a Markov chain model of the CPFSK modulated signal, describing the signal as a sequence of waveforms governed by Markovian probabilistic laws, is developed and used.

1.1 THESIS OUTLINE

Following this introductory chapter, several related digital transmission techniques are reviewed in chapter two, and the relation between MSK (or CPFSK with h = 1/2) and OQPSK is illustrated. Major published contributions on the generation and demodulation of CPFSK are summarized. This review is helpful for the understanding of the materials presented in later chapters.

A new approach of the generation of constant envelope, bandlimited CPFSK signals, with and without spectral lines, using a single modulator circuit has been developed and is introduced in chapter three. Furthermore, the hardware implementation of the modulator and the experimental results are presented.

In chapter four, a Markov chain model of the CPFSK modulated signal, describing the signal as a sequence of waveforms governed by Markovian probabilistic laws, is developed and is used to compute the modulated signal's average power spectral

density. These properties are compared to those obtained from experimental results.

In chapter five, a hardware block diagram for a new coherent method to demodulate the CPFSK signal, is proposed. The binary input data stream is demodulated through a comparison of successive beginning phases. Furthermore, it is shown that the error performance of binary CPFSK with modulation index $h=1/b$ is marginally worse than that of the differentially encoded and coherently detected M-ary PSK with $M=b$. The case of $h = 1/4$, is shown to be of interest, since it is worse than DE-MSK in E_b/N_o performance, by only 0.95 dB for a P(e) of 10^{-4}; yet its bandwidth is half that of MSK.

Finally, in chapter six, the conclusions and future research points are presented, as well as a suggestion for a possible extension of this work.

CHAPTER TWO

REVIEW OF PSK AND FSK BASED SIGNALS

2.1 INTRODUCTION

Before proceeding to the design of the CPFSK modulator, some other modulation schemes are outlined in this chapter. This outline is expected to provide a general understanding of the main features of the existing power and bandwidth efficient modulation techniques that are relevent to the thesis' topic. The well known QPSK, Offset QPSK, MSK and other recently developed digital modulation schemes are presented. Major contributions that have been published on full and partial response CPFSK modulation scheme are summarized. The literature on the implementation of CPFSK is reviewed. Moreover, the relationship between Offset QPSK with sinusoidal pulse shaping (MSK) and CPFSK is highlighted.

With this overview, we are able to justify the needs and objectives of our investigation of a new method to generate the CPFSK modulated signals.

2.2 M-ARY PHASE SHIFT KEYING

In the transmission of digital signals the modulator performs the function of impressing the digital information bearing signal on a carrier by modulating the carrier amplitude, the carrier phase, or the carrier frequency. In M-ary PSK systems, the modulator maps the sequence of binary digits into a corresponding set of discrete phases of the carrier [39,41]. Consequently, if $\{x_n\}$ denotes the sequence of binary bits appearing at the input of the modulator at a rate of R_b bits/sec, an M-phase-shift-keyed signal is generated by mapping blocks of $K = \log_2 M$ binary digits of the sequence $\{x_n\}$ into one of the M corresponding phases $\theta_m = 2\pi m/M$, $m = 0,1,...,M-1$ [41]. The M possible signals that would be transmitted during each signaling interval $T_s = (\log_2 M)T_b$, are [5,39]

$$s(t) = \cos\{2\pi f_c t + \theta_n\} \quad \text{for } (t-nT_s) \in [0,T_s) \tag{2.1}$$

where $m = 0,1,...,M-1$. The resulting equivalent low pass signal is represented as, [41]

$$u(t) = \exp(j\theta_n) \tag{2.2}$$

The digital M-ary PSK-waveform can also be represented in the form,

$$s(t) = I(t)\cos(\omega_c t) - Q(t)\sin(\omega_c t) \tag{2.3}$$

where $I(t) = \cos(\theta_n)$ and $Q(t) = \sin(\theta_n)$, which shows that the waveform s(t) is the difference of two AM signals using $\cos(\omega_c t)$ and $\sin(\omega_c t)$ as carriers.

2.2.1 QUADRATURE PHASE SHIFT KEYING

In Quadrature Phase Shift Keying (QPSK), the sequence of phases $\{\theta_n\}$ in (2.1) has four distinct states. These states are generated by a unique mapping scheme of consecutive dibits (pair of bits) to phase values. A block diagram of a conventional coherent QPSK system is shown in figure 2.1.a [4,5,37,39,40]. The serial input data stream, entering the modulator at the rate of $1/T_b$ bits/sec, is separated by a serial to parallel converter

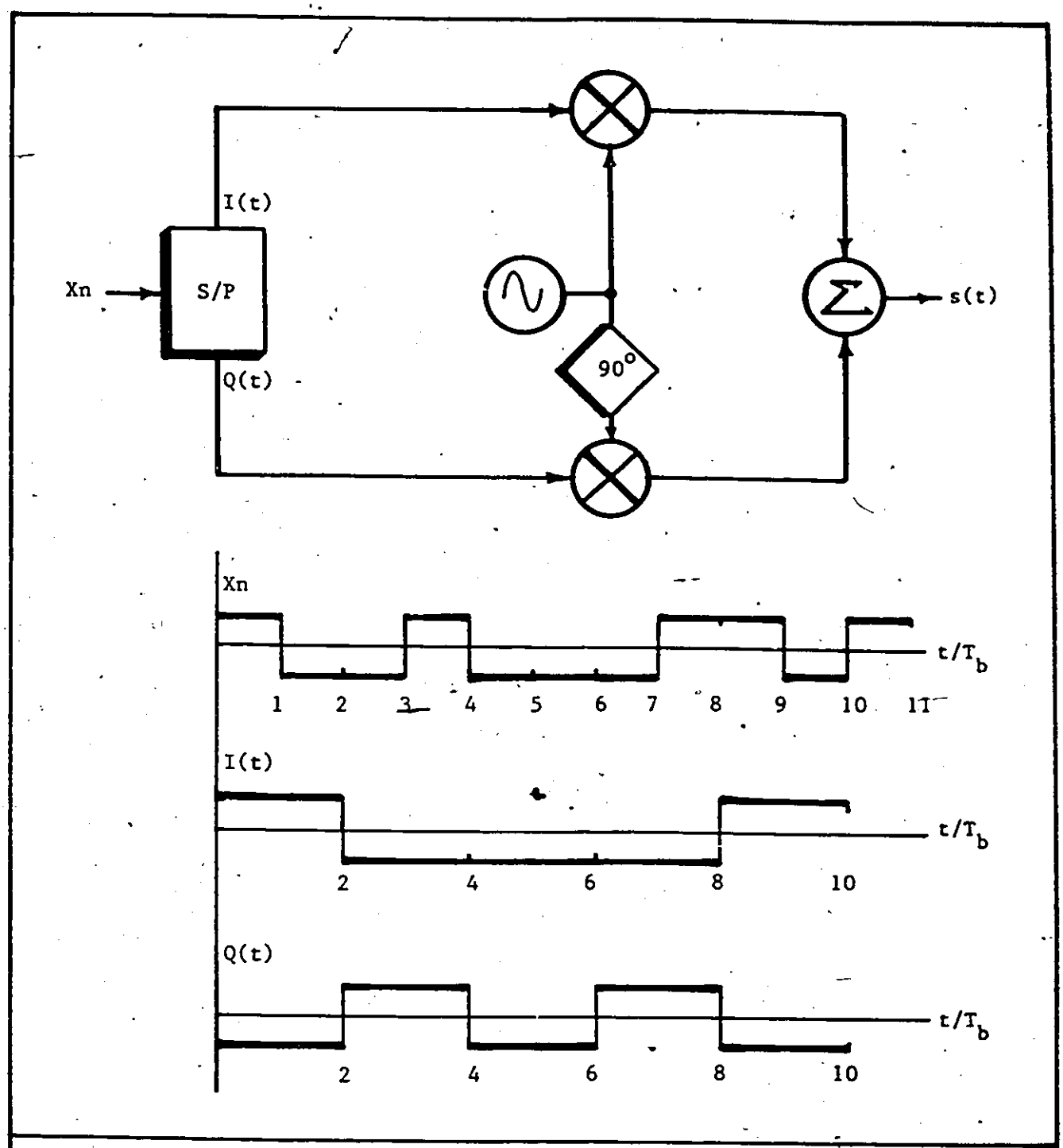

Figure 2.1.a block diagram of quadrature phase shift keying (QPSK) modulator.

into two streams, I(t) and Q(t), consisting of even and odd bits respectively, with half the incoming bit rate ($1/2T_b$). The two parallel pulse trains modulate the inphase and quadrature components of the carrier; and the sum s(t), the modulated QPSK signal can be expressed as

$$s(t) = I(t)\cos(\omega_c t) - Q(t)\sin(\omega_c t) \qquad (2.4)$$

The outputs of the multiplier, in figure 2.1.a, are BPSK signals. The I multiplier output signal has phase 0 or 180 degrees relative to the carrier, and the Q multiplier output signal has phase 90 or 270 degrees relative to the carrier. The four distinct states of the carrier phase are thus: $\theta(t) = \text{Arctan}(Q(t)/I(t)) = \pm 45, \pm 135$, corresponding to the four combinations of I(t) and Q(t). The carrier phase $\phi(t)$ can change only once every $T_s = 2T_b$. During the following $2T_b$ interval, if neither bit stream changes sign, the carrier phase remains the same. If one component, I(t) or Q(t), changes sign a phase shift of 90 degrees occurs. A change in both components results in a phase shift of 180 degrees. Since the I and Q modulated signals are in quadrature, the receiver is able to demodulate and regenerate them independently of each other, operating in effect as two BPSK

receivers. The regenerated I and Q streams are then recombined in a parallel to serial converter to form the original input data stream. However, it is subject to error because of waveform distortion and bit spreading resulting from noise and filtering.

2.2.2 OFFSET QUADRATURE PHASE SHIFT KEYING

Offset QPSK system is very similar to QPSK. The difference between the two modulation techniques lies in the phase relationship of the I and Q bit streams [37]. The odd and even bit streams, transmitted at the rate of $1/2T_b$ baud, are synchronously aligned in QPSK, as shown in figure 2.1.b, such that their transitions coincide. In the case of OQPSK, a shift is introduced in the relative alignment of the quadrature stream Q(t) with respect to the other by an amount equal to T_b. The OQPSK signal can be represented by 2.1 and 2.7, and the resulting instantaneous phase states at the modulator output are the same as for QPSK. However, a common representation of the OQPSK modulated signal is given by [22],

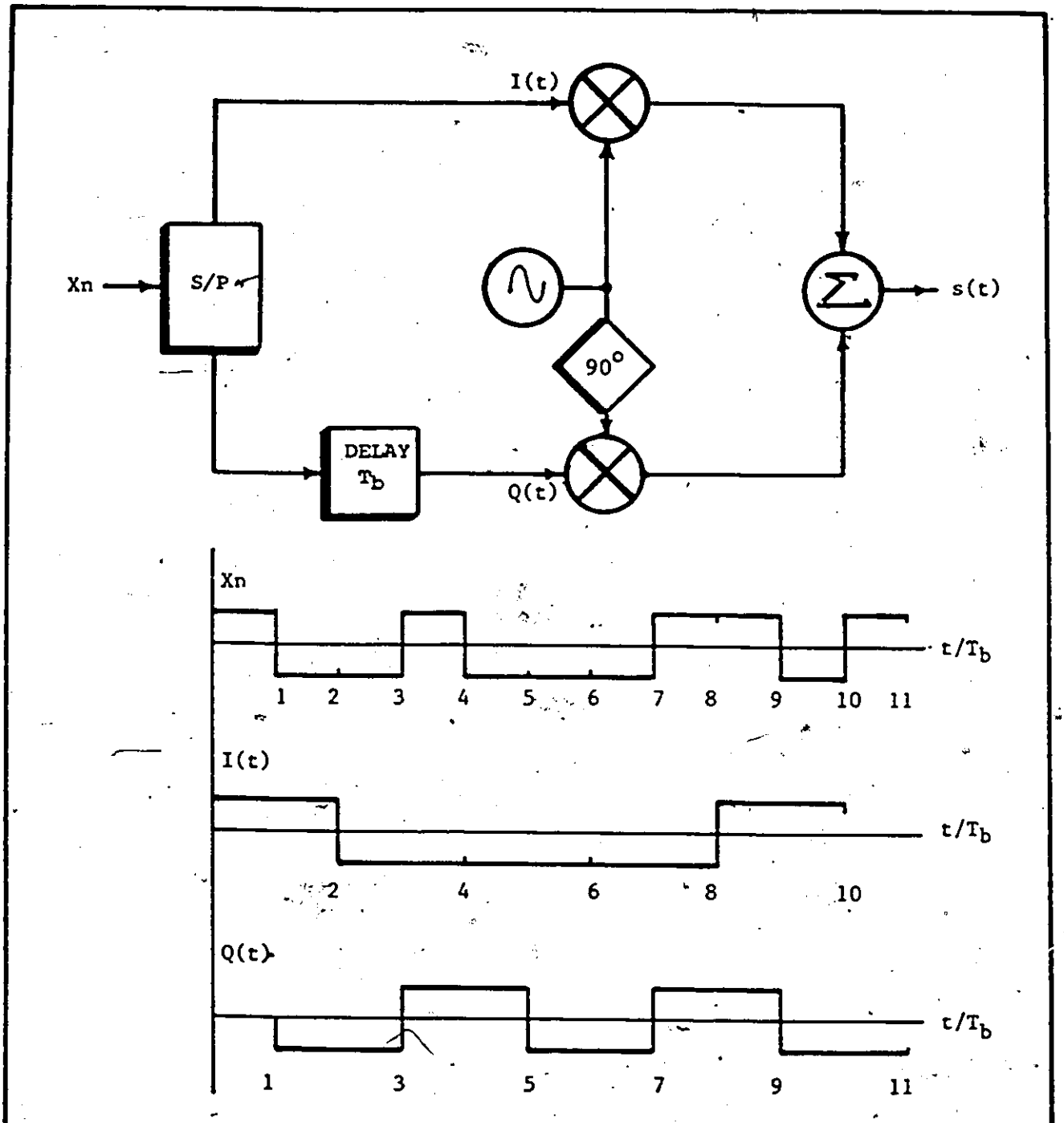

Figure 2.1.b block diagram of an offset quadrature phase shift keying (OQPSK) modulator.

$$s(t) = \begin{cases} x_{2n-1}\, S_{q_c}(t-2nT_b)\cos(\omega_c t) - x_{2n-2}\, S_{q_s}(t-(2n-2)T_b)\sin(\omega_c t) \\ \qquad\qquad (2n-1)T_b \le t \le 2nT_b \\ \\ x_{2n-1}\, S_{q_c}(t-2nT_b)\cos(\omega_c t) - x_{2n}\, S_{q_s}(t-2nT_b)\sin(\omega_c t) \\ \qquad\qquad 2nT_b \le t \le (2n+1)T_b \end{cases} \qquad (2.5)$$

where ω_c is the carrier frequency in rad/sec, $x_n = \pm 1$ is the input, binary bit stream at a rate of $1/T_b$ bits/sec, and $S_{q_s}(t)$ and $S_{q_c}(t)$ are two rectangular unit amplitude pulses each with a duration of $2T_b$:

$S_{q_s}(t) = u(t) - u(t-2T_b)$ and $S_{q_c}(t) = u(t+T_b) - u(t-T_b)$.

Since the binary components cannot change states simultaneously, one component changes in the centre of the other symbol and hence only one component switches at a time. The demodulator block diagram for both QPSK, and OQPSK is shown in figure 2.1.c.

Like QPSK, an unfiltered OQPSK signal has a constant amplitude envelope. Bandlimited OQPSK signals have a maximum amplitude variation of 70% (3 dB) compared to 100% amplitude variation for conventional QPSK systems [39].

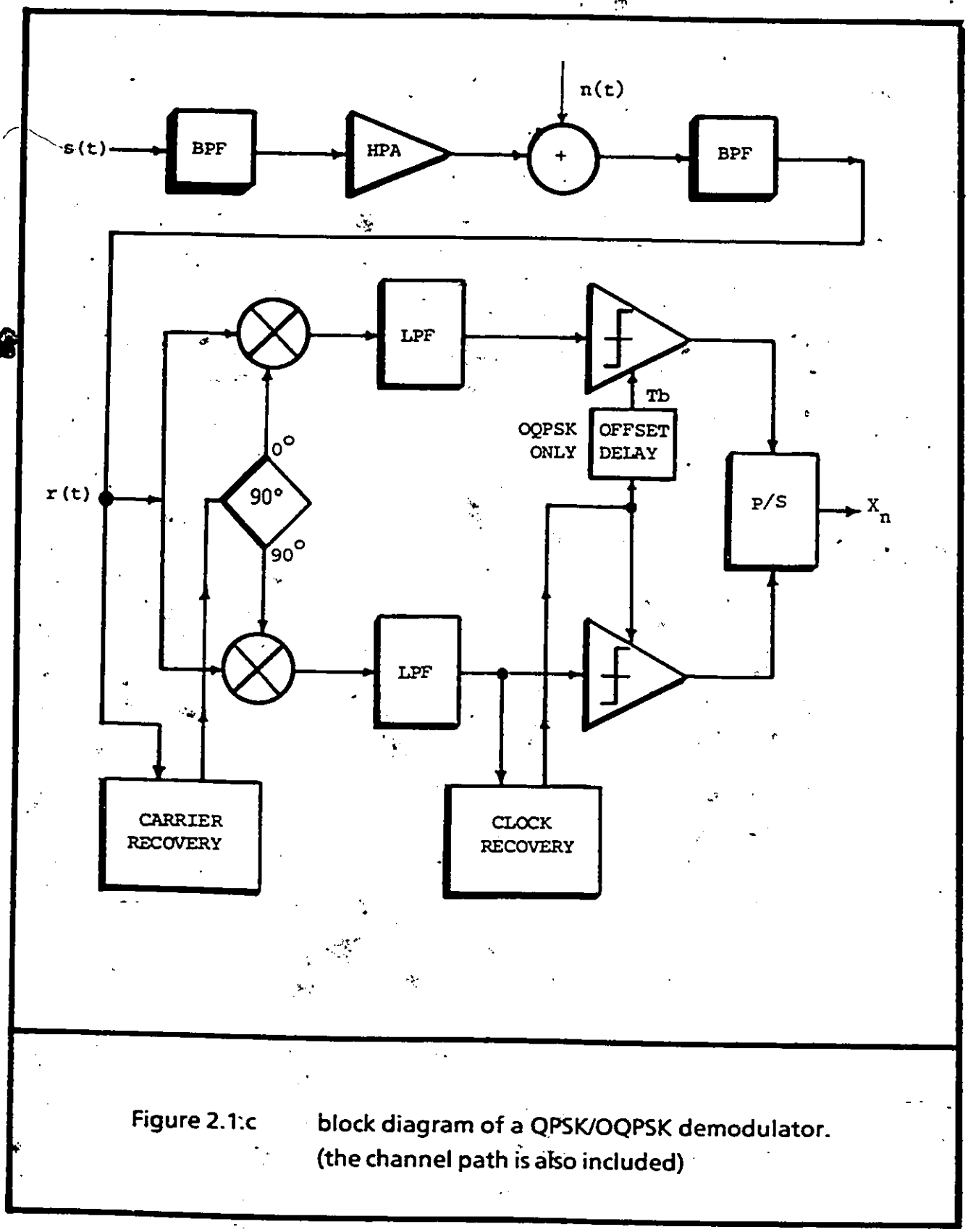

Figure 2.1:c block diagram of a QPSK/OQPSK demodulator. (the channel path is also included)

This lower amplitude envelope variation imparts certain advantages to OQPSK as compared to QPSK in non-linear systems [22,37,39,40]. This means that, when a bandlimited OQPSK signal is transmitted through an amplitude limiting device such as a high power amplifier (HPA) or a hard limiter, there is only partial regeneration of high frequency components, in the spectrum, prior to filtering [37,39]. For QPSK under the same circumstances, however, the regeneration to the unfiltered level is complete [39]. Thus, out of band interference in OQPSK is reduced, while in QPSK it is not [39].

2.3 MINIMUM SHIFT KEYING

Minimum Shift Keying (MSK) is a special case of OQPSK in which the OQPSK signal format is modified to avoid abrupt phase transitions all together [37]. This is accomplished by employing half-cycle sinusoidal pulses instead of the usual rectangular shapes [22,37,39]. Figure 2.2 shows the block diagram of an MSK system. As with OQPSK, the demultiplexer accepts bits at R_b, and routes these alternately to the I and Q phasor encoders at a rate of $R_s = R_b/2$, where R_s is the phasor

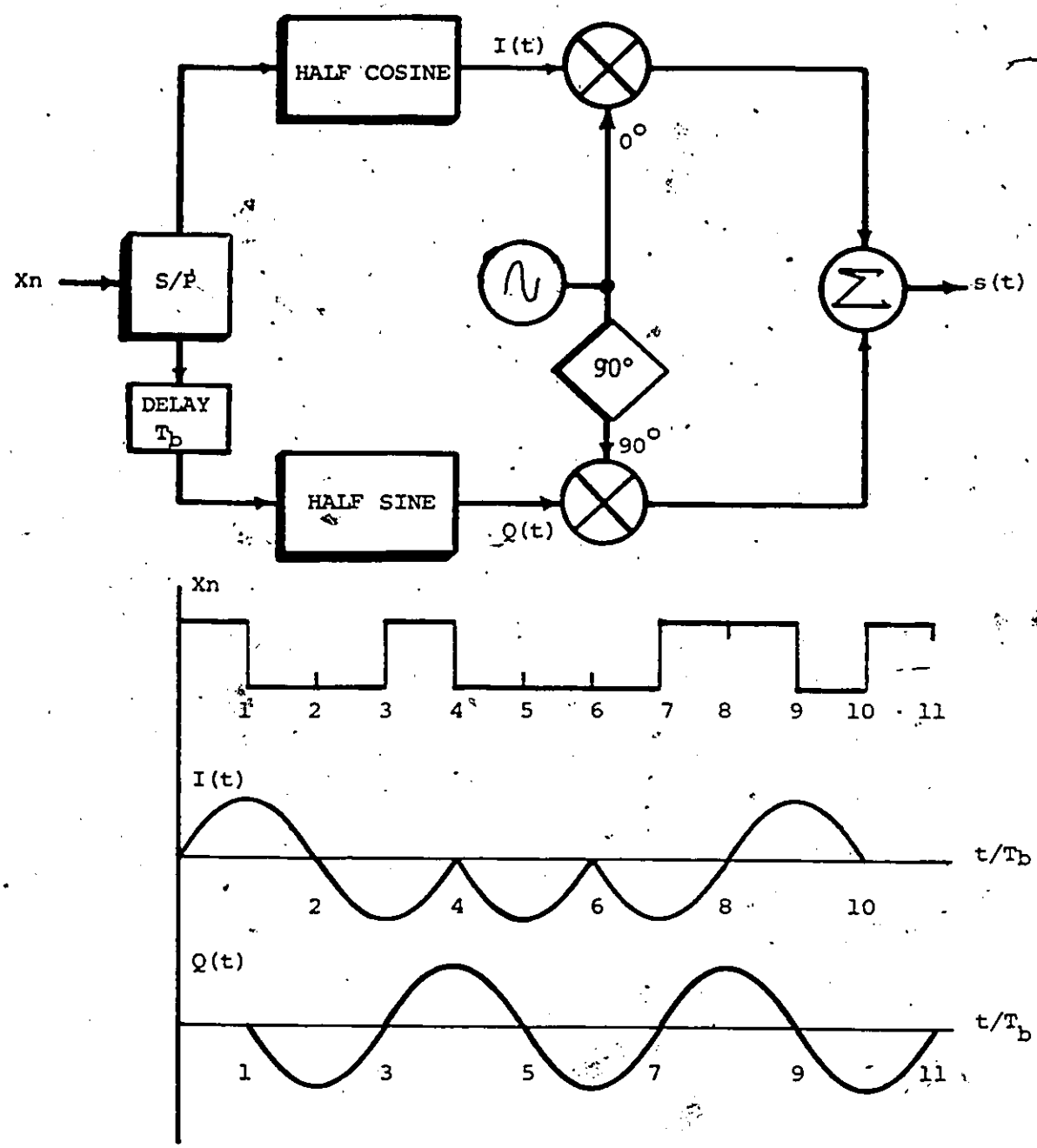

Figure 2.2.a block diagram of a minimum shift keying (MSK) modulator.

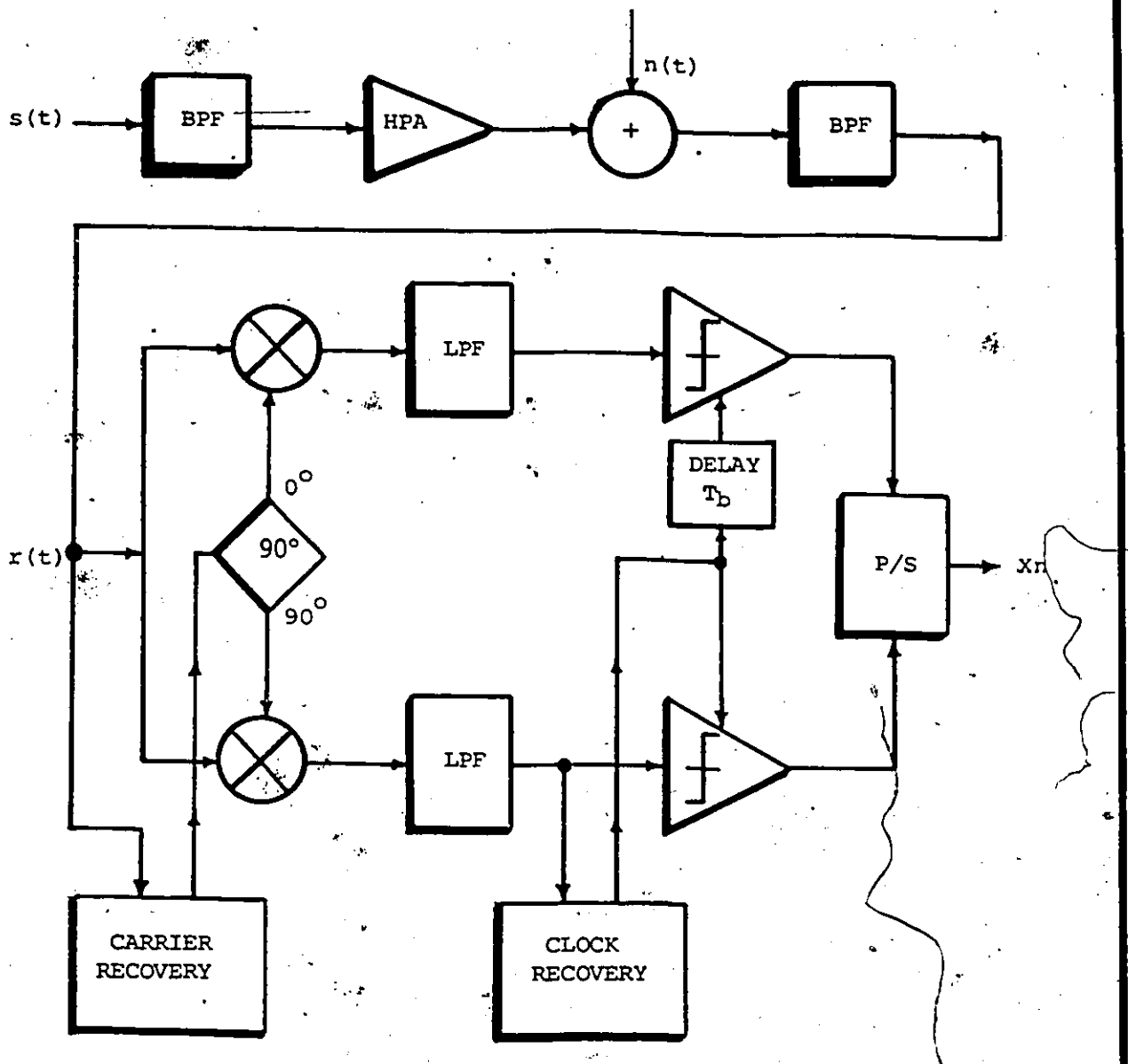

Figure 2.2.b block diagram of a minimum shift keying (MSK) demodulator. (the channel path is also included)

symbol rate. Each symbol is lengthened to $2T_b$. After passing through the two multiplexers and the summer, the resulting output is [22]

$$s(t)=\begin{cases} x_{2n-1}\,C(t-2nT_b)\cos(\omega_c t) - x_{2n-2}\,S(t-(2n-2)T_b)\sin(\omega_c t) \\ \qquad\qquad (2n-1)T_b \le t \le 2nT_b \\ \\ x_{2n-1}\,C(t-2nT_b)\cos(\omega_c t) - x_{2n}\,S(t-2nT_b)\sin(\omega_c t) \\ \qquad\qquad 2nT_b \le t \le (2n+1)T_b \end{cases} \tag{2.6}$$

where $C(t)=\cos(\pi t/2T_b)$ and $S(t)=\sin(\pi t/2T_b)$. A comparison between MSK, OQPSK and conventional QPSK waveforms is shown in figure 2.3.

Owing to its constant envelope and continuous phase nature, an unfiltered MSK signal, when non-linearly amplified, suffers no significant spectral spreading in the bandwidth of interest, and provides faster roll off and lower high-order spectral sidelobes than the filtered OQPSK signal [22,37]. It is illustrated that 99% of the power of a non-filtered MSK signal is contained within a channel bandwidth of $1.15R_b$ [22,38].

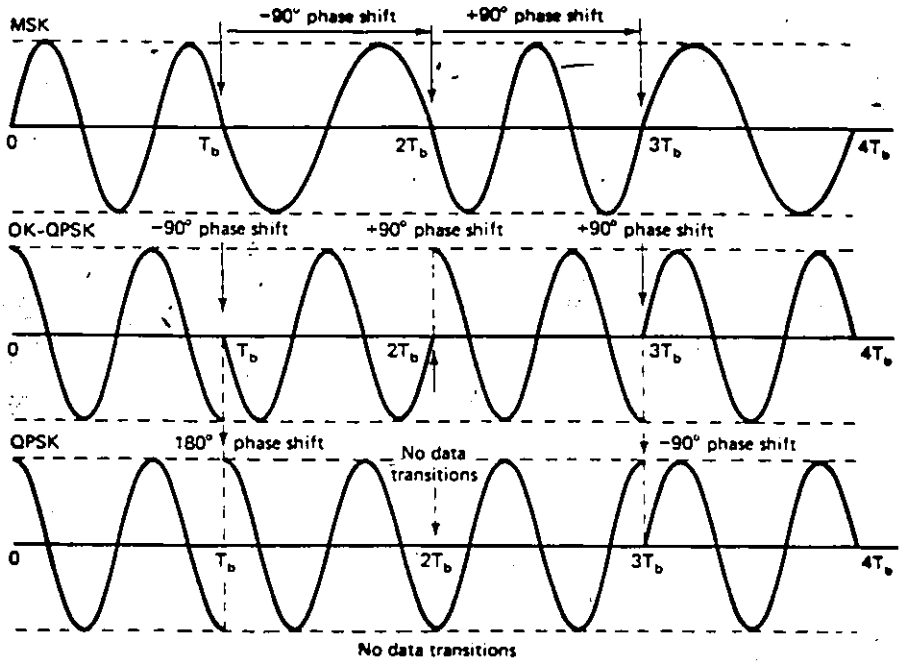

Figure 2.3 Typical waveforms for MSK, Offset QPSK and conventional QPSK.

Hence, less post modulation filtering will be required of MSK than of OQPSK to reduce the out of band power to a given value (for a channel bandwidth $B_c > 0.75R_b$) [21, 37,39,40]. In addition to its spectral properties, the ideal E_b/N_0 performance of MSK which is the same ideal E_b/N_0 as BPSK, QPSK or OQPSK [40], is of interest. As is well known, the probability of bit error p_e of coherently detected QPSK, OQPSK and MSK is [39,40]

$$p_e = Q((2E_b/N_0)^{1/2}) \tag{2.7}$$

This expression, however, omits considerations of data ambiguity resolution. Differential encoding may be used to provide such resolution in which case the probability of bit error P(e) is given by [3,39,40]

$$P(e) = 2p_e - (p_e)^2 \tag{2.8}$$

The spectral spreading and error probability performance of QPSK, OQPSK and MSK systems in various nonlinear channel models have been investigated by many authors. In general, it was found that E_b/N_0 degradation, due to both bandwidth and amplitude limiting, is less for wide channel spacing and worse for

narrow channel spacing, relative to QPSK and OQPSK [40]. However, since the MSK spectral main lobe is 50% wider than that of unfiltered QPSK and OQPSK signals [21,22,37,39], and since the power spectrum of the MSK signal has the same shape as the magnitude squared of the Fourier transform of the pulse shaping function m(t) [22,37], the spectral properties of the MSK type modulated signal can be further improved by using bandwidth efficient pulse shapes m(t). Different pulse shapes have been proposed by a number of authors [12,38,39,42,43,45]. Amoroso introduced Sinusoidal Frequency Shift Keying (SFSK) in which the pulse shape m(t) is synthesized by applying a keyed sinewave to a linear integrator followed by a linear frequency modulator [38], i.e.,

$$m(t) = \cos\left(\frac{\pi t}{2T_b} - U\sin\left(\frac{\pi t}{2T_b}\right)\right) \quad \text{for } |t| < T_b \tag{2.9}$$

where U is constant in the range (0,1/2). For U=0 the MSK signal is obtained. This results in a much smoother m(t) and produces an asymptotic spectral roll off that is twice as fast as in MSK. Rabzel and Pasupathy [42] applied the relationship between sharp spectral roll off and the pulse shape having many

continuous derivatives to present pulse shapes with smoother end-point behaviour, and thus sharp spectral roll off. Simon [45] derived a set of conditions on the input pulse shapes and derived the general power spectral densities of those shapes. Feher [4,39] introduced a non-linear switch filter (NLSF) which was later used [12] to develop a class of intersymbol-interference and jitter-free (IJF) baseband signals and IJF-OQPSK systems. A new class of IJF-OQPSK called two-symbol-interval (TSI) was later introduced [46]. Based on Feher's NLSF and IJF-OQPSK systems, cross-correlated phase-shift-keying (XPSK) was introduced by Kato [47]. In XPSK modulators, a controlled amount of cross correlation between the in-phase (I) and quadrature (Q) channels is introduced. I and Q cross correlation reduces the envelope fluctuation of the intersymbol interference and jitter free OQPSK (IJF-OQPSK) modulation scheme, from 3 dB to approximately 0 dB [47].

2.4 CPFSK MODULATION SCHEME

In continuous phase FSK (CPFSK) modulation, the transmitted signal is generated by varying the carrier frequency. In full

response CPFSK, each data symbol only affects the instantaneous frequency of the transmitted signal in one symbol interval while the phase is kept continuous. CPFSK scheme can handle M-ary signalling, various frequency pulse shapes and arbitrary set of modulation indices [18]. The transmitted constant envelope CPFSK signal can be expressed as [18,28]

$$s(t)=\cos(\omega_c t+\theta(t,x_i)+\theta_o) \tag{2.10}$$

where $\theta(t,x_i)$ is the continuous phase modulation induced by the data sequence $x_i=(x_1,x_2,.....,x_n)$, and is given by

$$\theta(t,x_i)=2\pi\int_0^t \sum_{n=-\infty}^{\infty} x_n h_n g(\zeta-nT_b)d\zeta \tag{2.11}$$

The symbols x_n are selected independently every T_b second in equiprobable fashion from the uncorrelated M-ary set {-1,.....,-M-1}. The variable h_n is the modulation index during the nth interval $[(n-1)T_b,nT_b)$. The amplitude of the baseband pulse g(t) is chosen such that the maximum phase change over the nth

interval is $x_n h_n \pi$. For continuous phase signal, the baseband pulse shape g(t) is not allowed to contain any impulses [28]. CPFSK systems can be divided into two major classes:

1. Full response CPFSK modulation scheme:

   In this case, the baseband pulse shape g(t) is limited within one bit interval T_b. Note that although the scheme is full response, the actual phase over any specific bit interval depends upon the previous data symbols. This case includes linear phase with constant h (i.e., binary CPFSK) or with multi-h [30,31] and with rectangular or smoother g(t) (e.g., SFSK [38]). As the baseband pulse g(t) gets smoother the power spectrum of the full response CPFSK signal rolls off faster but its main lobe becomes wider. A low modulation index yields a narrower main lobe but the complexity of practical implementation is increased [37].

2. Partial response CPFSK modulation scheme:

In this case, the baseband pulse shape extends over many bit intervals. Only constant h schemes with piecewise constant baseband pulses g(t) [15,36] or with smooth multiple-interval pulses [15,16,17,36] have been considered. The Tamed-Frequency Modulation (TFM) [16], uses correlation between phase shifts to achieve smoother phase and thus better spectrum (i.e., smoother pulse g(t)). This correlative encoded FM technique was generalized by Mulwijk [15], to a class of Correlative Phase Shift Keying (CORPSK) Modulation Techniques. Partial response CPFSK modulation schemes provide power spectra with both narrow main lobe and fast roll-off (see figure 2.4). However, because of multi-level correlation, phase variations are small; therefore, to obtain good error probability performance, careful carrier and clock synchronization is required.

2.4.1 IMPLEMENTATION OF CPFSK SYSTEMS

This section reviews the literature on the generation and demo-

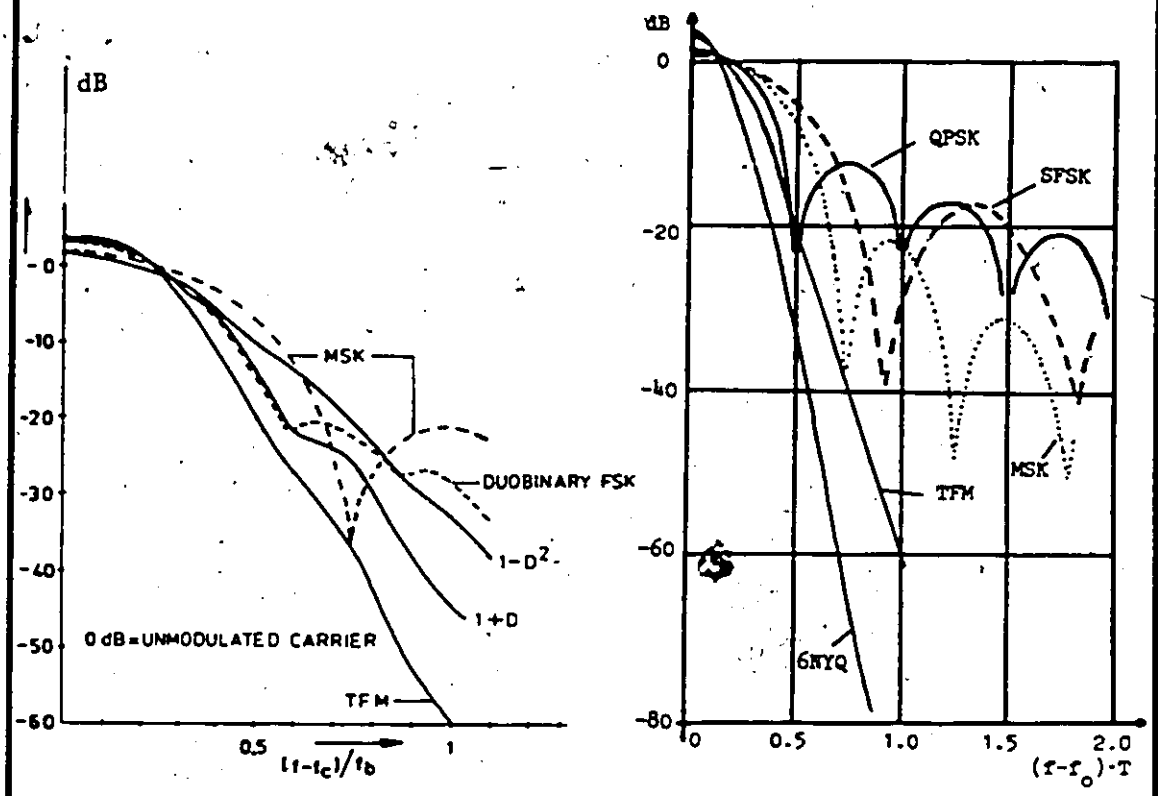

Figure 2.4, Spectra of MSK, duobinary FSK with h = 0.5, QPSK, SFSK, CORPSK(2-3, 1 + D), CORPSK(2-3, 1-D^2), and CORPSK (2-5, $(1 + D)^2$)(= TFM).

dulation of CPFSK modulation technique. Implementation of CPFSK modulation scheme with h = 1/2, also known as FFSK or MSK, can be accommodated in two equivalent fashions, namely parallel and serial. The parallel method is illustrated in figure 2.2.a; the serial method is an alternative approach to parallel modulation and demodulation of MSK. In the parallel approach, the quadrature channels of the modulator and demodulator must be time synchronized, amplitude balanced, and in phase quadrature to minimize overall system degradation. For high data rate, this becomes more difficult to maintain. The serial method, published by Amoroso and Kivett [7] and later implemented at 760 Mb/s by Ryan, Hambley and Vogt [48], avoids these problems. DeBuda, [20], included other values of h (h = 0.715) into CPFSK; a longer bit memory was used before the decision was to be made (larger observation intervals such as $3T_b$ or $5T_b$ were implemented). Only 0.8 dB of improvement has been reported; however, the complexity of the circuit involved does not seem to favor this scheme over the simple MSK scheme (CPFSK with h = 1/2) [37]. Davis [25] implemented an experimental 4-ary CPFSK MODEM with low modulation index (h = 1/8). The demodulation technique used on this modem is that of phase detection similar to that described by Brady [24]. Brady introduced coherent phase

shift detection that can be used to demodulate multilevel frequency modulated type signals. Tamed frequency modulation was implemented by Jager, Dekker, and Muilwijk[16,17]. Duo-binary FSK, also known as FSOQ, is analysed and implemented by Dagakis and Papadopoulos [49].

2.5 SUMMARY

So far, major contributions in the field of digital modulation techniques, (both PM and FM) have been reviewed. Baseband pulse shapes, phase transitions and envelope fluctuations are among the major parameters that affect spectral regeneration caused by non-linear amplification. Spectral improvements can be obtained if spectral efficient baseband pulse shapes and/or smooth phase transitions, as have been proposed by many authors, are used. The cost of the spectral improvement of these constant-envelope modulation schemes increases the system's complexity and synchronization problems. Special emphasis was done on CPFSK systems.

In the following chapters, we introduce and study a new

approach for the generation of CPFSK signals. Our studies include the spectral properties, error probability performance of a few CPFSK cases in a noisy environment, hardware feasibility, and potential applications of this system.

CHAPTER THREE

GENERATION OF CONSTANT ENVELOPE CPFSK SIGNALS

3.1 INTRODUCTION

In chapter two, several related digital modulation techniques were reviewed and it was shown that although the spectral shape of MSK is overall more concentrated than that of the M-ary PSK signal spectra, its main lobe is wider resulting in less bandwidth efficiency in bits/sec/Hz. Moreover, major contributions to CPFSK were summarized. However, because of the increase in hardware complexity, little work has been done on linear phase, binary CPFSK. Indeed, most of the work done, dealt mainly with MSK or with its derivatives (e.g., TFM, CORPSK, SFSK etc...).

This chapter will show that it is possible to generate constant envelope CPFSK signals using a single modulator circuit. To achieve improved spectral economy the new generation scheme has values of the peak frequency deviation f_d, less than or equal to one fourth of the bit rate. The resultant CPFSK signal is free

of amplitude variations, and hence is less affected by the non-linearities of the channel and of the power amplifiers of satellite repeaters.

3.2 SIGNAL CHARACTERIZATION

For binary CPFSK system the baseband information x(t) to be transmitted, is a sequence of uncorrelated bipolar random rectangular pulses, that is,

$$x(t)=\sum_{n=0}^{\infty} x_n m(t-nT_b) \tag{3.1}$$

where $\{x_n=\pm 1\}$ is the antipodal binary data stream and m(t) is a pulse of unit height. The modulation index h or frequency deviation ratio is defined as $h=2f_dT_b$ [20]. Assuming without loss of generality that $\theta_0=0$, and integrating the phase expression in (2.11), s(t) can be represented, during the nth interval, as

$$s(t)=\cos\{2\pi f_c t+x_n 2\pi f_d t+\theta_n(x_1,\ldots,x_n)\} \tag{3.2}$$

where θ_n represents an additive phase which is constant over the interval $[nT_b,(n+1)T_b)$ with a value determined by the requirement of phase continuity at the data transition instants $t=nT_b$. Rewriting (3.2) and replacing f_d by $h/2T_b$, we get (see appendix A)

$$s(t)=\cos\{\omega_c t+\frac{\pi h}{T_b}x_n(t-nT_b)+\pi h\sum_{k=1}^{n}x_k\} \tag{3.3}$$

for $t \in [nT_b,(n+1)T_b)$, where the function

$$\theta(t)=\frac{\pi h}{T_b}x_n(t-nT_b)+\pi h\sum_{k=1}^{n}x_k \tag{3.4}$$

satisfies both the condition of an equiprobable choice between the two frequencies (f_1,f_2) in each bit interval, and the required condition of phase continuity (see appendix A). Setting

$$L_n=\{n-x_n\sum_{k=1}^{n}x_k\} \tag{3.5}$$

s(t) can be expressed as,

$$s(t)=I(t)\cos(\omega_c t)+Q(t)\sin(\omega_c t) \tag{3.6}$$

where,

$$I(t) = \cos\{\frac{nh}{T_b}(t - L_nT_b)\} \text{ and,} \tag{3.7}$$

$$Q(t) = -x_n \sin\{\frac{nh}{T_b}(t - L_nT_b)\} \text{ on } [nT_b,(n+1)T_b) \tag{3.8}$$

respectively represent the in-phase and quadrature-phase components of the binary CPFSK signal and where L_nT_b represents the time offset from the origin for both components. The orthogonal components of the CPFSK modulated signal for three values of h (h = 1/2, 1/4 and 1/8), are shown in figures 3.1.a, 3.1.b and 3.1.c. Figure 3.2 shows the corresponding eye pattern of the various I(t) and Q(t) waveforms.

3.3 ON THE DESIGN OF THE CPFSK MODULATOR

A possible implementation of the binary CPFSK modulator is shown in figure 3.3. It basically consists of a voltage controlled oscillator (VCO) followed by a bandpass filter. This implementation, however, is far from being considered as practical. For, while a voltage controlled oscillator will have

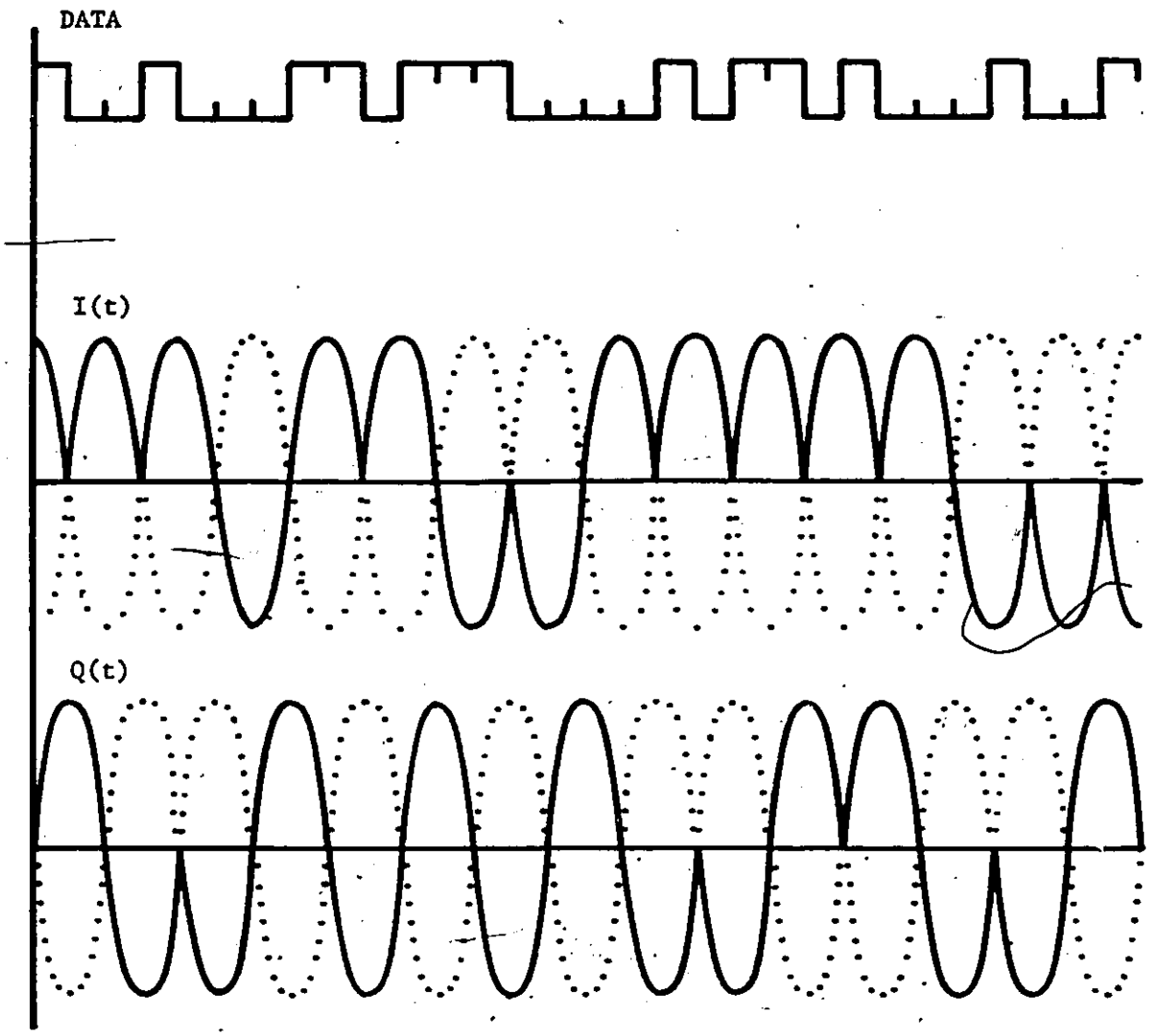

Figure 3.1.a Orthogonal components of the CPFSK modulated signal's complex preenvelope. (h = 1/2)

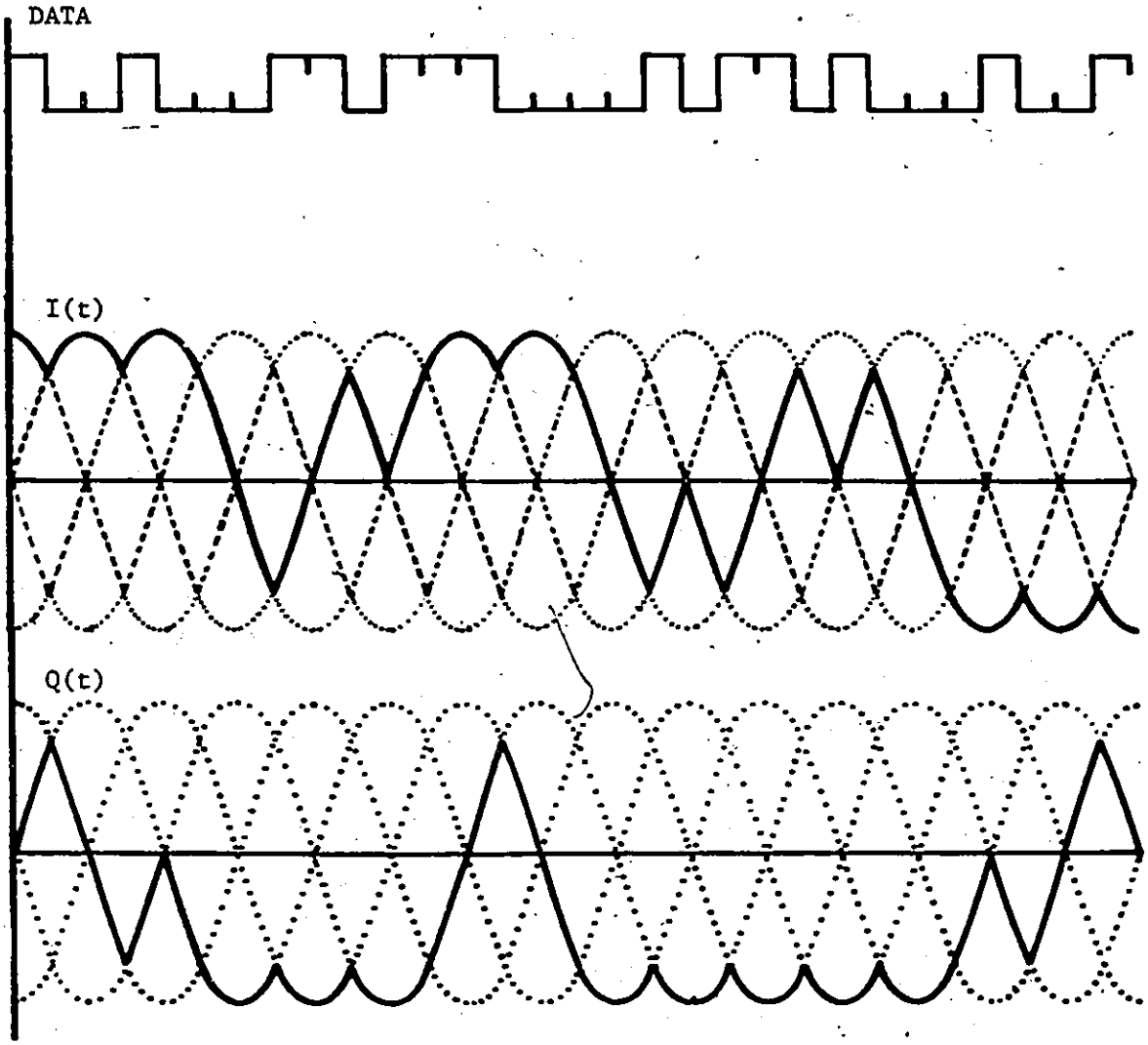

Figure 3.1.b Orthogonal components of the CPFSK modulated signal's complex preenvelope. (h = 1/4)

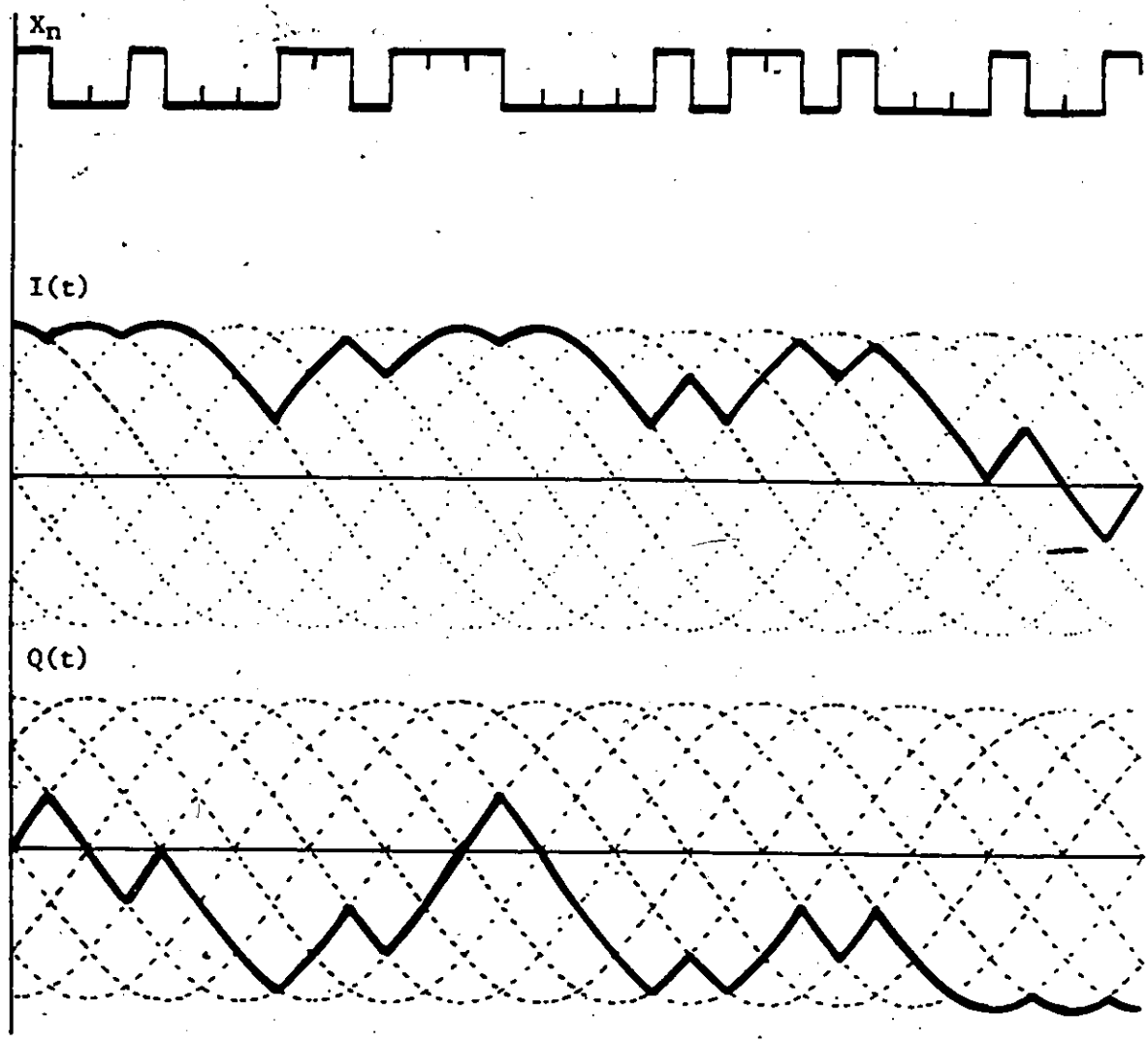

Figure 3.1.c Orthogonal components of the CPFSK modulated signal's complex preenvelope. (h = 1/8)

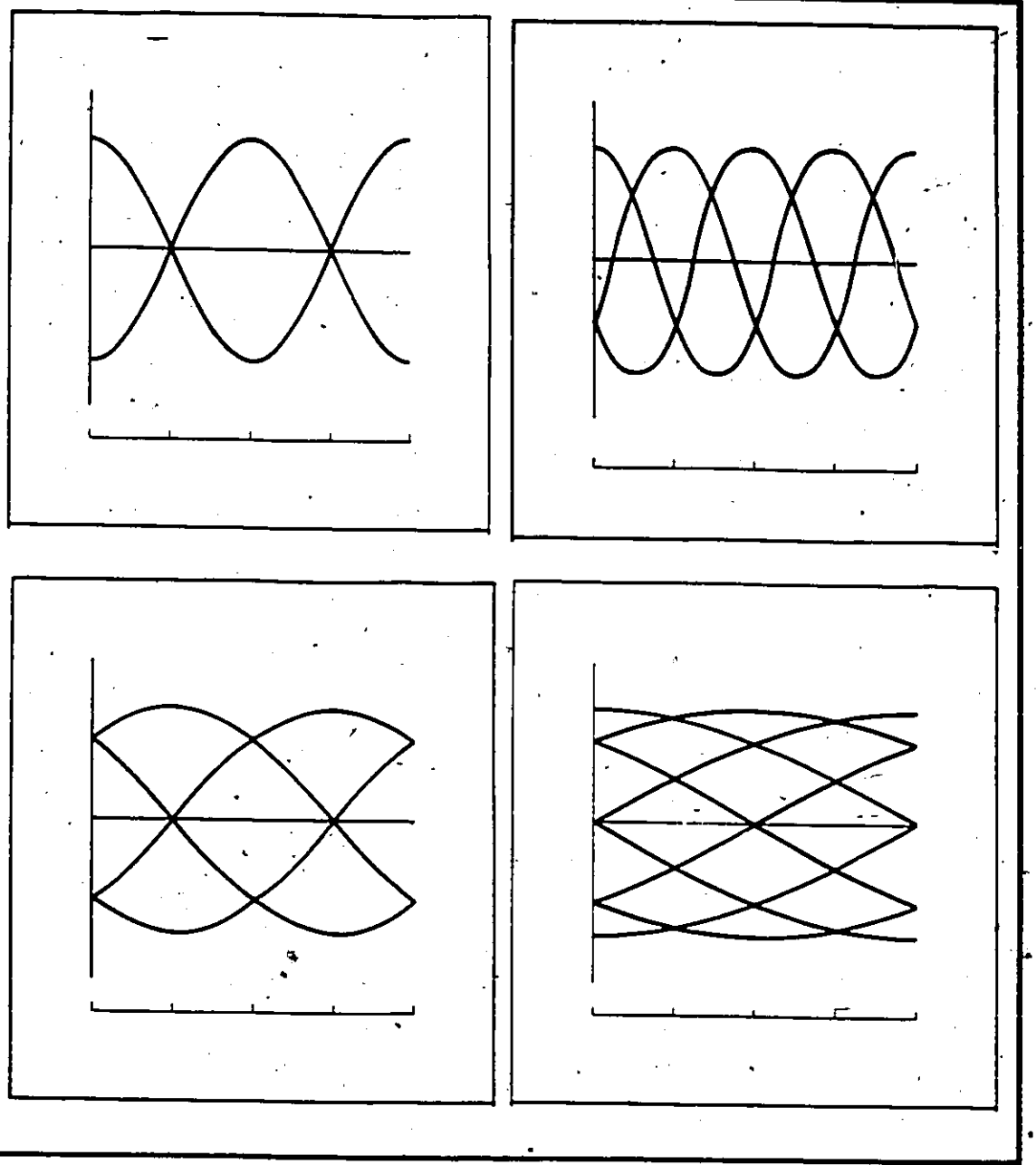

Figure 3.2 Computed CPFSK eye patterns for several values of h.
a) h = 1/2; b) h = 1/3; c) h = 1/4; d) h = 1/8.

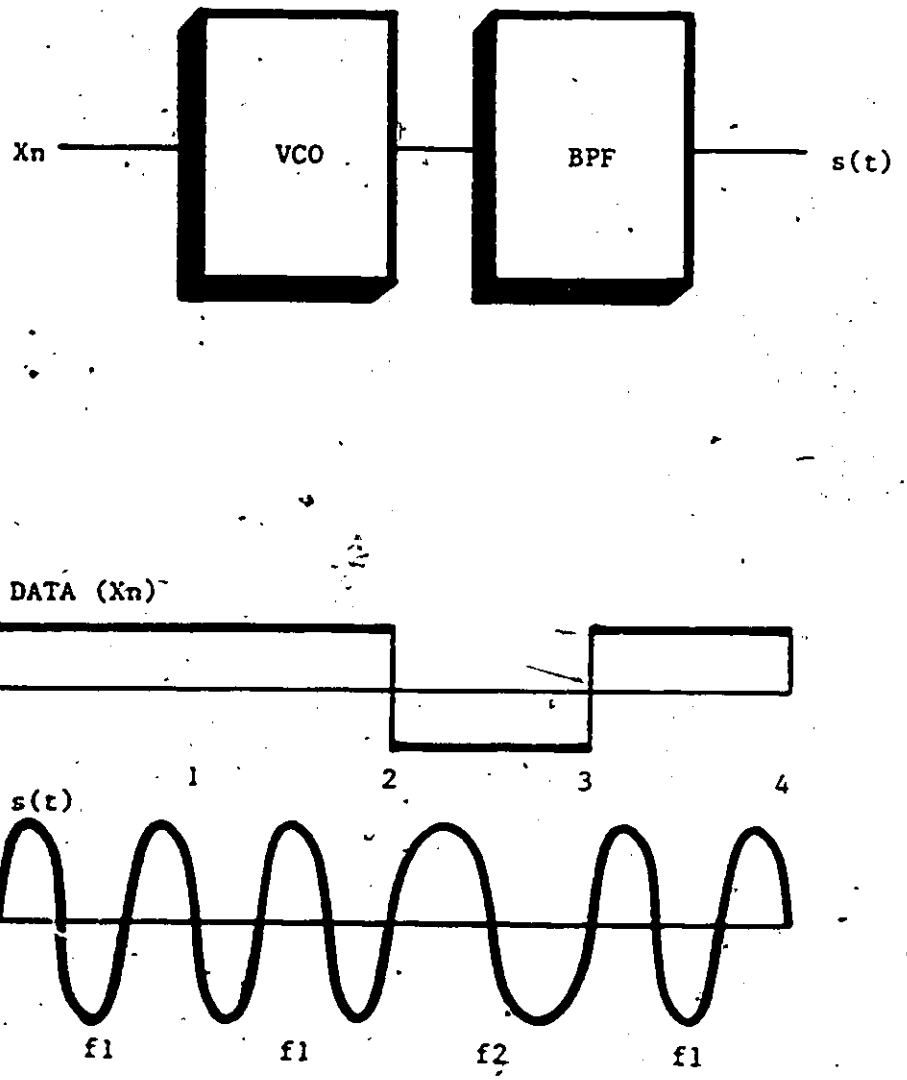

Figure 3.3 Block diagram of a CPFSK modulator.

continuous phase, the frequency of the output cannot be precisely controlled. Switching between precise oscillators will eventually cause phase discontinuities at the switching times (nT_b).

A practical implementation of a CPFSK modulator generates the modulated signal s(t) by balanced amplitude modulation of two carriers in quadrature; the I waveform modulates $\cos(\omega_c t)$ and the Q waveform modulates $\sin(\omega_c t)$. Following this implementation, the output frequency can be precisely controlled and the transmitted phase is kept continuous while the frequencies are switched. As shown in figure 3.4, both the I and Q waveforms are generated by the baseband processor. A straightforward realization of this processor is achieved, mainly, because of the special relationship between the two parameters L_n and h. The next section illustrates this further.

3.3.1 THE BASEBAND PROCESSOR

Since, for spectrally efficient full response binary CPFSK, rational values of the modulation index h range inside the

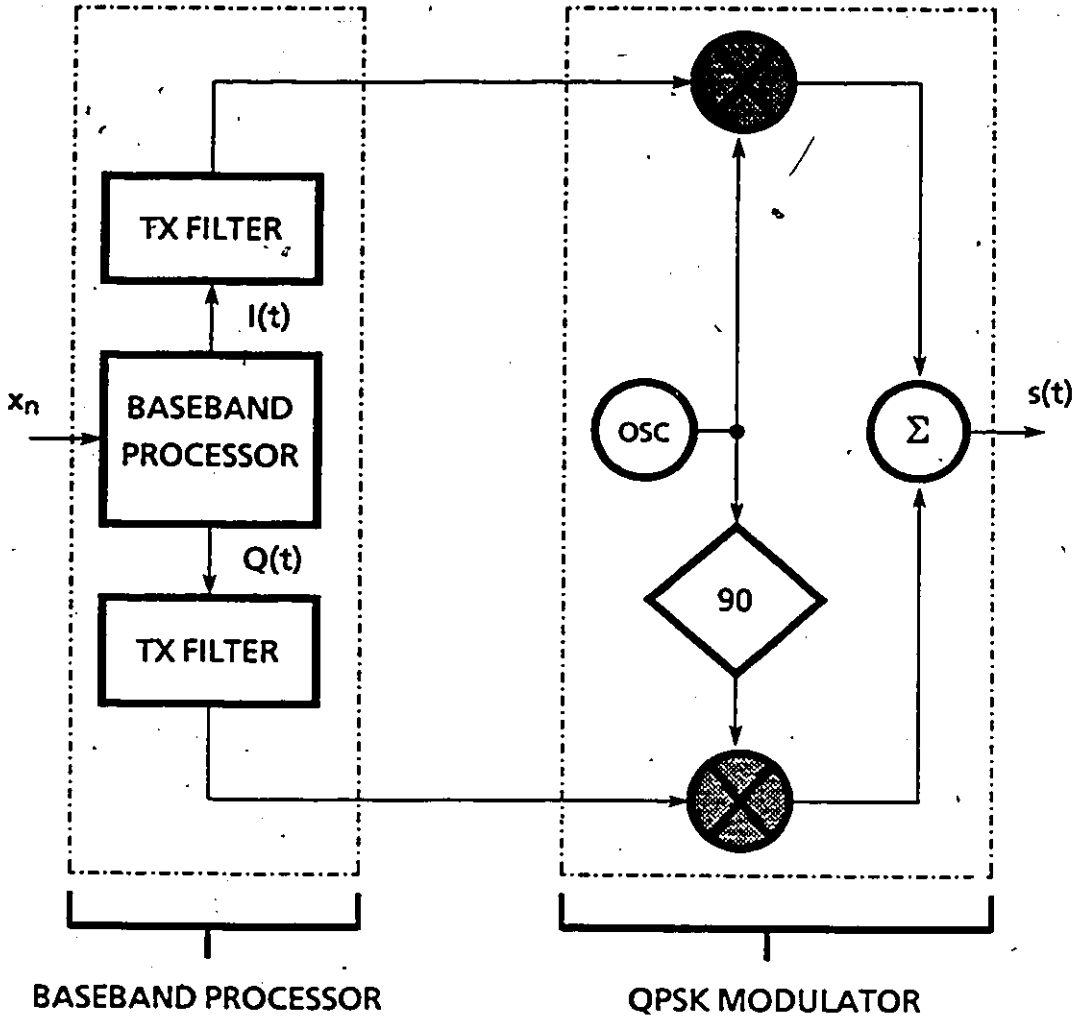

Figure 3.4 A practical CPFSK modulator

interval (0,1), a subset H of the rational number set Q, will be used to map selected values inside this interval. In other words, h will be considered to assume any value in the subset

$$H=\{h=a/b;\ a=1,2 \text{ and } b \in N^{+} \text{ and } a \leq b\} \tag{3.9}$$

where N^{+} represents the set of all positive integers. Note that since the numerator of h has one of two values (1 or 2), another degree of hardware complexity will be avoided.

From (3.5), it is clear that the time delay L_nT_h does not directly depend on the value of h. A further examination of (3.5, 3.7 & 3.8) yields 2(b-1)/b as the maximum value of the phase $L_n\pi h$ mod 2π, that is,

$$aL_n=0,2,.....,2(b-1) \bmod 2b \tag{3.10}$$

Consequently, only b different waveforms are to be generated by the baseband processor. Figure 3.5 shows the block diagram of the baseband processor. The incoming master clock is fed to a frequency generator; b distinct sinusoidal waveforms, all of

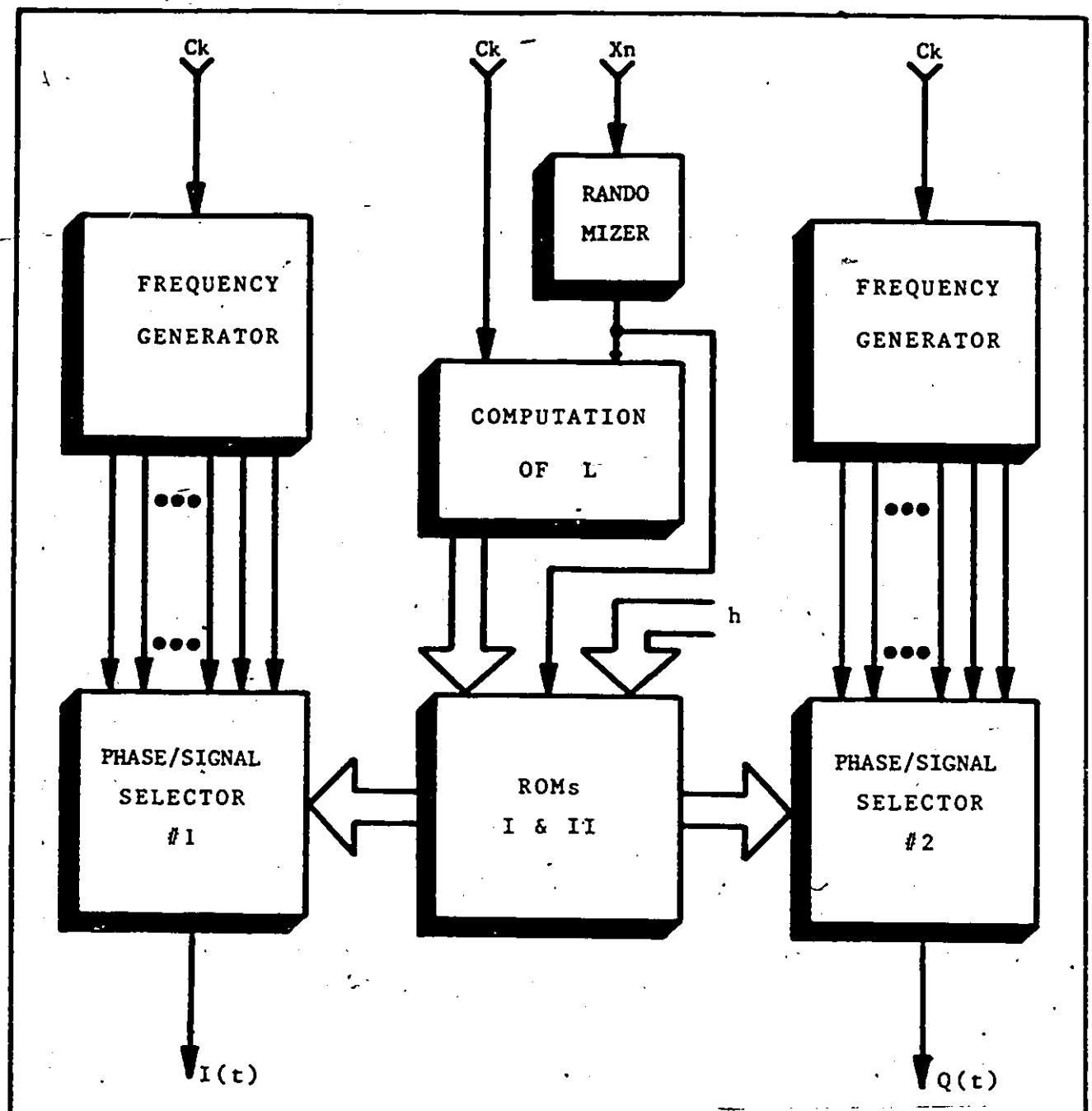

Figure 3.5 Block diagram of the baseband processor.

which have the frequency of f_d but are shifted apart by $2T_b$ sec, are generated for each channel. The generated waveforms are then phase-coded, using two phase selectors, to give the I and Q waveforms. The digital control signals, appearing at the input of each phase selector, indicate the phase of the appropriate waveform to be selected. The binary data is fed to a randomizer to ensure data spectral characteristics. The randomized data is then used to compute the delay factor L_n of (3.5). This delay factor is then combined with the frequency deviation ratio h to address the two ROMs shown in figure 3.5. The relationship that exists between the ROM output and its input, is the following:

FOR EACH NUMBER L_n PRESENT AT THE ROM INPUT, THE ROM OUTPUT IS L_n MOD 2b.

For the ROM that outputs the control signal of the Q channel's phase selector, the current bit x_n is joined to the input combination:

1. for positive x_n, the ROM output/input relationship is the same as above.

2. However, for negative x_n, this relationship becomes:

FOR EACH NUMBER L_n PRESENT AT THE ROM INPUT, THE ROM OUTPUT IS $(b+L_n)$ MOD 2b.

The block diagram of the frequency generator is shown in figure 3.6. The incoming master clock is fed to a divide-by-2/h counter (in the case where 2/h is not an integer, a PLL combined with a binary rate multiplier performs the division). Hence, the frequency of the divided clock is the peak frequency deviation of the CPFSK signal. During the division, the divided clock is digitally shifted b/2 times, resulting in b/2 periodic clocks shifted $2T_b$ sec apart. Narrow bandpass filters, centered at f_d, are used to extract the fundamental frequency of each periodic clock. Using analog inverters, the sinusoidal waveforms are then inverted. Consequently, b sinusoidal waveforms are available to input the phase selector of the I channel:

$$I_1(t) = \cos\{\frac{\pi}{bT_b}(t-0T_b)\}$$

$$I_2(t) = \cos\{\frac{\pi}{bT_b}(t-2T_b)\}$$

$$I_b(t) = \cos\{\frac{\pi}{bT_b}(t-2(b-1)T_b)$$

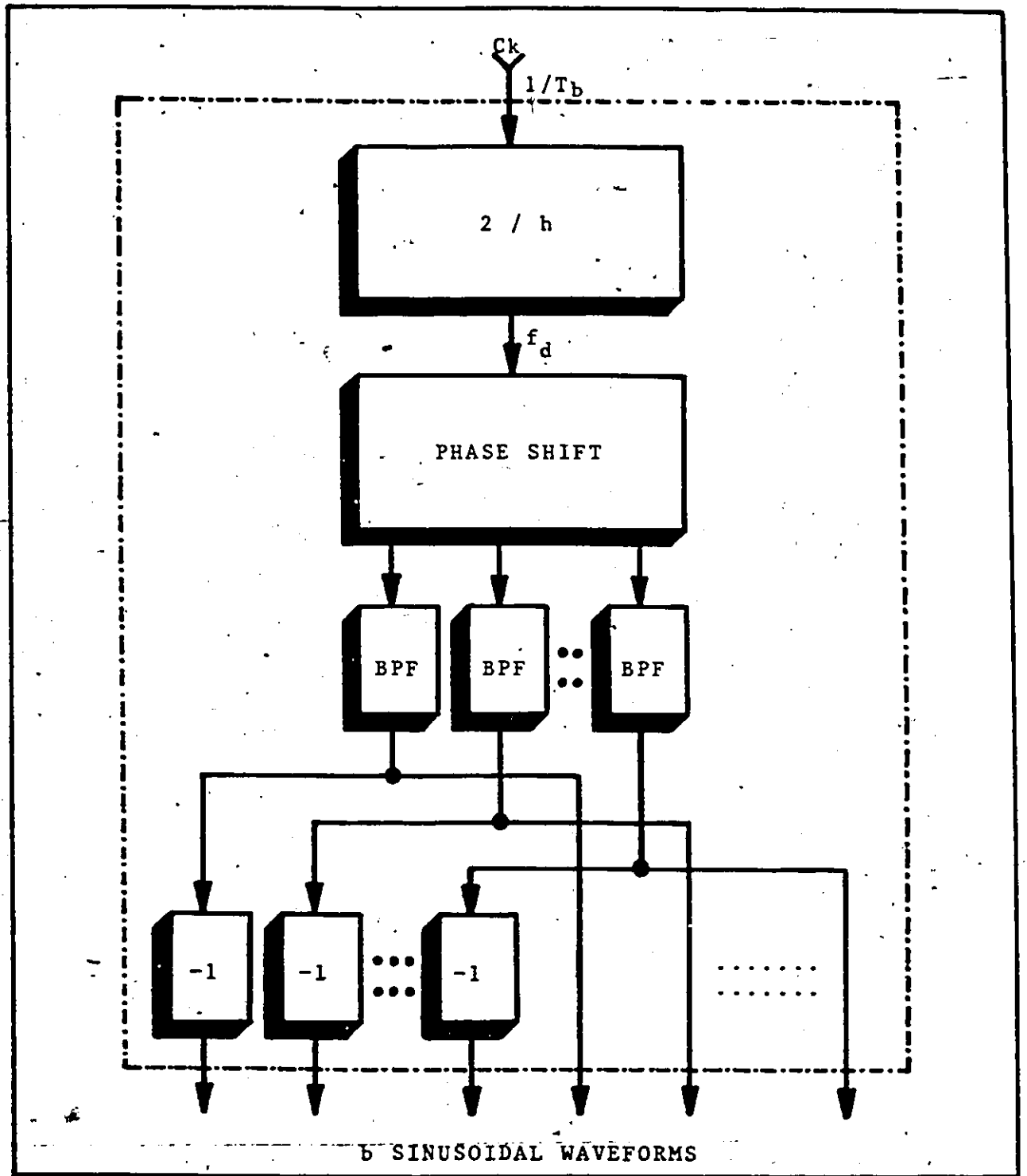

Figure 3.6, The frequency generator.

The phase selector input of the other channel is also made out of b sinusoidal waveforms, which in addition of being $2T_b$ sec shifted apart, they have the property that each of them is orthogonal to its I channel's waveform equivalent. In other words, the inputs are:

$$Q_1(t)=\sin\{\frac{\pi}{bT_b}(t-0T_b)\}$$

$$Q_2(t)=\sin\{\frac{\pi}{bT_b}(t-2T_b)\}$$

$$Q_b(t)=\sin\{\frac{\pi}{bT_b}(t-2(b-1)T_b)$$

The delay factor L_n is obtained by subtracting $x_n\sum x_k$ from the number n. This operation is done using two's complement technique, that is, n is added to the two's complement of $-x_n\sum x_k$, for positive x_n; or it is added to $-x_n\sum x_k$ itself, for negative x_n. A data selector, controlled by the binary input data stream, selects between $+\sum x_k$ and $-\sum x_k$ two's complement. The accumulation of bits up to time nT_b ($+\sum x_k$) and the two's complement of ($-\sum x_k$) are obtained by means of programmable up/down counters.

As shown in figure 3.7, the number "n" is easily obtained by counting up the master clock pulses. The output delay factor L_n is available in digital form.

3.3.2 HARDWARE IMPLEMENTATION

This section describes the binary CPFSK baseband processor's hardware implementation for two modulation indices, $h = 1/2$ and $h = 1/4$. In figure 3.8, the hardware block diagram is shown, and in figure 3.9, the detailed circuit diagram is presented. In the following subsections, each part of the baseband processor is described in the order outlined by the hardware block diagram in figure 3.8.

3.3.2.1 NRZ

The input binary data stream enters the circuit in the form of non-return-to-zero (NRZ) data, at a rate of 64 kb/sec. The NRZ code is a pulse transmission system wherein the pulse lasts for the duration of a signaling interval T_b.

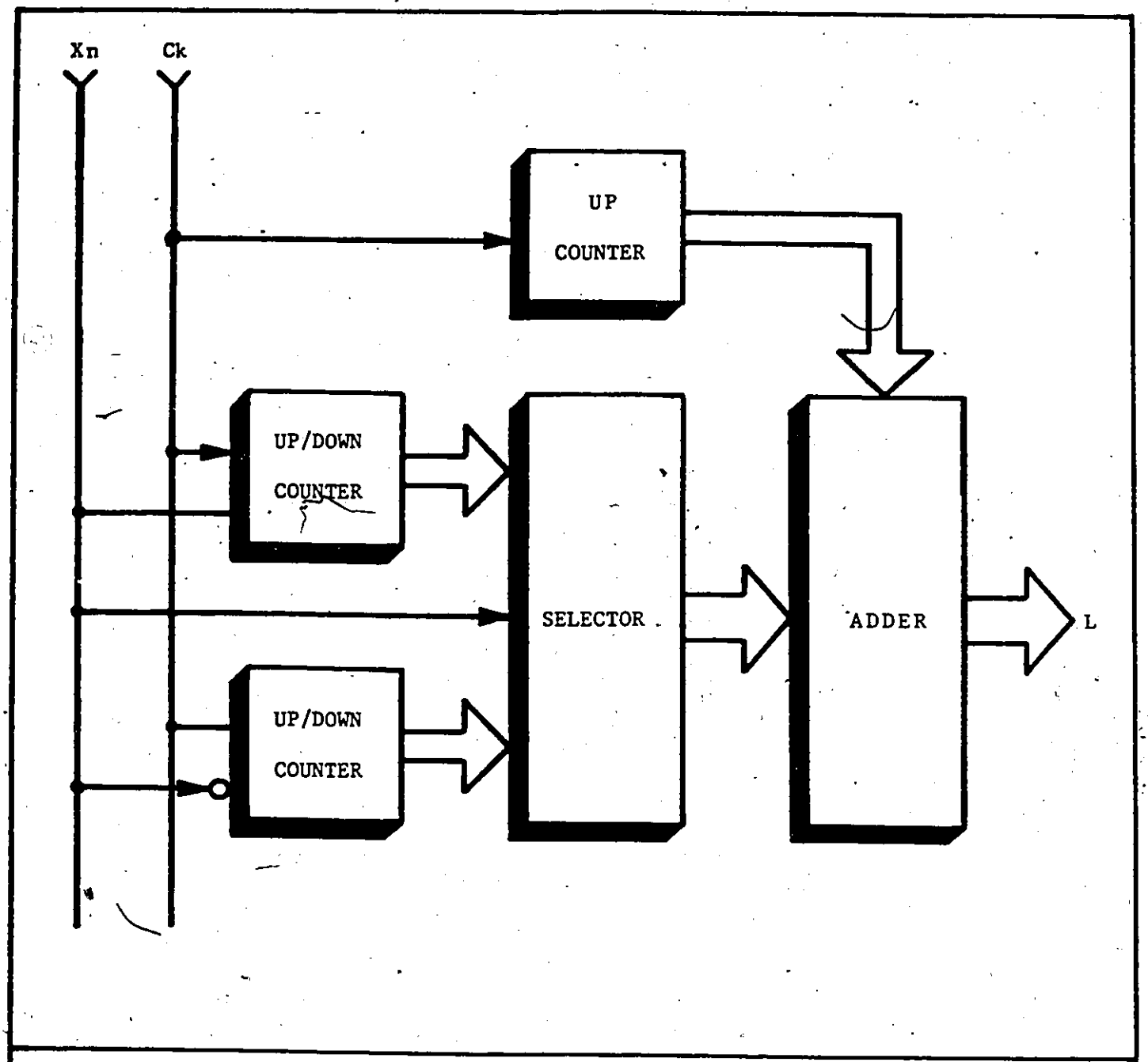

Figure 3.7 Computation of the delay factor L_n.

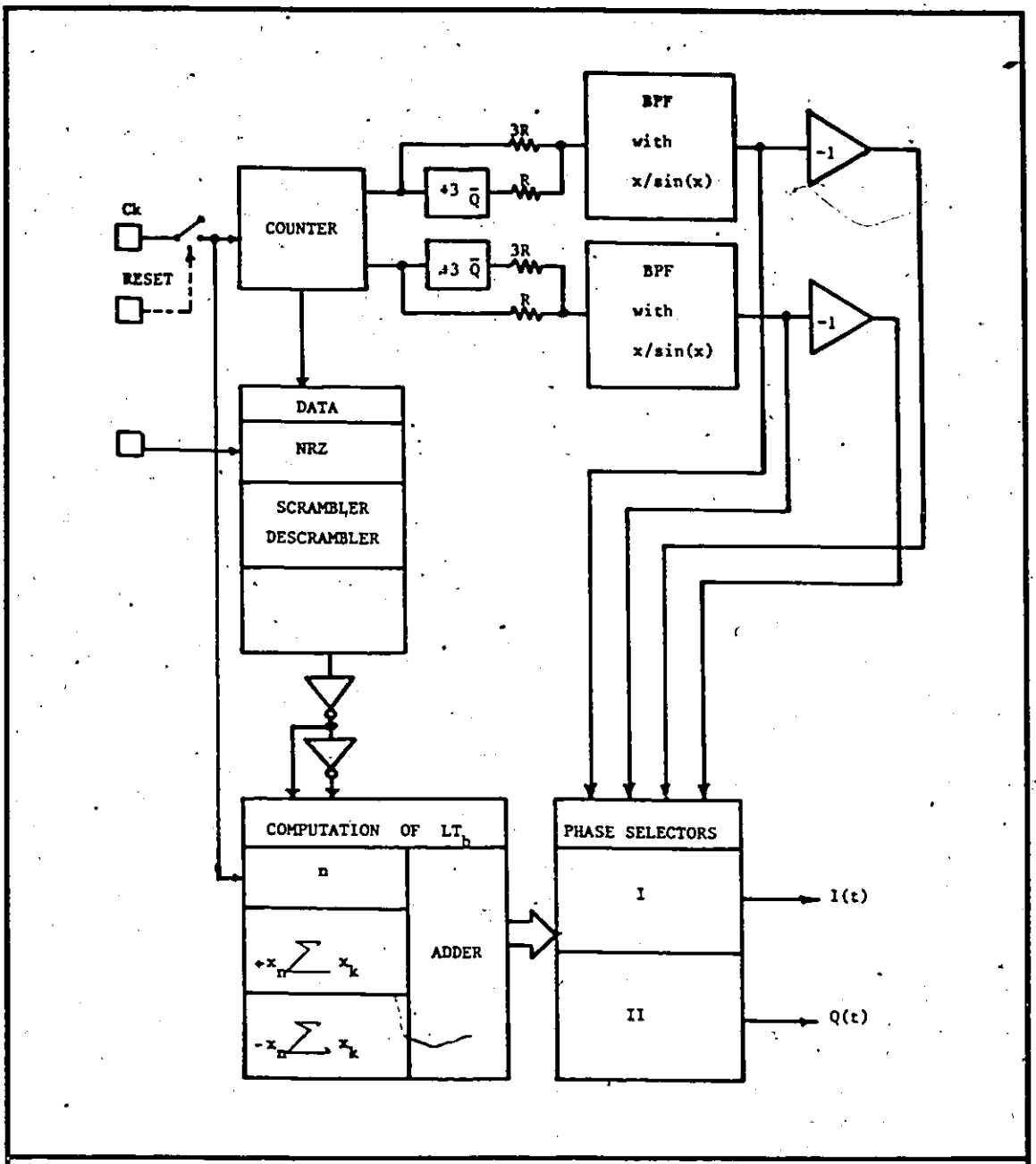

Figure 3.8, HARDWARE BLOCK DIAGRAM OF THE CPFSK MODULATOR

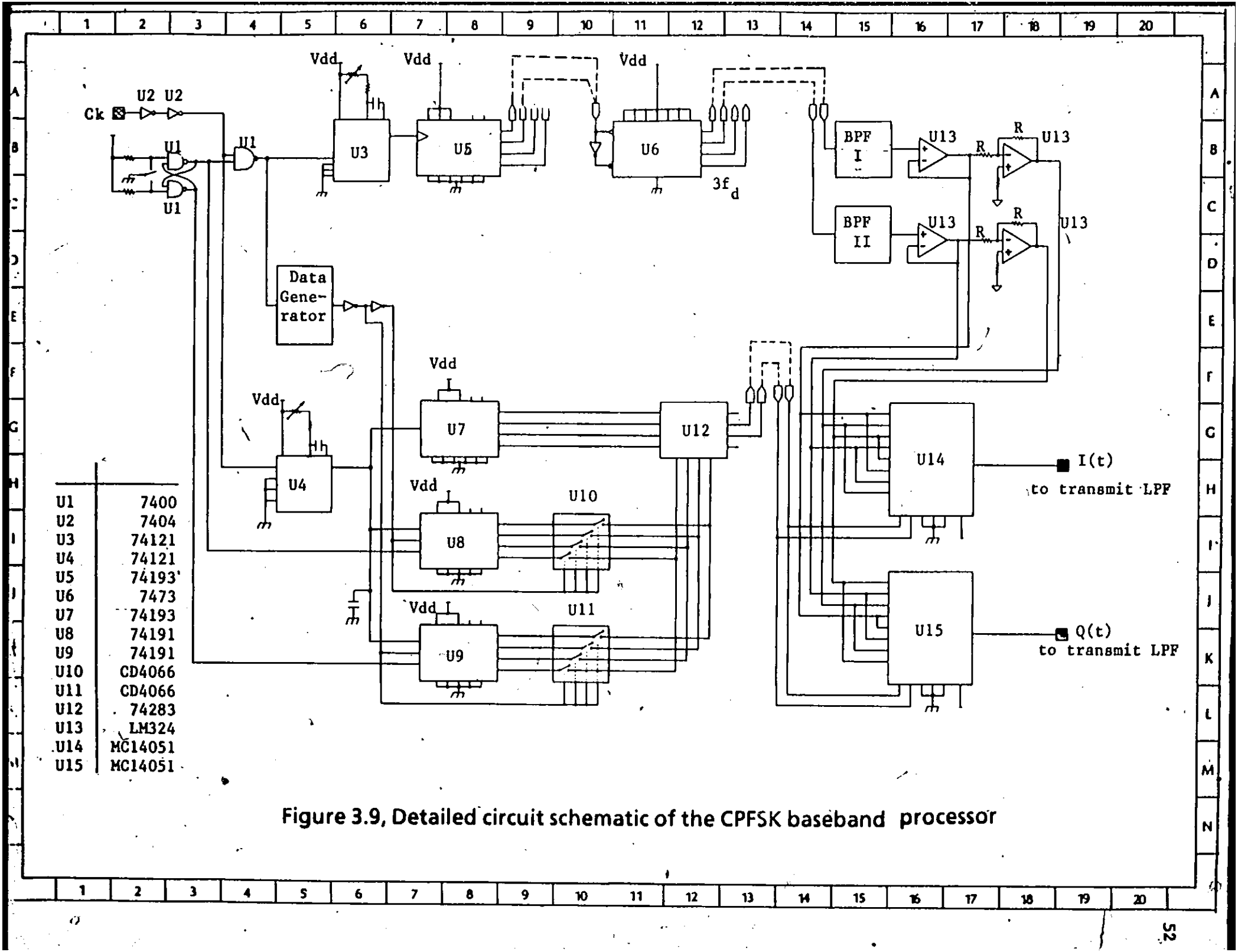

U1	7400
U2	7404
U3	74121
U4	74121
U5	74193
U6	7473
U7	74193
U8	74191
U9	74191
U10	CD4066
U11	CD4066
U12	74283
U13	LM324
U14	MC14051
U15	MC14051

Figure 3.9, Detailed circuit schematic of the CPFSK baseband processor

3.3.2.2 DATA SCRAMBLING/DESCRAMBLING

The fundamental purpose of the scrambler is to prevent the transmission of repetitive data patterns and to ensure spectral properties. Repetitive data patterns generate line spectra that can be significantly more degrading from an interference point of view than continuously distributed spectra produced by random data [49]. Moreover, digital radio systems are required by the FCC to not transmit line spectra. Even when not required, scramblers are useful in transforming data sequences with low transmit densities into sequences with strong timing components, thus facilitating symbol clock recovery.

The block diagram of data scrambler/descrambler is shown in figure 3.10. The binary data stream D_i is modulo-2 added in an EXCLUSIVE-OR gate to the R_i bit stream. This bit stream has been obtained from a predetermined combination of a finite length m-bit shift register and a set of coefficients $C_1 \ldots C_m$. These coefficients take on values of 0 and 1. The self-synchronizing descrambler has the same structure as the scrambler.

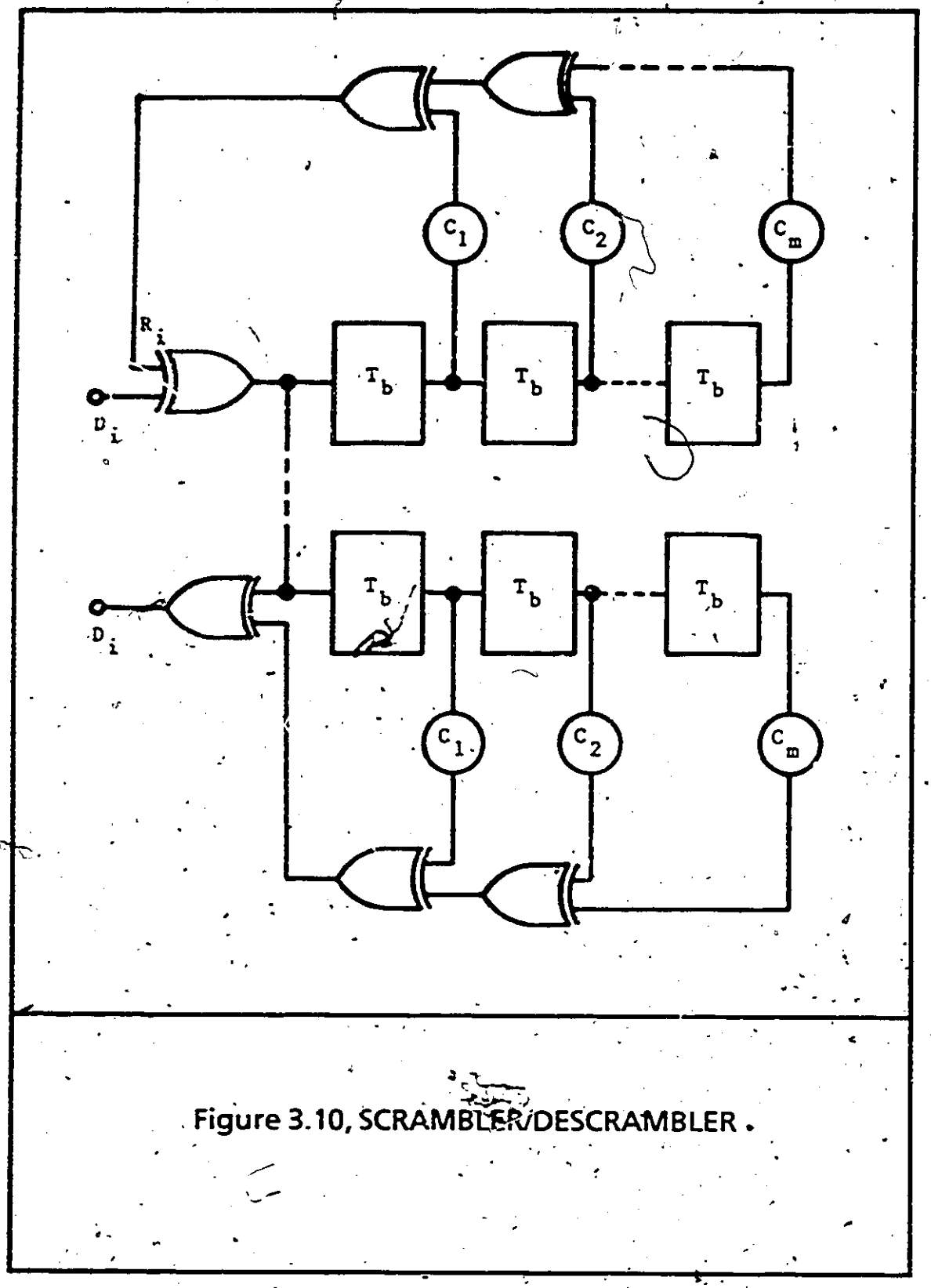

Figure 3.10, SCRAMBLER/DESCRAMBLER.

3.3.2.3 GENERATION OF SINUSOIDAL WAVEFORMS

This section presents the generation of the waveforms in (3.7) and (3.8). In figure 3.9, U1 resets the circuit; U2 provides the necessary inversion and/or buffering of signals. A monostable multivibrator, U3, provides the necessary time delay between the master clock and the randomized data. Using the 64 KHz clock pulse, U5 and U6 generate two square waves, at three times the peak frequency deviation ($3f_d$), and are shifted apart by $T_b/4$ sec. Filters I and II extract the fundamental frequency of the two square waves. The block diagram of the filter is shown in figure 3.11. As seen, the fundamental frequency is extracted by dividing the input frequency ($3f_d$) by three. The third harmonic ($3f_d$) is then removed using a two bit D/A converter. The resulting waveform is then input to a second order continuous filter with an x/sin(x) correction factor, where $x = f/6f_d$. The filter removes the harmonics at greater or equal to $5f_d$. The output signal is a sine wave at the desired frequency (f_d). U13 provides the buffering and inversion of both signals to generate the necessary 180 and 270 degrees shifted signals. U4 is a monostable multivibrator which is used to compensate the time delay introduced by filters I and II and therefore helps to align

the four synthesized signals and the data in a common zero phase at the bit switching times in order to maintain continuous phase at the output of the signal selector.

3.3.2.4 COMPUTATION OF L_n

U7-U12 generate the four bits representing the number L_n in (3.10). In the case of $h=1/4$ ($h=1/2$), two of those four bits, pins 1 and 13 (pin 13), will be used as two bits control signal to both channel multiplexers.

3.3.2.5 PHASE SELECTORS

For each consecutive T_b bit interval, one of these signals is switched to the transmission system. The required switching function is performed by two four channel analog multiplexers (MUXs) U14 and U15. The I and Q waveforms, available at the MUXs output (pin #3 of U1 and pin #3 of U15), are directed to the transmitter bandlimiting filters.

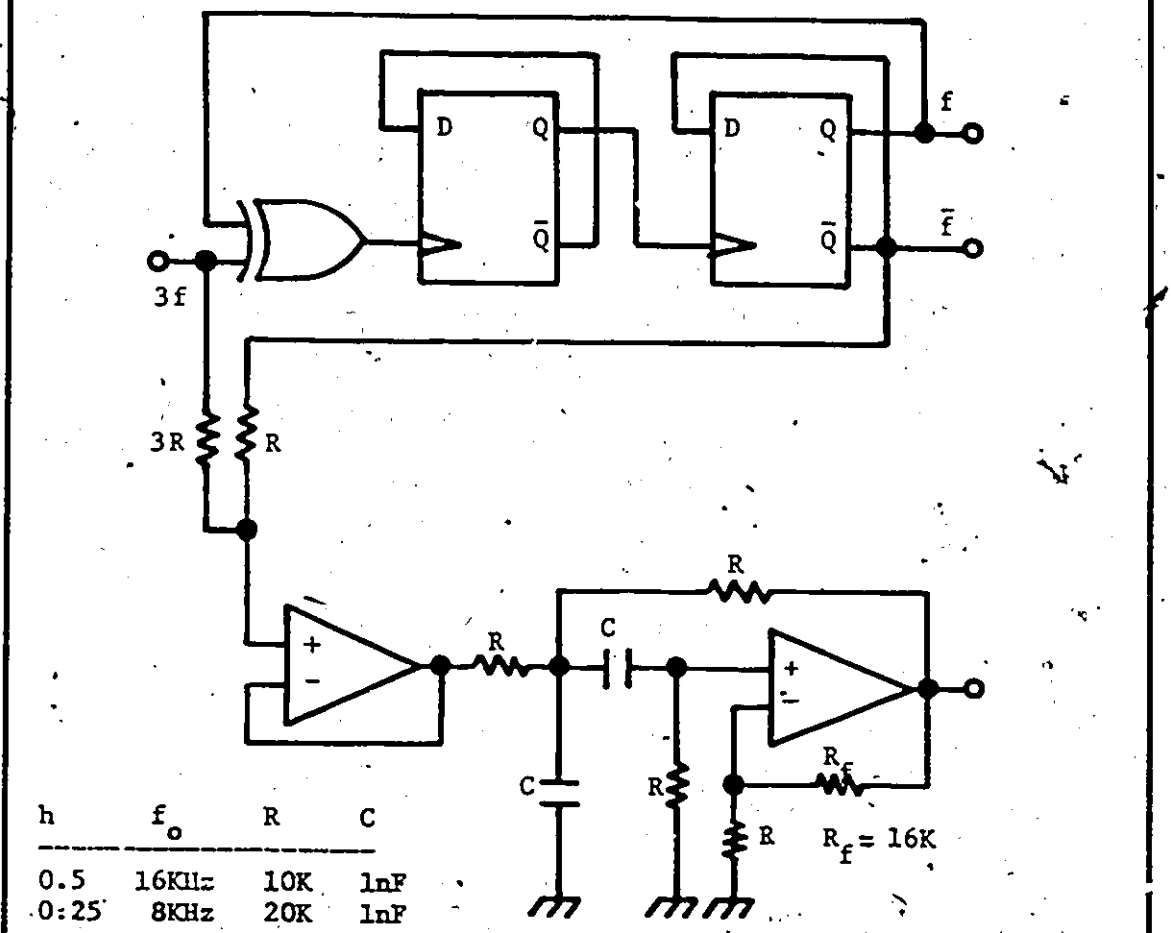

h	f_o	R	C
0.5	16KHz	10K	1nF
0:25	8KHz	20K	1nF

Figure 3.11, Filter used in the generation of the sinusoidal waveforms

3.3.2.6 TRANSMIT FILTER

To filter the sinusoidally shaped baseband CPFSK (I(t) and Q(t)), two phase-equalized fourth-order Butterworth low-pass filters, having a 3 dB cut off frequency of $0.55f_b$ for $h=1/2$ ($0.3f_b$ for $h=1/4$), are used. The filters approximate the $\alpha=0.5$ raised-cosine channel (50% excess bandwidth). The amplitude characteristics of the 0.5 raised-cosine channel for sinusoidally shaped pulse transmission is shown on a linear scale in figure 3.12. The schematic diagram of the fourth-order LPF is shown in figure 3.13.

3.3.2.7 EXPERIMENTAL RESULTS

Figures 3.14 and 3.15 show the measured I and Q channel eye patterns of the CPFSK for $h=1/2$ and $h=1/4$ respectively, in a linear channel environment. Note that the $h=1/2$ CPFSK (MSK) eye diagram is intersymbol interference and jitter free. Figures 3.16 and 3.17 show the baseband I and Q channel CPFSK signal ($h=1/2$ and 1/4) for several digital input patterns. The CPFSK signal space diagram for both cases, shown in figure

3.18, shows the constant envelope property of the CPFSK signal.

3.3.3 ADVANTAGES OF THE TX IMPLEMENTATION

The transmitter implementation advantages for binary CPFSK with $h = 1/b$, can be summarized as follows:

1) digital circuits employed.
2) many values of h can be implemented.
3) less sensitivity to deviations.
4) switching between two oscillators is avoided.
5) no VCO is used.
6) simpler method that avoids circuit complexity (more systematic approach).

3.4 SUMMARY

A new method of generating constant envelope, binary CPFSK signals has been introduced. The CPFSK signal is generated by balanced amplitude modulation of two carriers in quadrature.

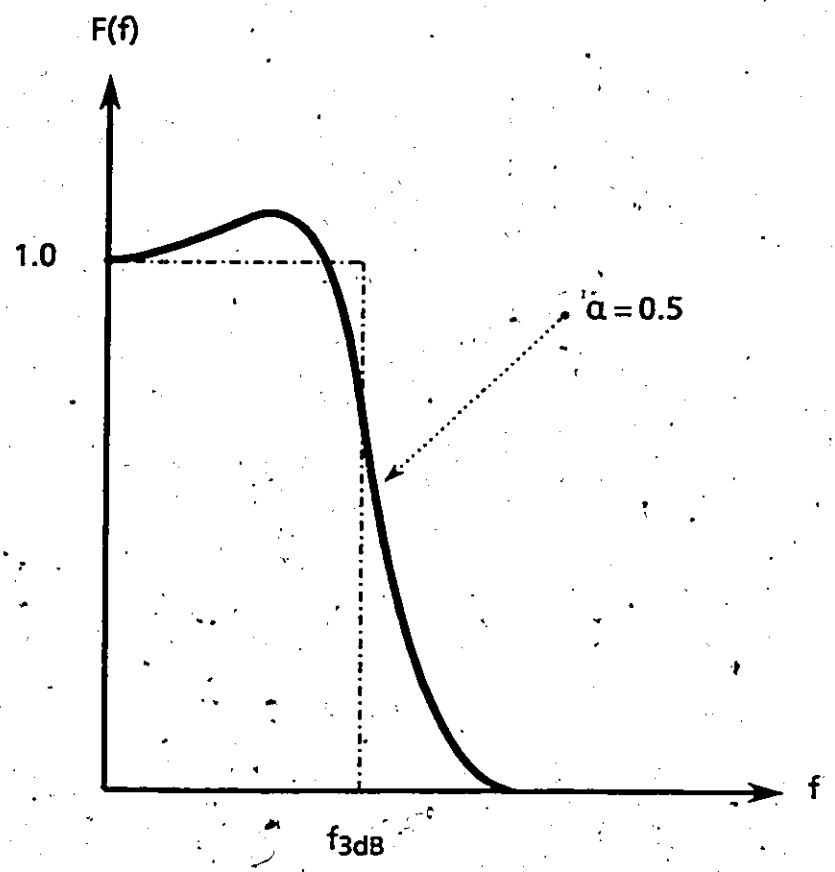

Figure 3.12, Transfer function of the baseband transmit low-pass filter on a linear scale.

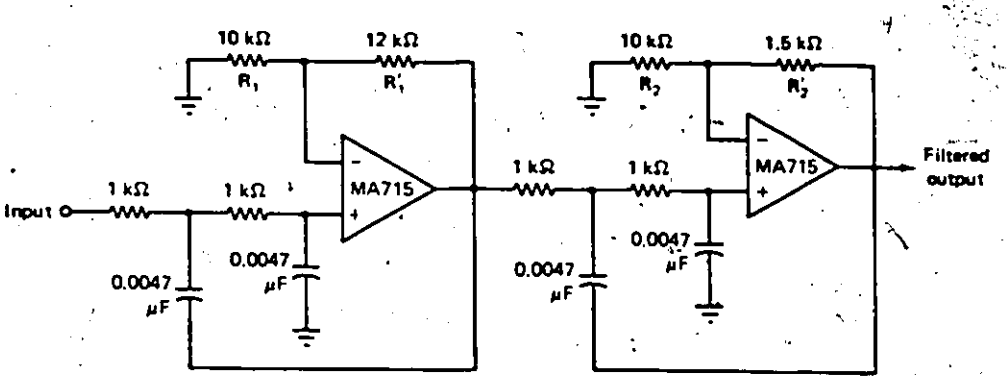

Figure 3.13, Circuit schematic of the fourth order Butterworth low-pass transmit filter. ($\alpha = 0.5$ channel)

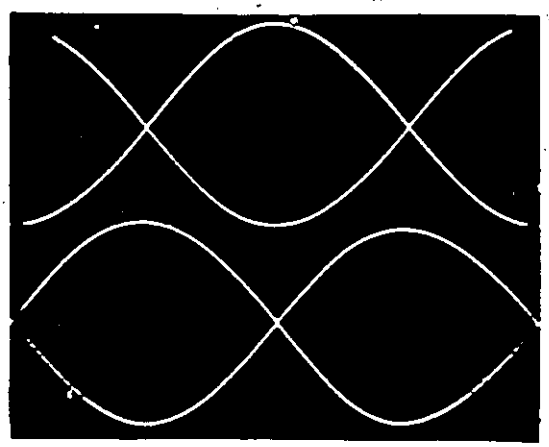

Figure 3.14, Measured eye pattern of the CPFSK signal with

$h = 1/2$ (MSK)

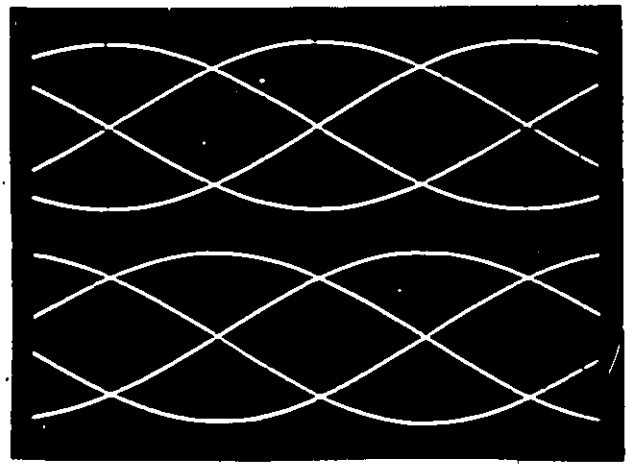

Figure 3.15, Measured eye pattern of the CPFSK signal with h = 1/4.

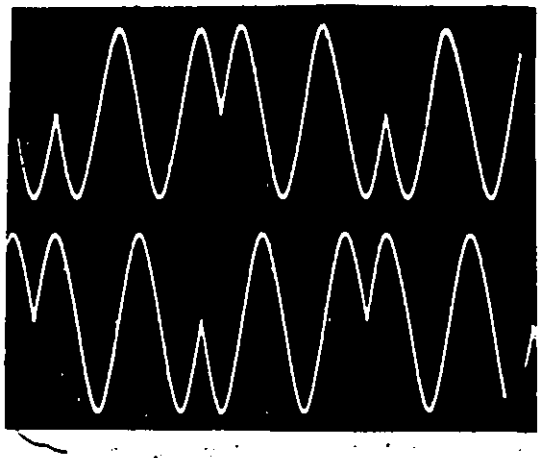

a) digital input pattern: 7 one, 1 zero

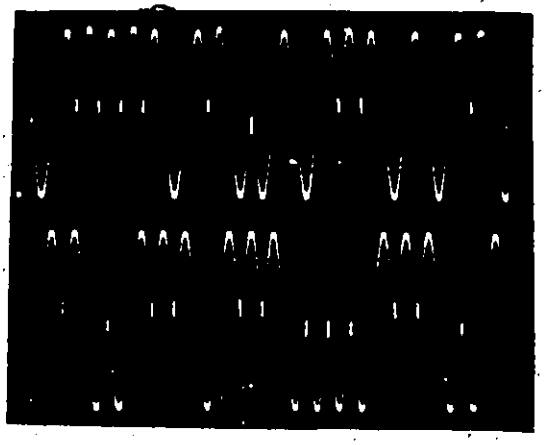

b) digital input pattern: 6 one, 3 zero

Figure 3.16, Measured I and Q channels of the CPFSK signal for h = 1/2. (MSK)

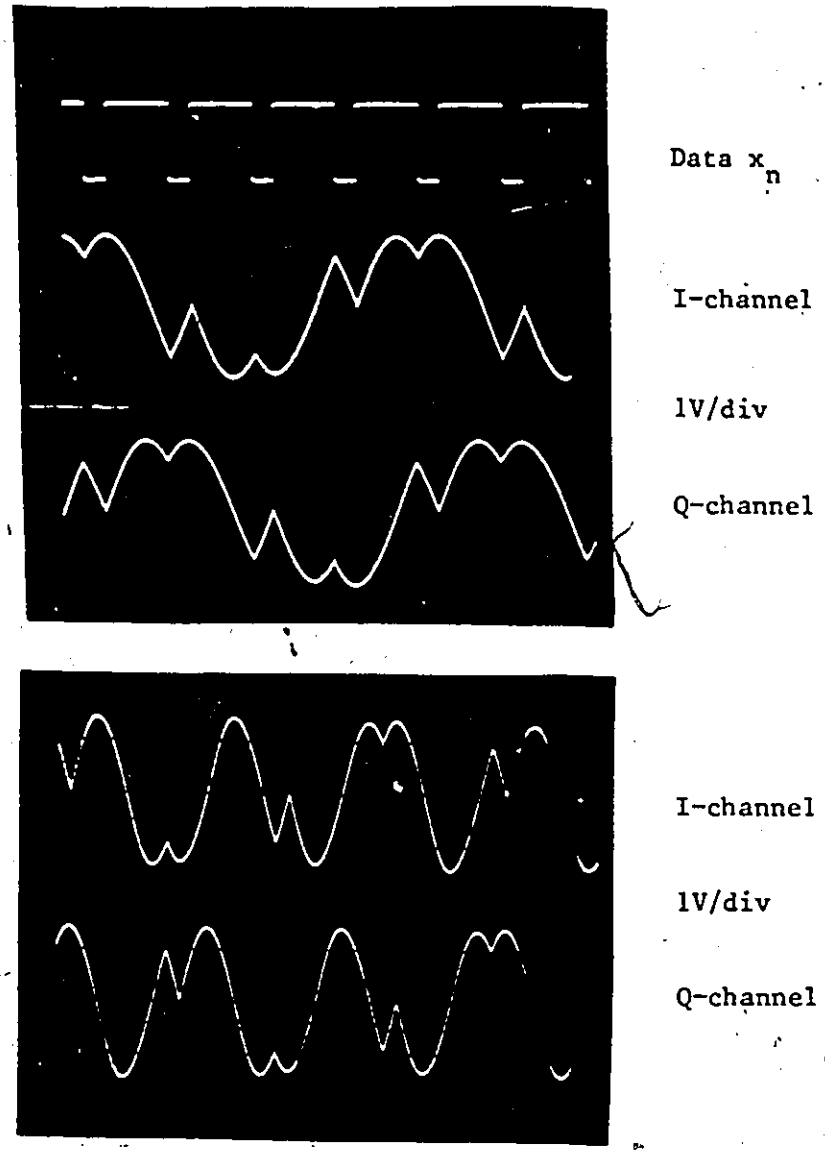

Figure 3.17, Measured I and Q components of the CPFSK signal for h = 1/4.

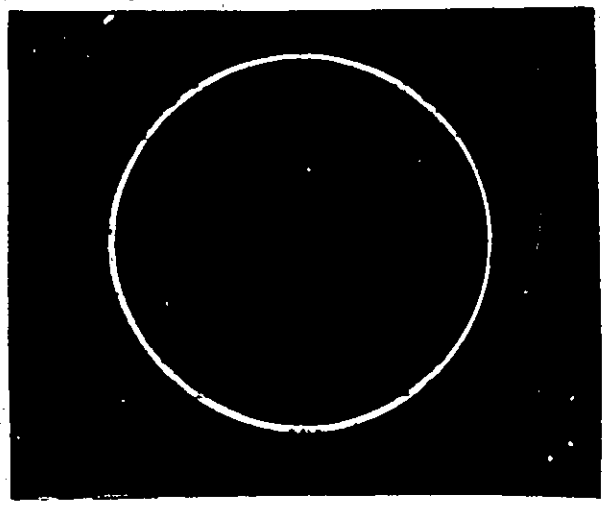

Figure 3.18, Measured CPFSK signal space diagram.

The I waveform modulates $\cos(\omega_c t)$ and the Q waveform modulates $\sin(\omega_c t)$. The baseband processor has been implemented for two values of h, and experimental results have shown that theory and practice are in full agreement. The resultant CPFSK signal is shown experimentally to have constant envelope and to be free of amplitude variations. Moreover, the I and Q waveforms are shown to have good eye-diagrams.

CHAPTER FOUR

SPECTRAL ANALYSIS OF CPFSK SIGNALS

4.1 INTRODUCTION

An important parameter in the statistical description of a signal is its power spectral density. For spectrum conservation, the band occupancy of the chosen modulation scheme must be small so that as many channels as possible can be accommodated in a given band. Therefore, the knowledge of the power spectral density provides an estimation of bandwidth requirements, and is essential in the evaluation of mutual interference between channels. In this chapter, we present the power spectrum of a sinusoidal carrier, frequency modulated by a random baseband binary pulse train in which the signaling pulse duration is finite and the binary signal pulses do not overlap. For the spectrum calculations, the Markov process representation of the CPFSK signal, is developed and used to compute the autocorrelation function and power spectrum.

4.2 MARKOV PROCESS ANALYSIS

This section develops a general procedure for calculating power spectra of CPFSK signals, and presents results for several examples of interest. The procedure can accommodate any modulation index belonging to the subset H. As will be seen, the approach is a rather straightforward extension of [22,38]. The CPFSK signal was given earlier by (3.6), in which I(t) and Q(t) were given by (3.7) and (3.8) respectively. Since the modulated signal is a narrowband (IF or RF) signal, it is more convenient to describe it by its low-pass equivalent notation, also called preenvelope, r(t); i.e., the actual signal is represented by [41]

$$s(t) = \mathrm{Re}\{r(t)\exp(-j\omega_c t)\} \text{ and,} \tag{4.1}$$

$$r(t) = I(t) + jQ(t) \tag{4.2}$$

By definition, the CPFSK signal has continuous phase. As a result, when every T_b seconds, the signal or its preenvelope changes from one state to another, only the phase trajectory of the current symbol is needed in deciding the initial value of the

phase, of the waveform, in the next T_b seconds. Other values of the phase at previous transition instants are not really valuable in that decision. It follows that the CPFSK signal or its preenvelope can be modeled by a Markov chain model describing the envelope as a sequence of waveforms governed by Markovian probabilistic laws. The preenvelope r(t) is therefore the superposition of these waveforms and thus may be written as,

$$r(t) = \sum r_i(t - mT_b) \qquad (4.3)$$

wherein a random N-ary source emits $r_i(t)$, every bit interval of duration T_b, from the set $\{r_i(t); i = 1,2,.....,N\}$ with probability p_i; in which $r_i(t)$ is represented by

$$r_i(t) = I_i(t) + jQ_i(t) \qquad (4.4)$$

where,

$$I_i(t) = \cos\{\frac{\pi h}{T_b}(t - (N/2 - (i-1))T_b)\} \quad \text{for } i = 1,2,....N \qquad (4.4.a)$$

and,

$$Q_i(t) = \begin{cases} \sin\{\frac{\pi h}{T_b}(t - (N/2 - (i-1))T_b)\} & \text{for } i = 1,2,....N/2 \\ \\ -\sin\{\frac{\pi h}{T_b}(t - (N/2 - (i-1))T_b)\} & \text{for } i - N/2 = 1,2,....N/2 \end{cases} \quad (4.4.b)$$

respectively represent the real and imaginary parts of the CPFSK low-pass equivalent state waveforms. Replacing h by a/b in (4.4.b) yields,

$$r_i(t) = \begin{cases} \exp(j\eta_i) & \text{for } i = 1,2,....N/2 \\ \\ \exp(-j\eta_i) & \text{for } i - N/2 = 1,2,....N/2 \end{cases} \quad (4.5)$$

where,

$$\eta_i = \frac{\pi a}{bT_b}(t - (N/2 - (i-1))T_b) \quad (4.6)$$

Since the source is Markov, the sequence of waveforms generated is characterized by the set of initial probabilities $\{p_i; i=1,2,.....,N\}$, and the set of transition probabilities $\{p_{ik}; i,k=1,2,.....,N\}$, where p_{ik} is the probability of the transition from state i to state k at the transition instant given that the process is currently in state i. These transition probabilities are arranged in the transition probability matrix $P=\|p_{ik}\|$. The procees remains in a given state i, for T_b seconds; the corresponding waveform is generated, the chain then makes a transition to some state k according to the next data value. The state transition diagram, the waveforms associated with each state, and the transition probability matrix of the process of interest, are shown along with appropriate examples in figures 4.1 to 4.6. The Markov process representation described above can be used to compute the autocorrelation function of the CPFSK signal, where the autocorrelation function is defined as

$$R(t,t+\tau)=E[r(t)r^*(t+\tau)] \tag{4.7}$$

The power spectral density $G_r(f)$ is the Fourier Transform of $R(t,\tau)$, and is given by [10]

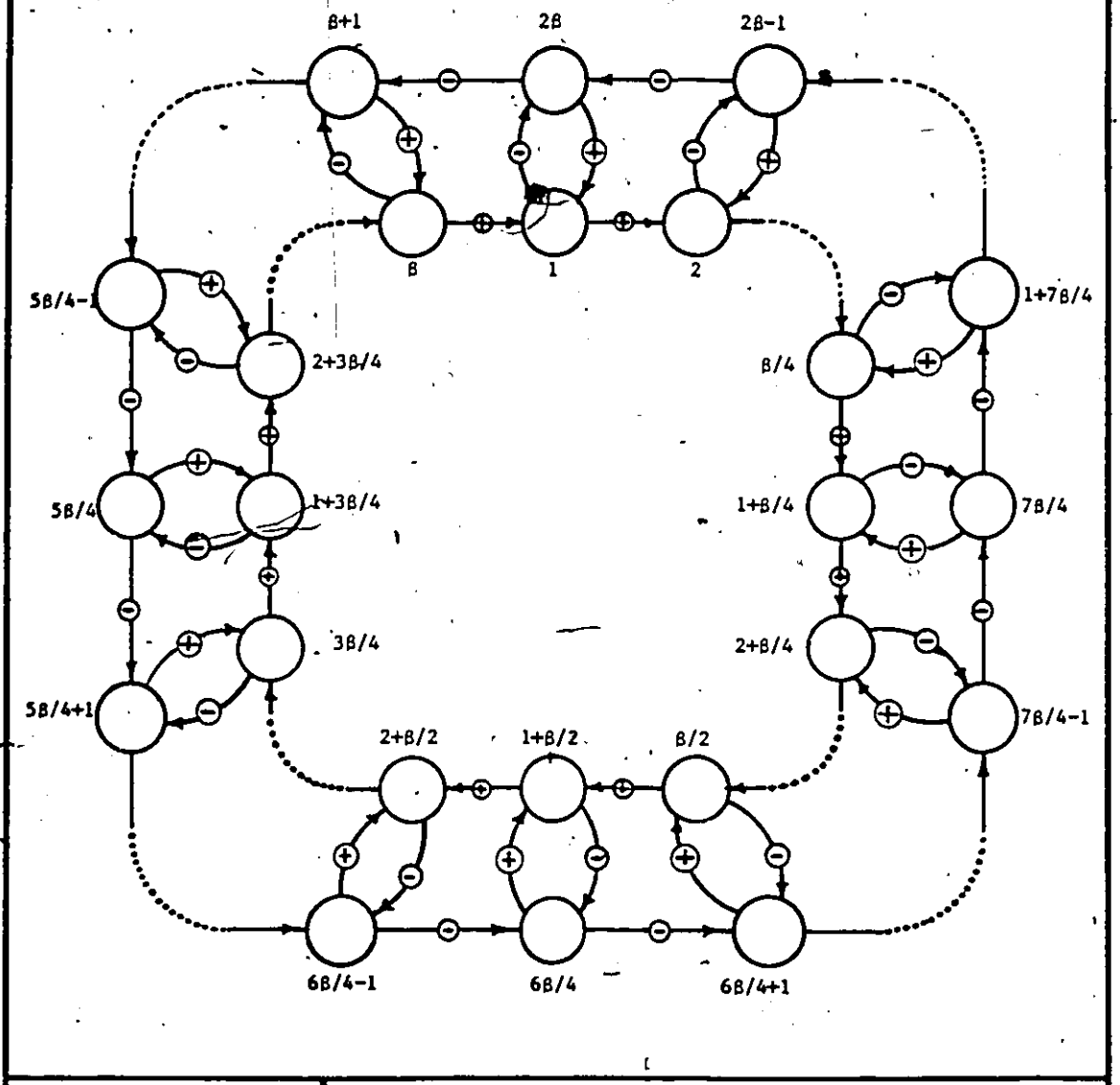

Figure 4.1, Markov process state transition diagram of CPFSK,

$\beta = b$ for a = 2 or a&b even

$\beta = 2b$ otherwise

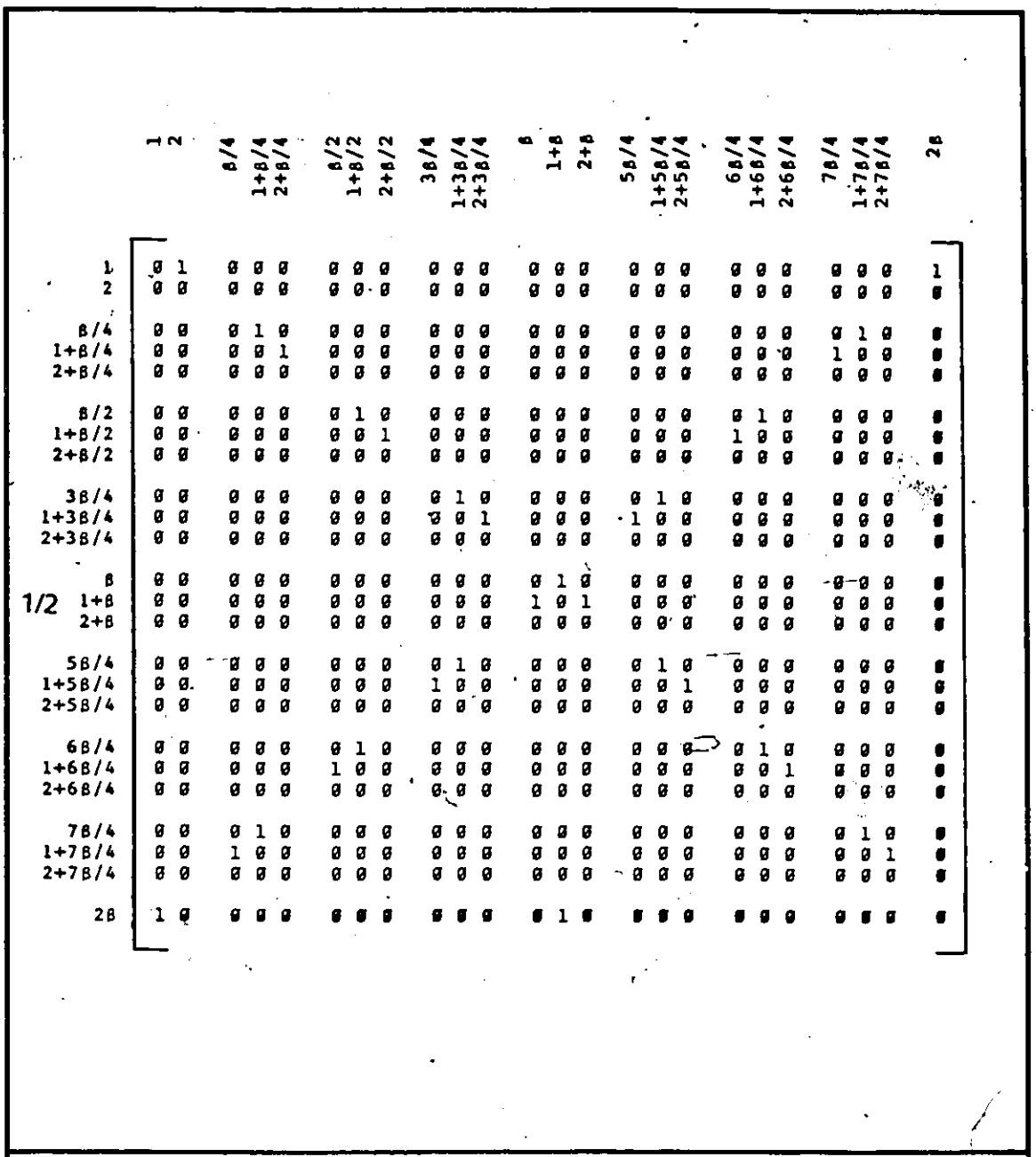

Figure 4.2, Transition probability matrix P corresponding to the transition diagram of CPFSK signals of figure 4.1. (h = a/b)

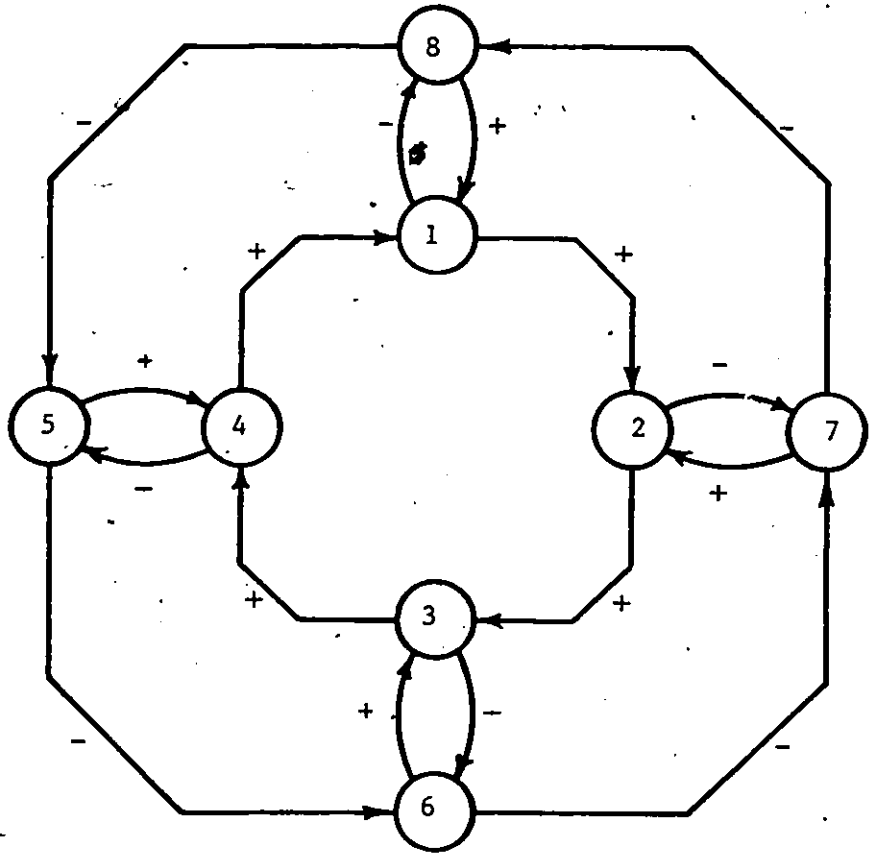

Figure 4.3.a, Markov state transition diagram of CPFSK with h = 1/2. (MSK)

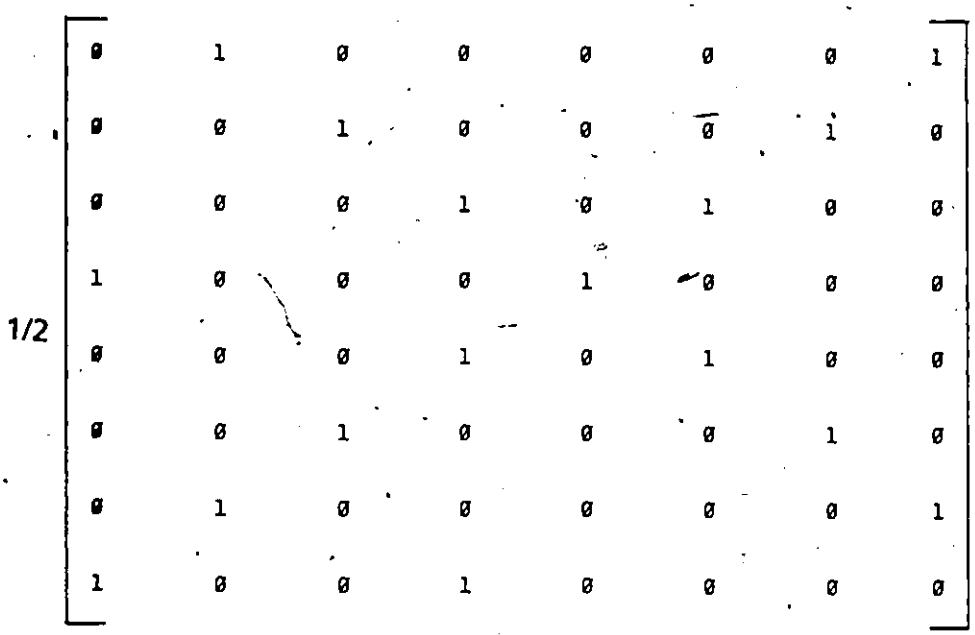

Figure 4.3.b, Transition probability matrix corresponding to the transition diagram of CPFSK signals with h = 1/2.

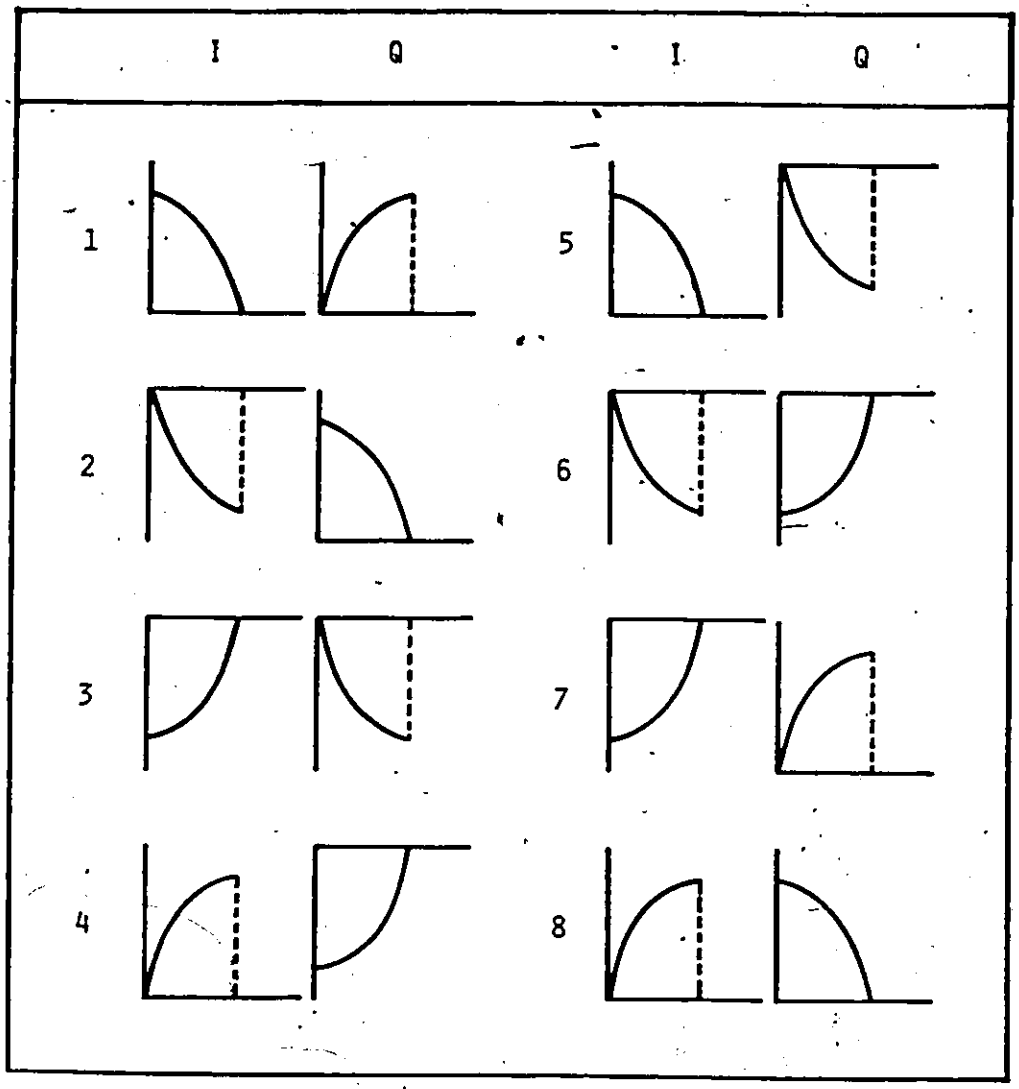

Figure 4.3.c, CPFSK low pass equivalent state waveforms for

h = 1/2. (MSK)

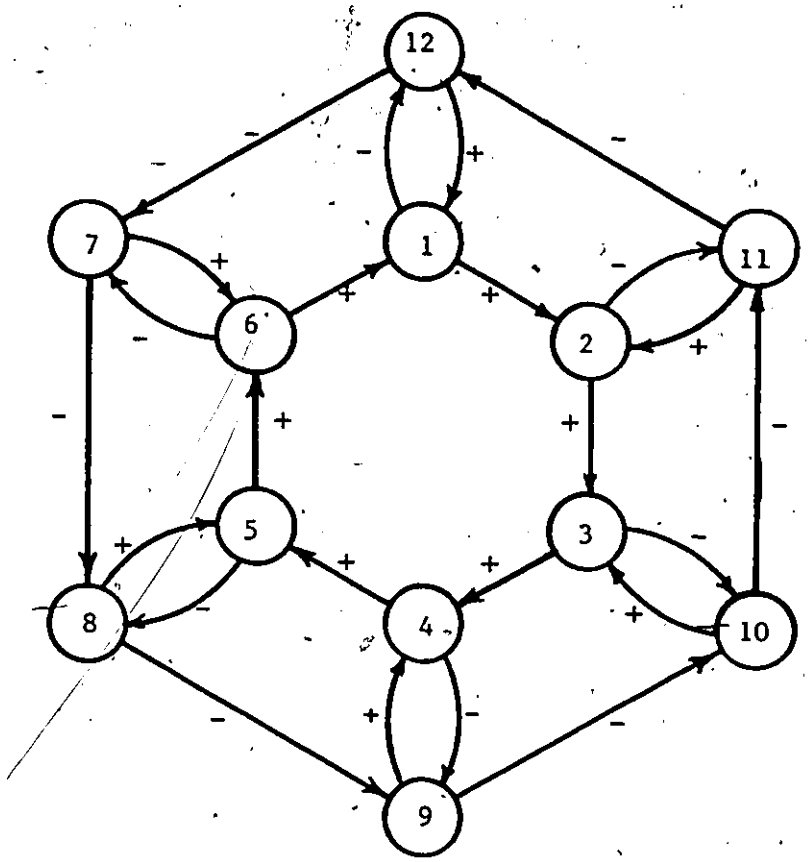

Figure 4.4.a, Markov process state transition diagram of CPFSK with h = 1/3.

1/2

$$\begin{bmatrix}
0 & 1 & 0 & 0 & 0 & 0 & 0 & 0 & 0 & 0 & 0 & 1 \\
0 & 0 & 1 & 0 & 0 & 0 & 0 & 0 & 0 & 0 & 1 & 0 \\
0 & 0 & 0 & 1 & 0 & 0 & 0 & 0 & 0 & 1 & 0 & 0 \\
0 & 0 & 0 & 0 & 1 & 0 & 0 & 0 & 1 & 0 & 0 & 0 \\
0 & 0 & 0 & 0 & 0 & 1 & 0 & 1 & 0 & 0 & 0 & 0 \\
0 & 0 & 0 & 0 & 0 & 0 & 1 & 0 & 0 & 0 & 0 & 0 \\
0 & 0 & 0 & 0 & 0 & 1 & 0 & 1 & 0 & 0 & 0 & 0 \\
0 & 0 & 0 & 0 & 1 & 0 & 0 & 0 & 1 & 0 & 0 & 0 \\
0 & 0 & 0 & 1 & 0 & 0 & 0 & 0 & 0 & 1 & 0 & 0 \\
0 & 0 & 1 & 0 & 0 & 0 & 0 & 0 & 0 & 0 & 1 & 0 \\
0 & 1 & 0 & 0 & 0 & 0 & 0 & 0 & 0 & 0 & 0 & 1 \\
1 & 0 & 0 & 0 & 0 & 0 & 1 & 0 & 0 & 0 & 0 & 0
\end{bmatrix}$$

Figure 4.4.b, Transition probability matrix corresponding to the transition diagram of h = 1/3 CPFSK signal.

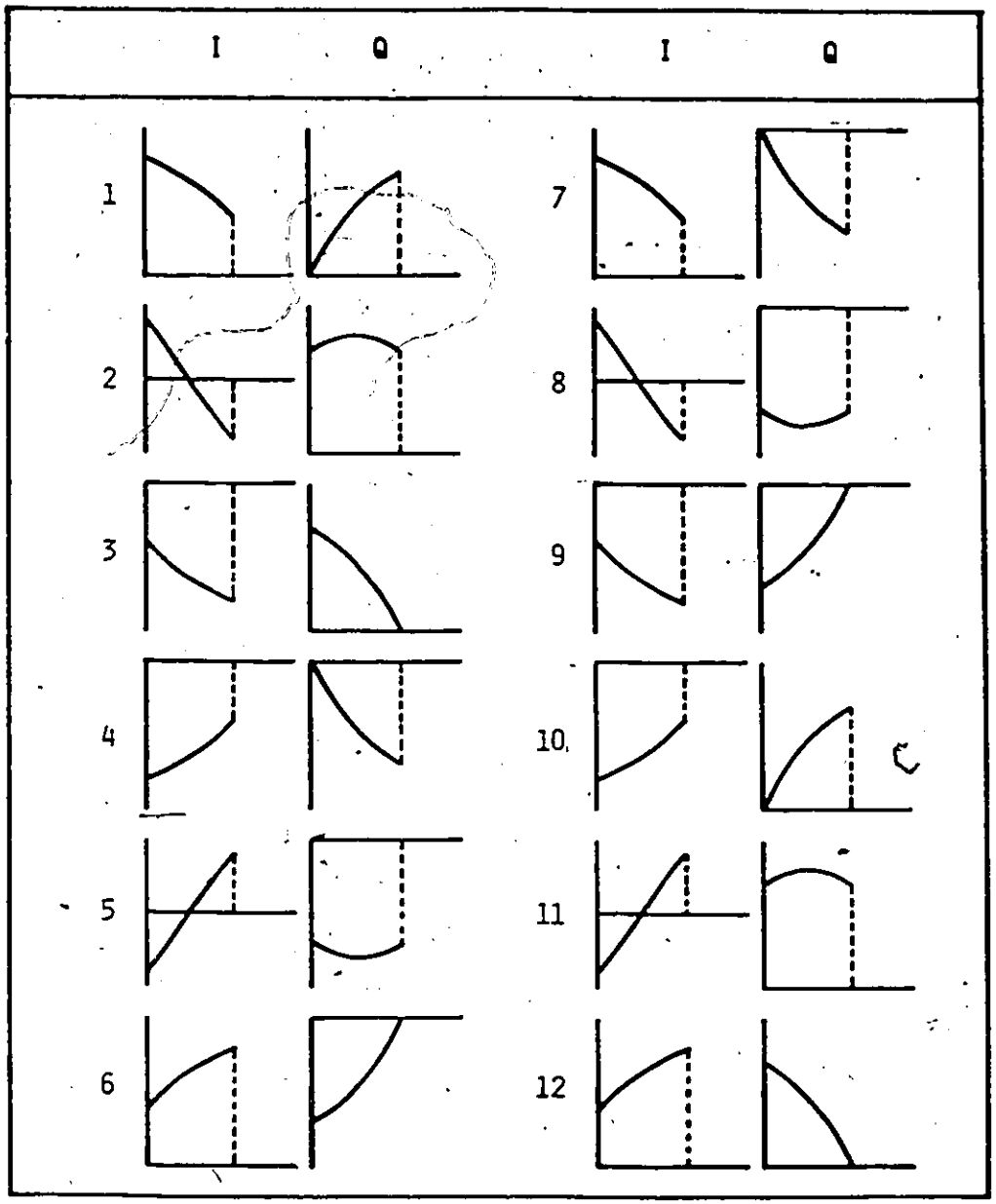

Figure 4.4.c, CPFSK low pass equivalent state waveforms for $h = 1/3$. ($\beta = 6$)

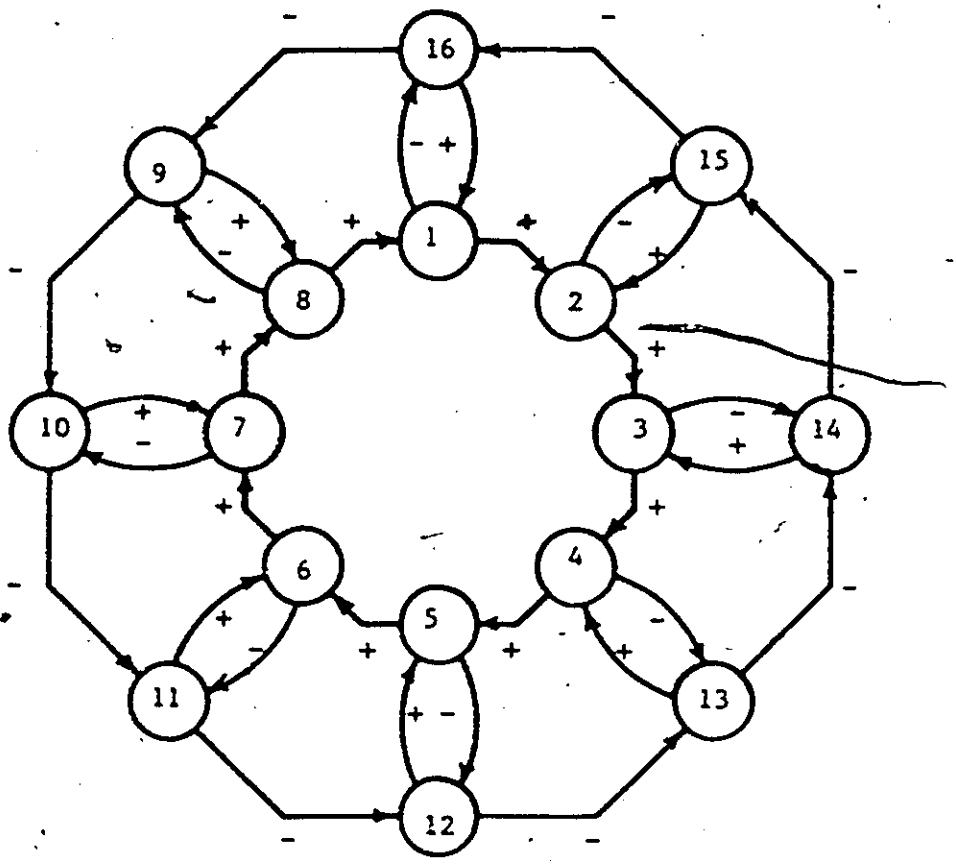

Figure 4.5.a, Markov process state transition diagram of h = 1/4 CPFSK signal.

1/2

$$\begin{bmatrix}
0 & 1 & 0 & 0 & 0 & 0 & 0 & 0 & 0 & 0 & 0 & 0 & 0 & 0 & 0 & 1 \\
0 & 0 & 1 & 0 & 0 & 0 & 0 & 0 & 0 & 0 & 0 & 0 & 0 & 0 & 1 & 0 \\
0 & 0 & 0 & 1 & 0 & 0 & 0 & 0 & 0 & 0 & 0 & 0 & 0 & 1 & 0 & 0 \\
0 & 0 & 0 & 0 & 1 & 0 & 0 & 0 & 0 & 0 & 0 & 0 & 1 & 0 & 0 & 0 \\
0 & 0 & 0 & 0 & 0 & 1 & 0 & 0 & 0 & 0 & 0 & 1 & 0 & 0 & 0 & 0 \\
0 & 0 & 0 & 0 & 0 & 0 & 1 & 0 & 0 & 0 & 1 & 0 & 0 & 0 & 0 & 0 \\
0 & 0 & 0 & 0 & 0 & 0 & 0 & 1 & 0 & 1 & 0 & 0 & 0 & 0 & 0 & 0 \\
0 & 0 & 0 & 0 & 0 & 0 & 0 & 0 & 1 & 0 & 0 & 0 & 0 & 0 & 0 & 0 \\
0 & 0 & 0 & 0 & 0 & 0 & 0 & 1 & 0 & 1 & 0 & 0 & 0 & 0 & 0 & 0 \\
0 & 0 & 0 & 0 & 0 & 0 & 1 & 0 & 0 & 0 & 1 & 0 & 0 & 0 & 0 & 0 \\
0 & 0 & 0 & 0 & 0 & 1 & 0 & 0 & 0 & 0 & 0 & 1 & 0 & 0 & 0 & 0 \\
0 & 0 & 0 & 0 & 1 & 0 & 0 & 0 & 0 & 0 & 0 & 0 & 1 & 0 & 0 & 0 \\
0 & 0 & 0 & 0 & 0 & 0 & 0 & 0 & 0 & 0 & 0 & 0 & 0 & 1 & 0 & 0 \\
0 & 0 & 1 & 0 & 0 & 0 & 0 & 0 & 0 & 0 & 0 & 0 & 0 & 0 & 1 & 0 \\
0 & 1 & 0 & 0 & 0 & 0 & 0 & 0 & 0 & 0 & 0 & 0 & 0 & 0 & 0 & 1 \\
1 & 0 & 0 & 0 & 0 & 0 & 0 & 1 & 0 & 0 & 0 & 0 & 0 & 0 & 0 & 0
\end{bmatrix}$$

Figure 4.5.b, Transition probability matrix corresponding to the transition diagram of h = 1/4 CPFSK signal.

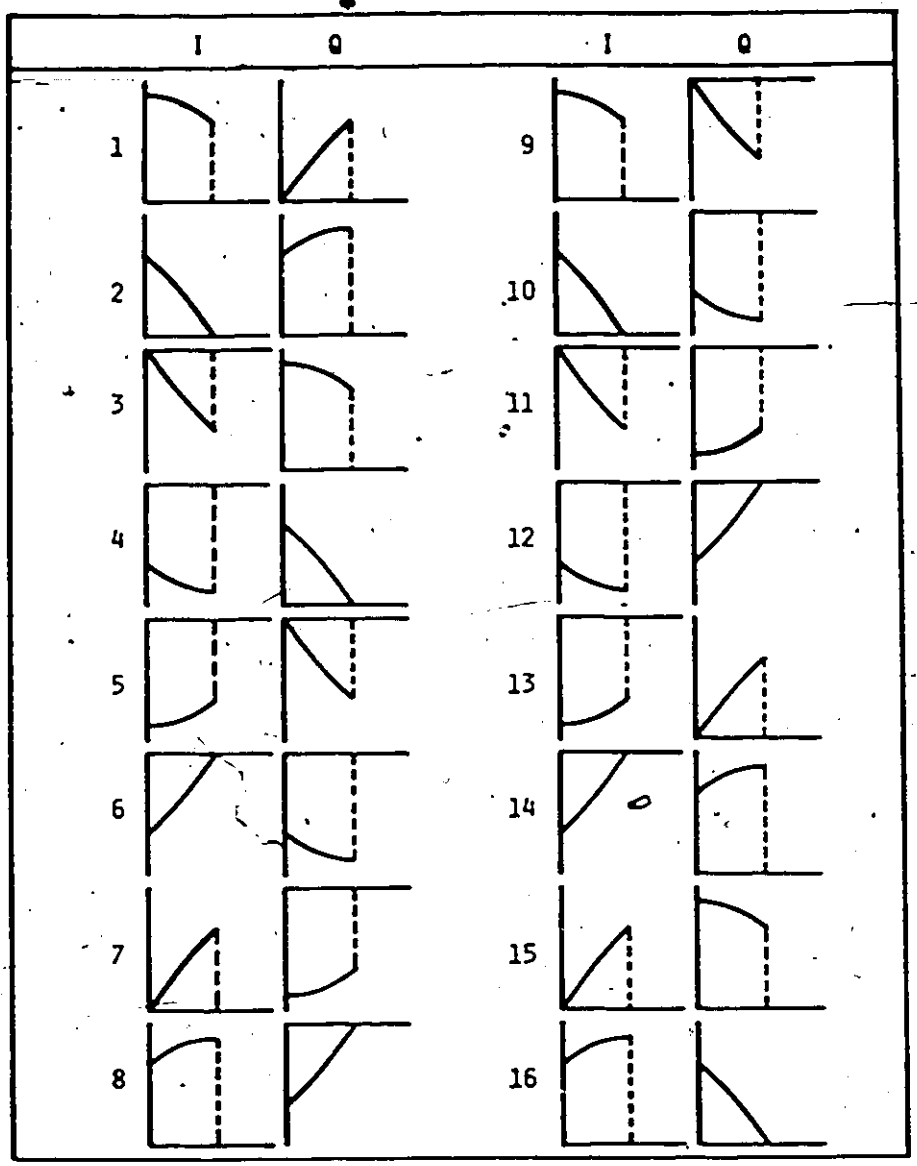

Figure 4.5.c, CPFSK low pass equivalent state waveforms for $h = 1/4$.

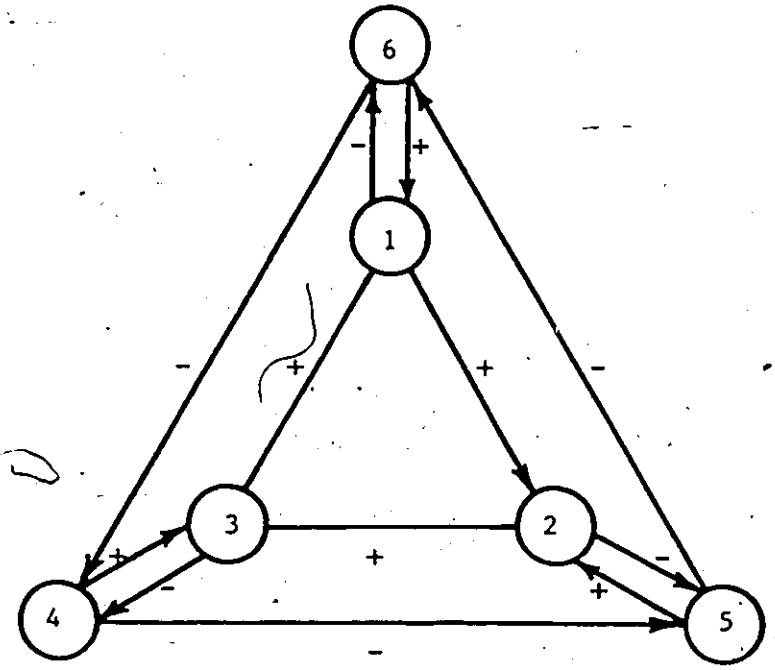

Figure 4.6.a, Markov process state transition diagram of h = 2/3 CPFSK signal.

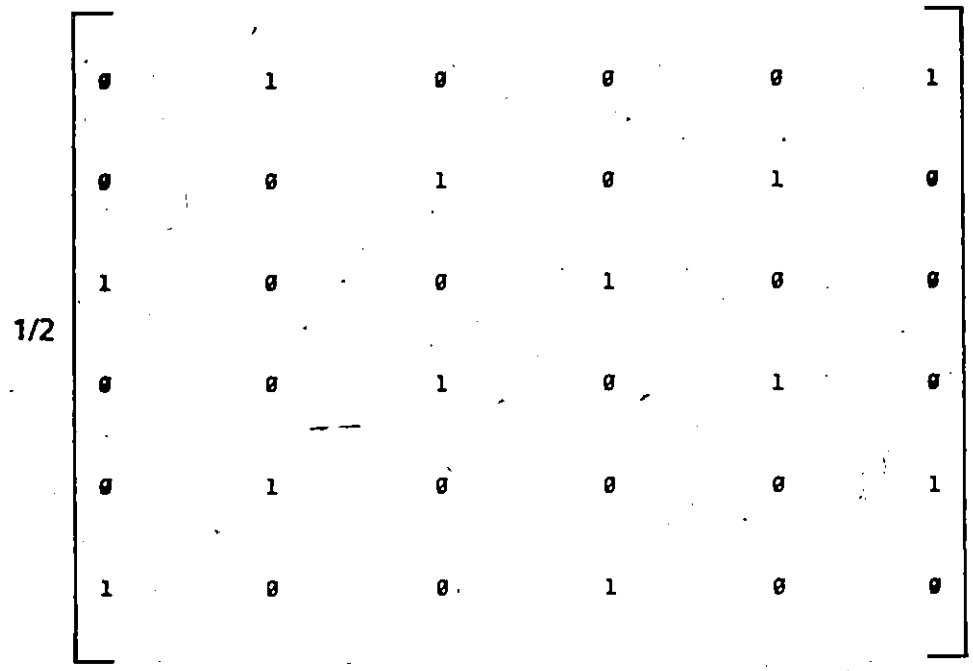

Figure 4.6.b, Transition probability matrix corresponding to the transition diagram of h = 2/3 CPFSK signals.

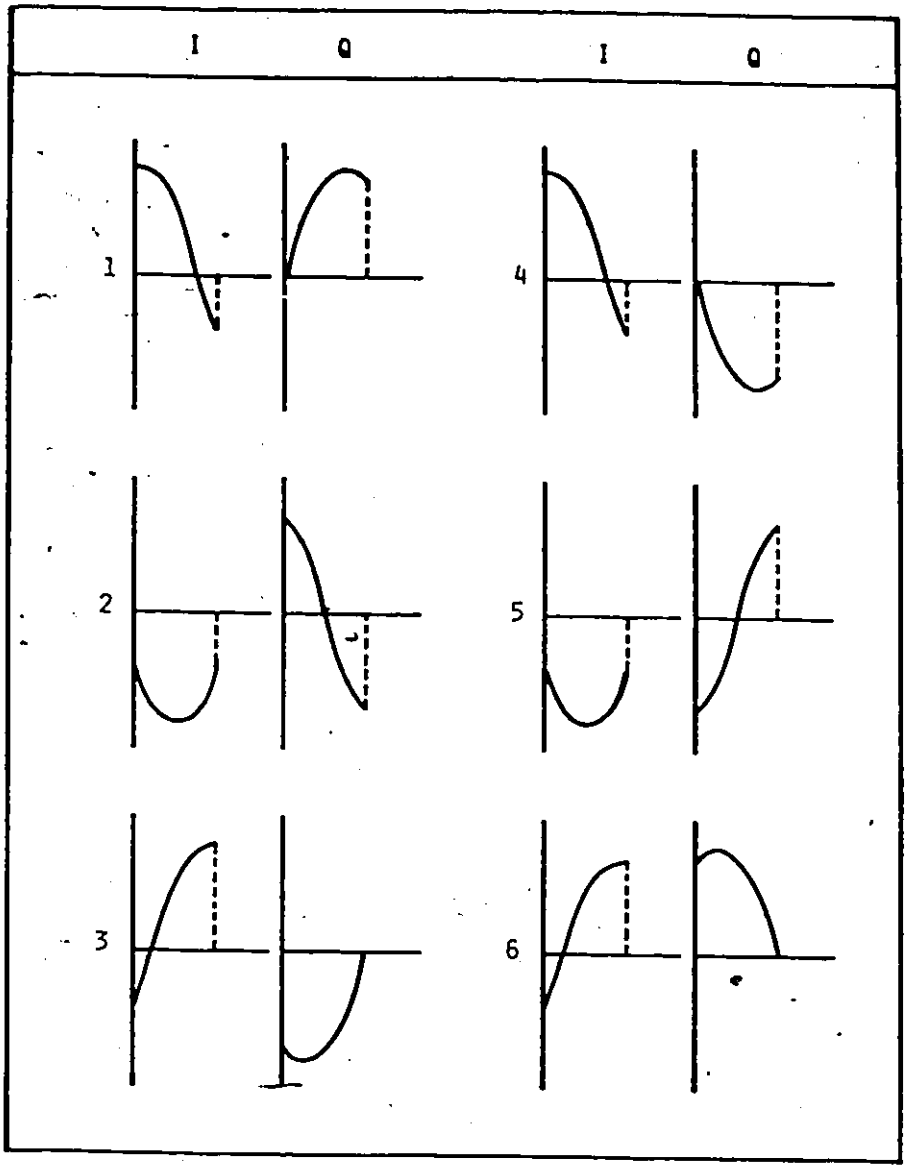

Figure 4.6.c, CPFSK low pass equivalent state waveforms for $h = 2/3$.

$$G_r(f) = \frac{1}{T_b^2} \sum_{n=-\infty}^{\infty} \sum_{i=1}^{N} p_i F_i(n/T_b)\ ^2 \delta(f - n/T_b)$$

$$+ \frac{1}{T_b} \sum_{i=1}^{N} p_i\ F_i'(f)\ ^2$$

$$+ \frac{2}{T_b} \mathrm{Re}\{ \sum_{i=1}^{N} \sum_{k=1}^{N} p_i F_i'^*(f) F_k'(f) p_{ik}(\exp(-j2\pi f T_b))\} \qquad (4.8)$$

where,

$\delta(f)$ is the Dirac delta function,

$F_i(f)$ is the Fourier transform of $r_i(t)$,

$F_i'(f)$ is the Fourier transform of $r_i'(t)$,

$$r_i(t) = r_i'(t) - \sum_{k=1}^{N} p_k r_k(t) \qquad (4.9)$$

$$p_{ik}(z) = \sum_{\ell=1}^{\infty} p^{\ell}_{ik} z^{\ell} \qquad (4.10)$$

and p^{ℓ}_{ik} is the probability that the elementary signal $r_k(t)$ is transmitted ℓ signaling intervals after the occurrance of $r_i(t)$.

We notice that the first term in (4.8), i.e., the line spectrum, vanishes when

$$\sum_{i=1}^{N} p_i F_i(n/T_b) = 0 \qquad (4.11)$$

which implies that a sufficient condition for the absence of a line spectrum includes the following two points:

1. that for each signal waveform $r_i(t)$ of the set, the negative $-r_i(t)$ also belongs to the set.
2. that the stationary probability on $r_i(t)$ and $-r_i(t)$ are equal. In other words,

$$\sum_{i=1}^{N} p_i r_i(t) = 0 \qquad (4.12)$$

From (4.5), it is seen that condition (1) is satisfied for $h = a/b$. Condition (2) is statisfied for random data. The computed power spectral densities for $h = 1/2$, 1/3, 1/4, and 1/5 are presented in figures 4.7 - 4.10. In the case of $h = 1/2$, the usual MSK spectrum is obtained; $h = 1/3$ and 1/4 yield a spectrum with narrower main lobe and should be considered for bandwidth efficient schemes

(h = 1/4 main lobe is almost half that of MSK). Figures 4.11.a and 4.11.b show measured power spectra of CPFSK signal for h = 1/2, 1/4 in a linear channel. As indicated above, the measured spectrum main lobe of h = 1/4 is narrower than that of h = 1/2. The set-up described in chapter three, was used to obtain these results. Experimental results in figure 4.11 indicate that the circuit of chapter three does give results identical to theory.

4.3 SUMMARY

The Markov process representation of the CPFSK signal (or its preenvelope) was developed and used to compute the power spectrum. The transition state diagram, the transition probability matrix and the low-pass equivalent state waveforms were also shown. As h decreases in value, the autocorrelation function extends over more bits and the power spectra main lobe becomes narrower (h = 1/4 main lobe is almost half that of MSK).

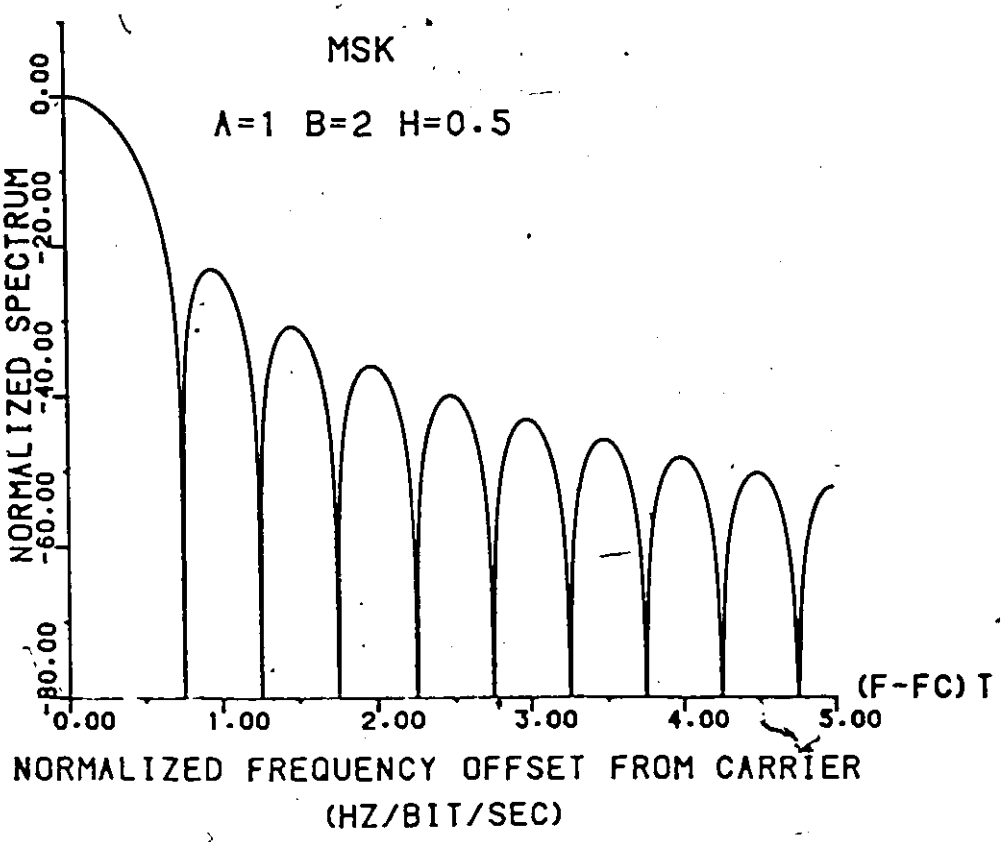

Figure 4.7 Computed power spectral density of h = 1/2 CPFSK. (MSK)

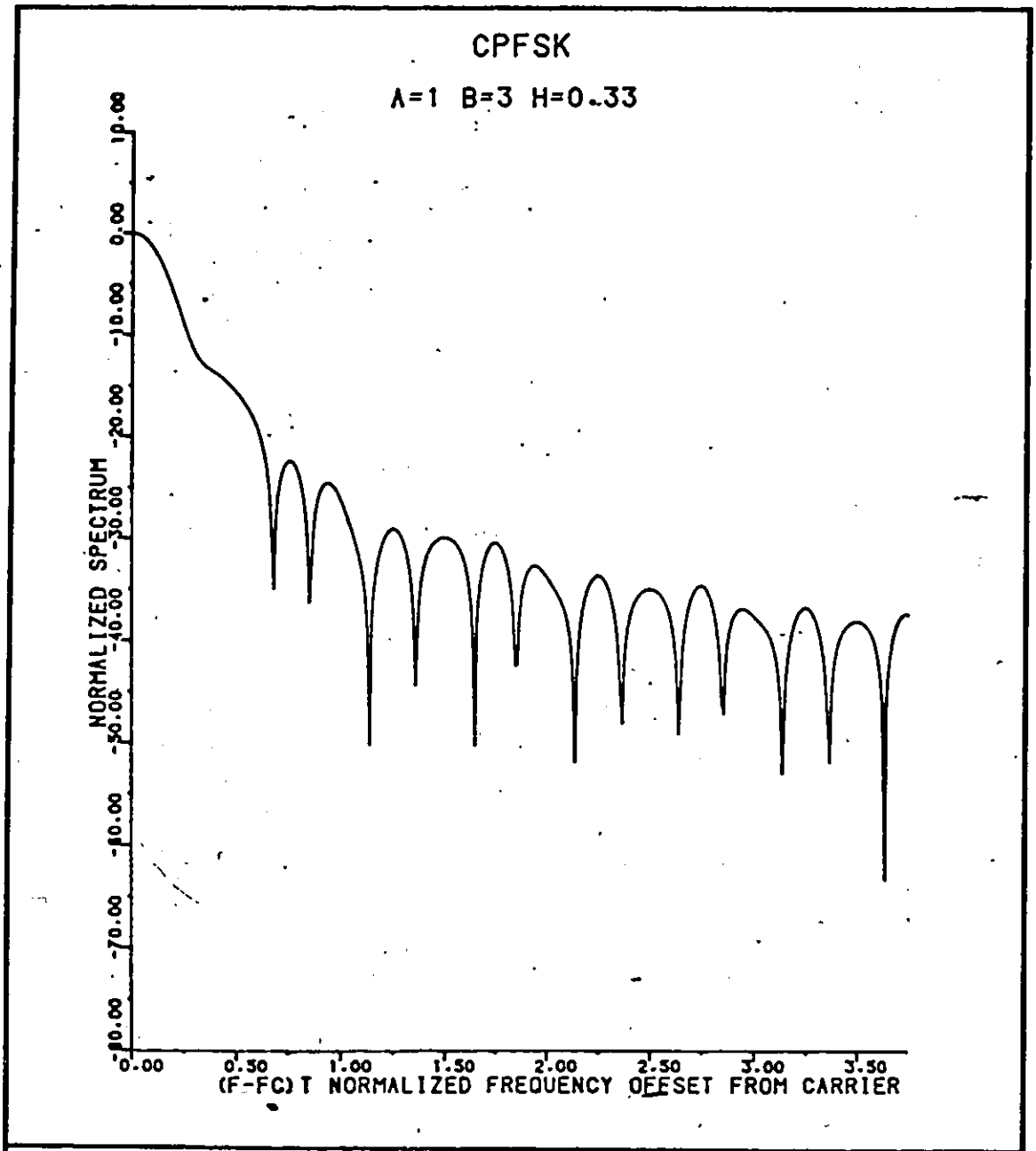

Figure 4.8 Computed power spectral density of h = 1/3 CPFSK.

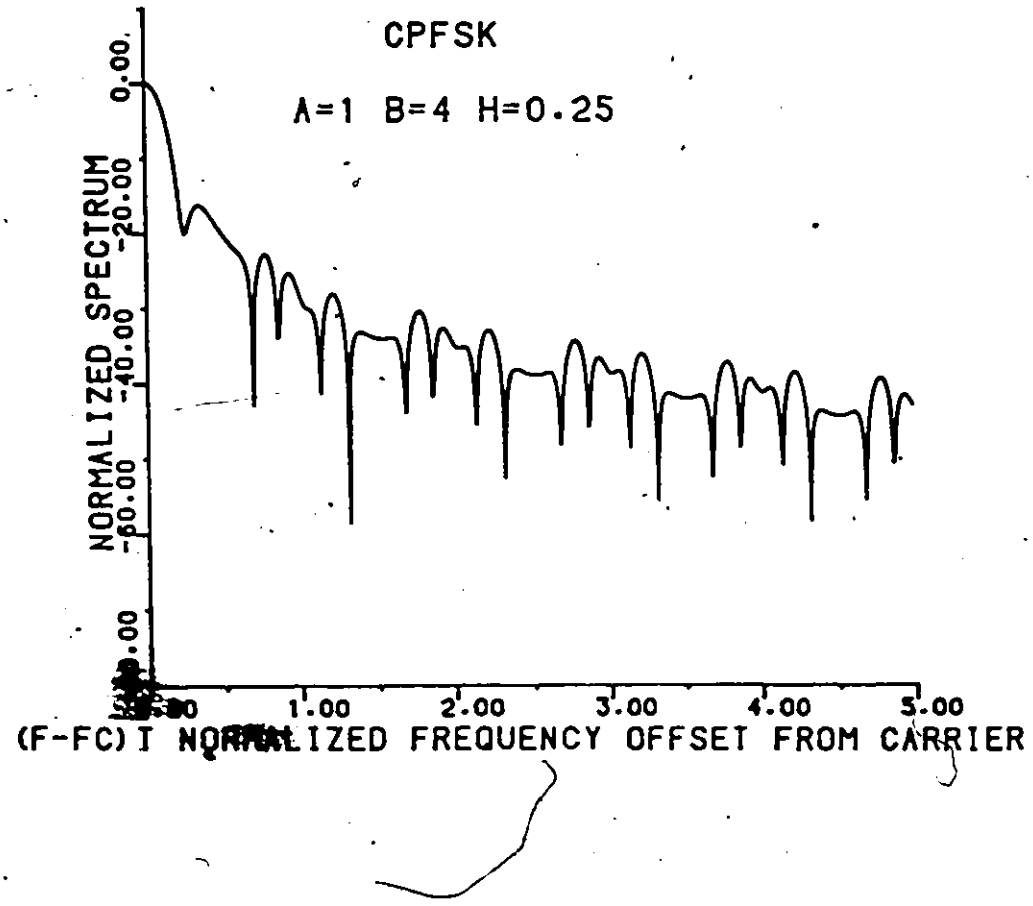

Figure 4.9 Computed power spectral density of h = 1/4 CPFSK.

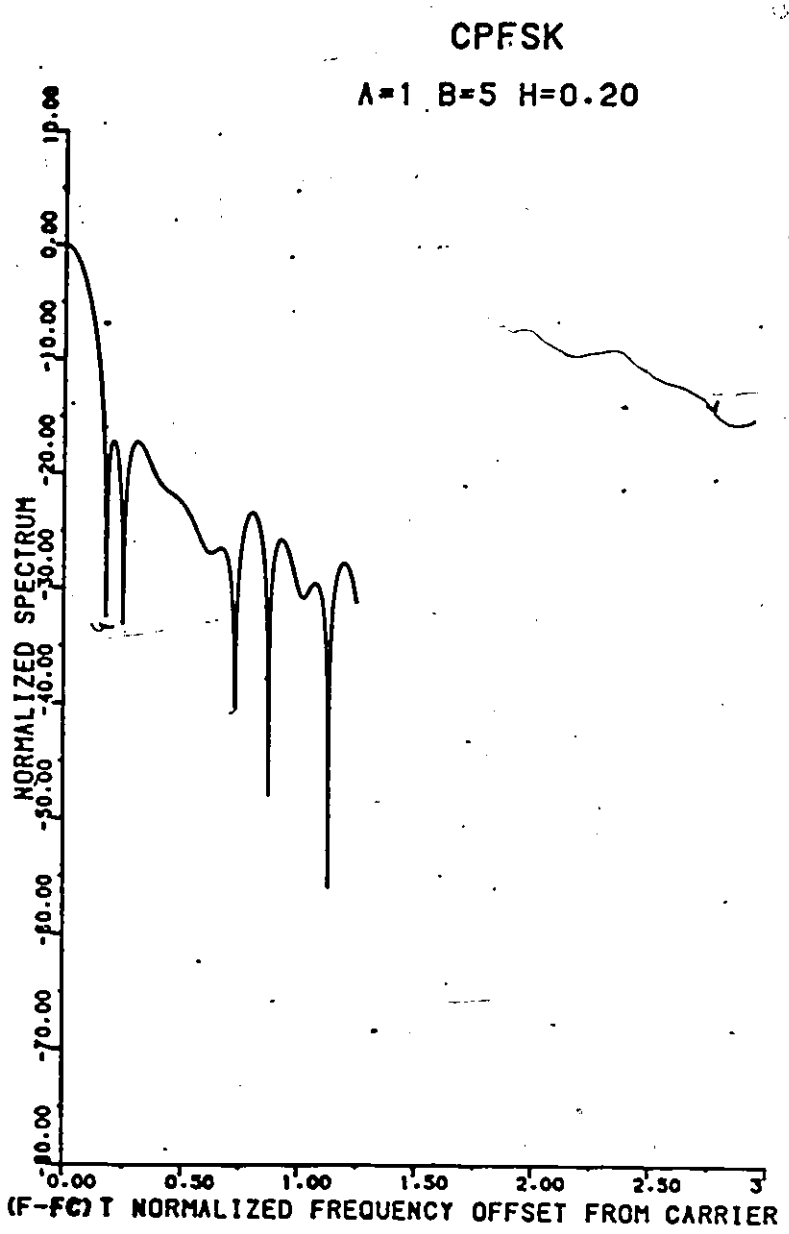

Figure 4.10 Computed power spectral density of h = 1/5 CPFSK.

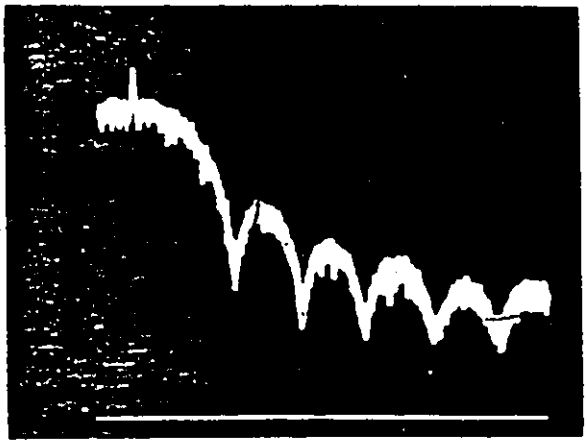

$(f - f_c)T_b$

Figure 4.11.a, Measured power spectra of h = 1/2 CPFSK (MSK) in al linear channel.

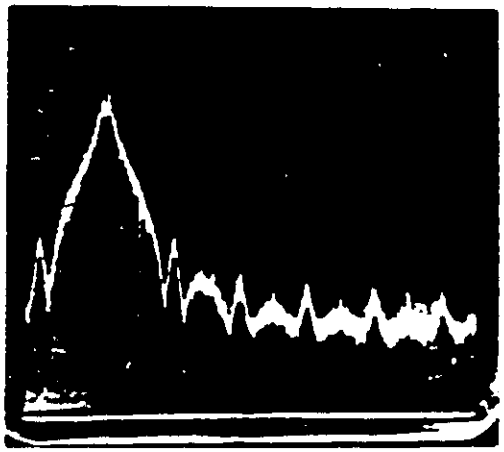

Figure 4.11.b, Measured power spectra of h = 1/4 CPFSK in a linear channel.

CHAPTER FIVE

DEMODULATION OF BINARY CPFSK SIGNALS

5.1 INTRODUCTION

The binary CPFSK signal, at the receiver input, r(t), can be demodulated using a coherent correlation receiver [48], or using a suboptimal scheme consisting of two bandpass filters (BPFs), with center frequencies f_1 and f_2, followed by envelope detectors (or squarers) and detector filters [48;51]. Narrowband FSK can also be detected using a discriminator, which is a frequency-to-voltage converter, followed sometimes by a detector filter, which is usually a filter matched to the shaping function [51]. Other noncoherent schemes include a one-bit and two-bit differential detection, in which the received signal is multiplied by a version of itself delayed by one (or two) bit time. The phase difference, over one (or two) bit time, is then used to demodulate the signal [50].

In this chapter, a new coherent technique for demodulation of binary CPFSK, is presented. The transmitted binary data is

recovered through a coherent comparison of successive beginning phases. The decoder also looks at two time intervals before making a decision. The threshold is selected such that the interphase interference effect, resulting from the transmit and receive filters, is minimized. A possible hardware implementation of this decoder is proposed. Further, it is shown that a slightly modified MSK quadrature receiver structure can still be used to demodulate the CPFSK signal, with $h = 1/2$, when generated in the manner shown in chapter three.

Another interesting aspect of this demodulation method is that the computed probability of error of binary CPFSK signals is found to be marginally less than the differentially encoded and coherently detected ϕ-ary PSK. Furthermore, the case of linear phase, $h = 1/4$, binary CPFSK is found to be of interest, as it is similar to MSK in E_b/N_o performance (figure 5.10); however, it occupies approximately half the bandwidth that MSK occupies (figures 4.7 and 4.9).

5.2 DEMODULATION OF BINARY CPFSK

In its basic form, CPFSK is a technique where binary

information is transmitted on two frequencies. However, because of the continuous phase characteristic (3.2), the binary data is carried in the difference between two successive beginning phases. i.e.,

$$\theta_{n+1} - \theta_n = x_n \pi h \qquad (5.1)$$

where $\theta_n = \theta(nT_b)$. Therefore, estimating successive phases at the transition instants should be sufficient to demodulate the input data conveyed by the transmitted signal. Moreover, because of the continuous phase requirement, CPFSK retains useful information beyond the time of the bit transmission and it would be of interest to take it into account. In the binary case, this bit-phase interrelation is shown in figure 5.1, and it extends over two time intervals. At the end of even (odd) signalling intervals, the phase θ_n assumes one of the phases of the set $S_1 = \{0, 2\pi h, \ldots, 2\pi\}$ ($S_2 = \{\pi h, 3\pi h, \ldots, 2\pi - \pi h\}$). This is shown in figure 5.2 for two values of h ($h = 1/2$, $h = 1/4$).

The demodulation technique described in this chapter, uses this property of bit-phase interrelation and looks over two bit

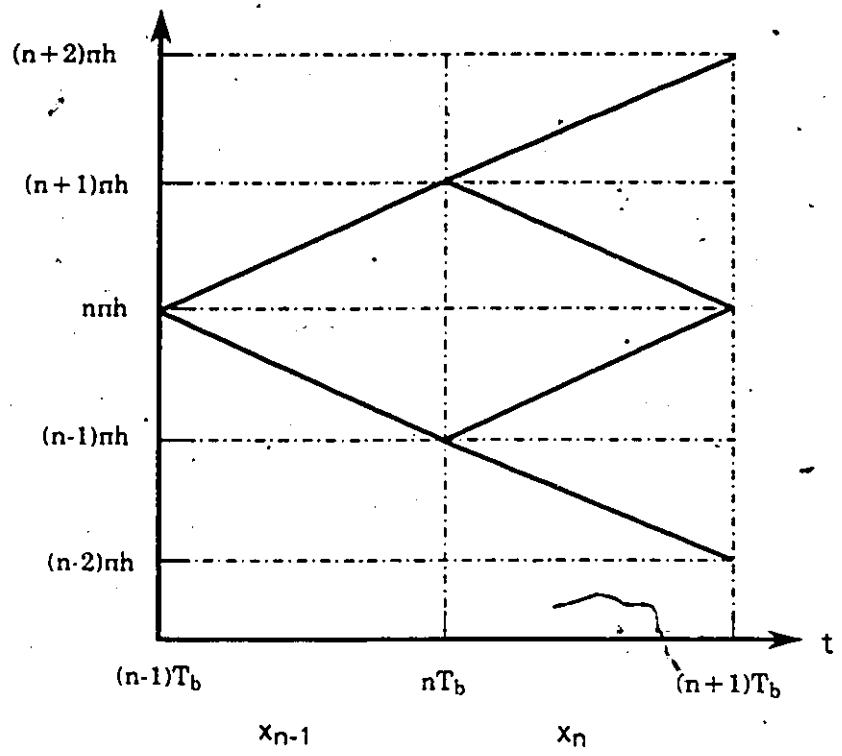

Figure 5.1 Phase trajectories of CPFSK signals over two symbol intervals

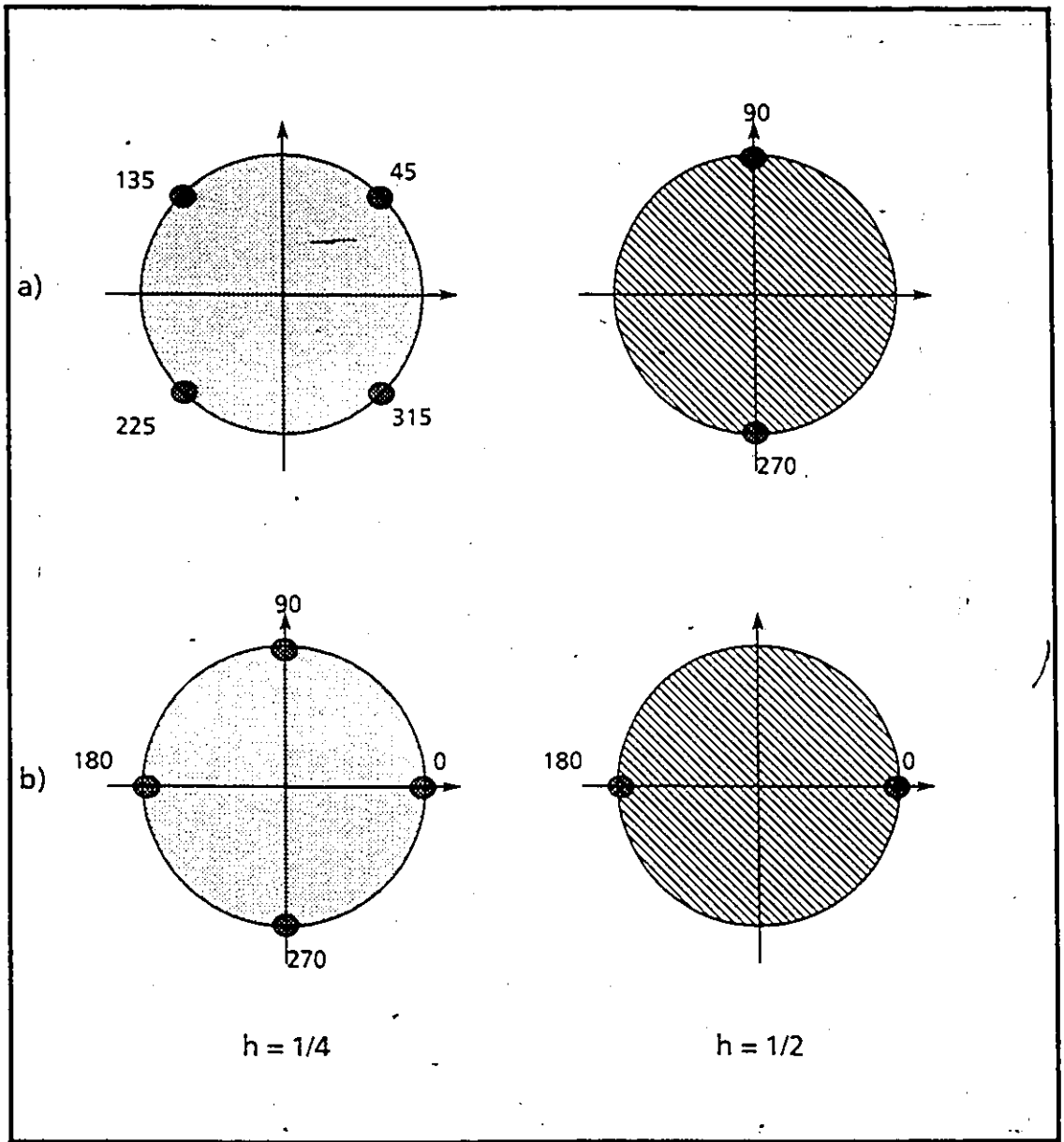

Figure 5.2 Constellation diagram of CPFSK with h = 1/4, h = 1/2:
a) n odd
b) n even

intervals before making the decision. To perform this, a coherent reference, at the carrier frequency f_c, is chosen. Comparison between the coherent reference and the received signal is then performed, and the sequence $\{\theta_n\}$ is decoded, as described in the next section, using techniques adapted from M-ary PSK. A differential phase processor computes the phase shifts (5.1), and an estimate of the transmitted symbol x_n, is obtained.

5.2.1 PHASE PROCESSOR

Since the proposed demodulation technique is adapted from that of M-ary PSK, a brief description of the phase detection in M-ary PSK, will first be given.

5.2.1.1 M-ary PSK phase detection

The M-ary PSK transmitted signal was defined in (2.1), along with its complex envelope in (2.2). Optimal decoding is achieved by coherent correlation of the receiver baseband signal with each member of the signals set, selecting the largest correlator output as the signaling phase state. Each correlator computes

$$z(nT)=z_n=\int_{(n-1)T}^{nT} r(t)s(t)dt=r_{I,n}\cos\theta_k+r_{Q,n}\sin\theta_k \qquad (5.2)$$

where

$$r_{I,n}=\int_{(n-1)T}^{nT} r(t)\cos\omega_c t\,dt \qquad (5.3)$$

$$r_{Q,n}=\int_{(n-1)T}^{nT} r(t)\sin\omega_c t\,dt \qquad (5.4)$$

$$\text{Let } r_n=|r_n|\exp(j\phi_n), \qquad (5.5)$$

$$\text{where, } |r_n|=(r_{I,n}+r_{Q,n})^{\frac{1}{2}} \text{ and } \phi_n=\tan^{-1}(r_{I,n}/r_{Q,n}); \qquad (5.6)$$

and let DR_i, $i=1,...,M$ be a partition of the two-dimensional plane into decision regions, so that if $r_n \in DR_k$, the decision is that $r_n=\exp(j\theta_k)$. The decision region DR_k is $DR_k=\{r_n: |r_n-\exp(j\theta_k)|\leq |r_n-\exp(j\theta_i)|, i=1,...,M\}$. We see that (5.2) is identical to writing

$$z_n=|r_n|\cos(\theta_k-\phi_n) \qquad (5.7)$$

The decoding decision as to which y_n is largest is therefore equivalent to determining which DR_k, $k=1,...,M$, r_n belongs to. That is, determining which $(\theta_k-\phi_n)$ is smallest, over all k. In other words, determining which θ_k the ϕ_n is closest to. The decoder can therefore be reduced to a pair of channels in which

$r_{I,n}$ and $r_{Q,n}$ in (5.3) and (5.4) are separately determined, and the decoder decisioning is based only on a computation of ϕ_n in (5.6) and a decision comparison to $\{\theta_k\}$ (figure 5.3). In essence, the decoder uses the phase of the received signal to make the decision. Note that the decoder uses quadrature mixing followed by an integrate-and-dump detector. This approach is taken from [10,53], and will be adapted and applied to the CPFSK signal. The probability of error is computed in (10,52,53) and will be shown later along with that of binary CPFSK.

5.2.1.2 Binary CPFSK phase detection

A similar scheme to the one shown above for PSK, can be modified to accomodate the phase detection of binary CPFSK. The received signal is multiplied with two coherent carriers in quadrature as shown in figure 5.6. The resulting inphase and quadrature waveforms are lowpass filtered and sampled synchronously at $t=nT_b$. The resulting $r_{I,n}$ and $r_{Q,n}$ are used to compute ϕ_n, which is used to obtain an estimate of θ_n ($\hat{\theta}_n$).

In figure 5.1, all six possibe phase trajectories of the unfiltered

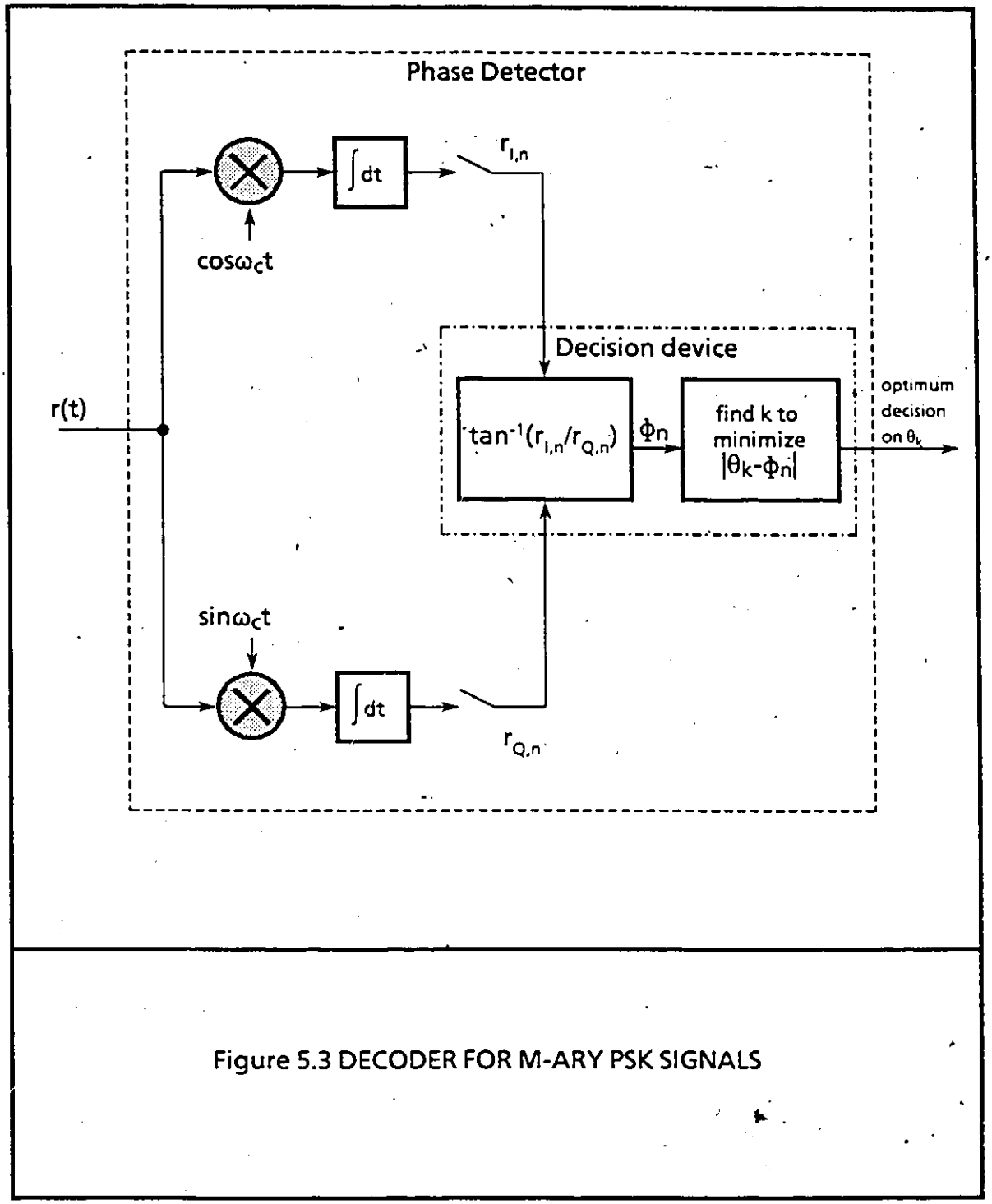

Figure 5.3 DECODER FOR M-ARY PSK SIGNALS

binary CPFSK, interconnecting the six possible phase values over two successive symbols, are shown. As can be seen, the unfiltered phase functions are piecewise linear and have sharp edges. With distortion and noise present at the receive side, it is difficult to precisely estimate θ_n'. However, it can be decided, with relative reliability, whether or not the transmitted phase value was within a range of $2\pi h$; i.e., that the transmitted value was one of two possible phases (belonging to the set S_1 for n even and to the set S_2 for n odd) between which the measured phase fell. Since the difference between two adjacent phases is $2\pi h$, it can be seen that at least $2\overline{\pi h}$ ($(2\pi h - \delta)$ taking into account the effect of filtering, where δ is the phase deviation from the ideal), of distortion plus noise, must occur before the correct value is eliminated from the retained pair.

In this initial phase, the contribution to the global probability of error, resulting from the elimination of the correct phase value, is considered to be virtually negligible. Figure 5.4 shows the retained pairs over the duration of two symbols, where the transmitted phase trajectory is assumed to be included. A threshold is then set between the retained pair (see section 5.2.2

for details), and a temporary phase decision is made. The phase estimate is stored in order to be used in the second phase of the algorithm.

The second phase provides a final decision on θ_n. This is done by observing again the sequence θ_{n-1}, θ_n, and θ_{n+1}. The decision on θ_{n-1} (which is final) is then used along with the temporary decision on θ_{n+1} (which is assumed to be correct), to decide on the middle phase θ_n. The threshold is again selected and a new and final decision is output. The difference between two successive final phase decisions is then decoded to yield a data symbol x_n according to (5.1).

5.2.2 SETTING THE THRESHOLD

The transmit and receive filters will cause the phase trajectories, of the received signal, to deviate from the ideal phase displayed in figure 5.1. For the filters chosen, the phase deviation from the ideal is approximately $\delta \approx 0.2\pi h$ (20° for $h=1/2$, 10° for $h=1/4$; a transition from f_1 to f_2 lifts the measured phase $0.2\pi h$ relative to the ideal phase value; f_2 to f_1 drops the phase $-0.2\pi h$). Since the closest phase value is only $2\pi h$ away, a threshold on phase measurements at the midpoint between two nodes is only πh

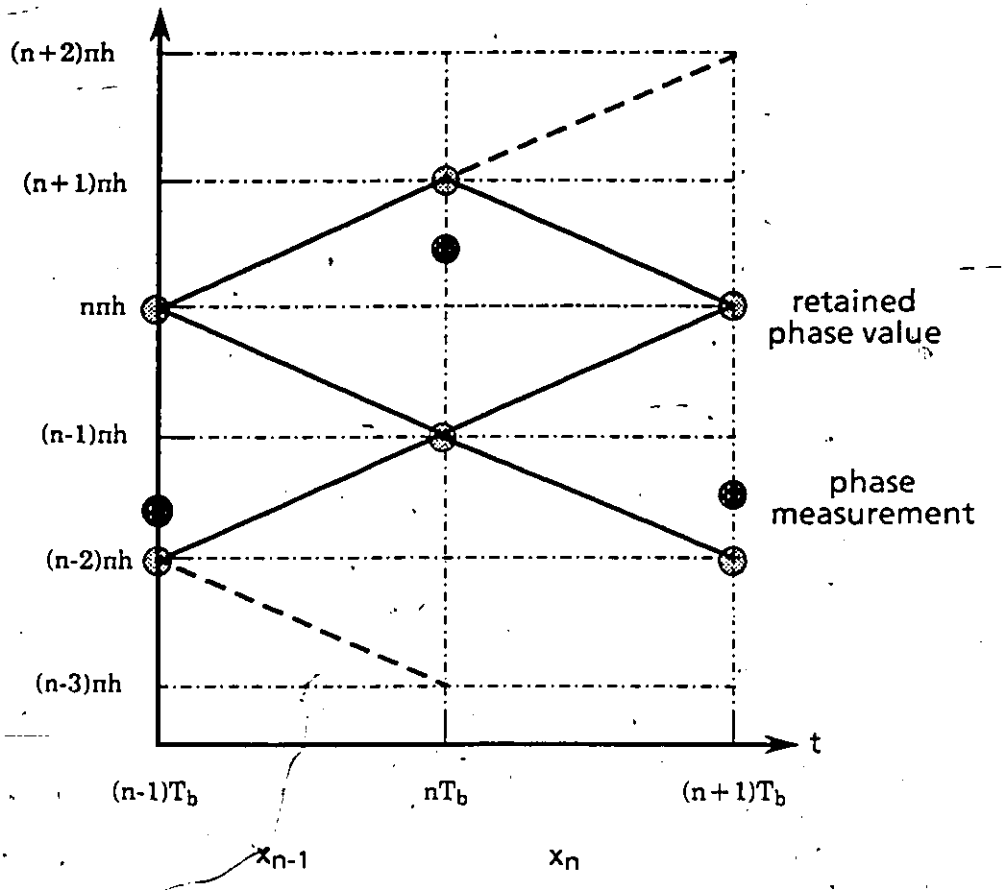

Figure 5.4 Three typical retained phase value pairs

away from an ideal phase value. Consequently, $0.2\pi h$ of distortion would leave only $0.8\pi h$ of distance to the threshold, as compared with πh in the ideal case. As a result, this would cause some degradation on the ultimate performance.

To alleviate the degrading effect of the interphase interference, the retained phases at the end of every two symbols are used to determine a threshold setting midway between the two possible phases (with distortion) at θ_n. For all possible combinations of θ_{n+1} and θ_{n-1}, the thresholds found are πh and $(1 \pm 0.1)\pi h$. In the case of binary CPFSK, the use of a variable threshold gives a moderate improvement; however, this improvement is more apparent and perhaps necessary for M-ary CPFSK. The algorithm presented above is summarized in the following steps:

1. Phase measurements are made at the beginning of each symbol period. All measurements are referenced to θ_0 (these measurements deviate from the ideal due to noise and interphase interference).

2. The phase measurements are quantized into the regions shown in figure 5.2.

3. The two ideal phase nodes closest to the measured phase are retained as decision candidates.

4. A threshold is selected and a tentative decision is made on the phase.

5. Decisions, two symbols apart, are recycled to obtain a new decision on θ_n.

6. Phase shifts (5.1) are then computed, and a decision on x_n is made.

Thus the data x_n decision output is influenced by three successive surrounding phase measurements. The above steps are also illustrated in figure 5.5.

5.2.3 DEMODULATOR BLOCK DIAGRAM

The block diagram for the linear phase, binary CPFSK demodulator is shown in figure 5.6. The demodulator is based on the phase processing algorithm presented above. As shown in figure 5.6, the received h=1/b, CPFSK IF signal is filtered, limited, and passed on to the phase detector. The CPFSK

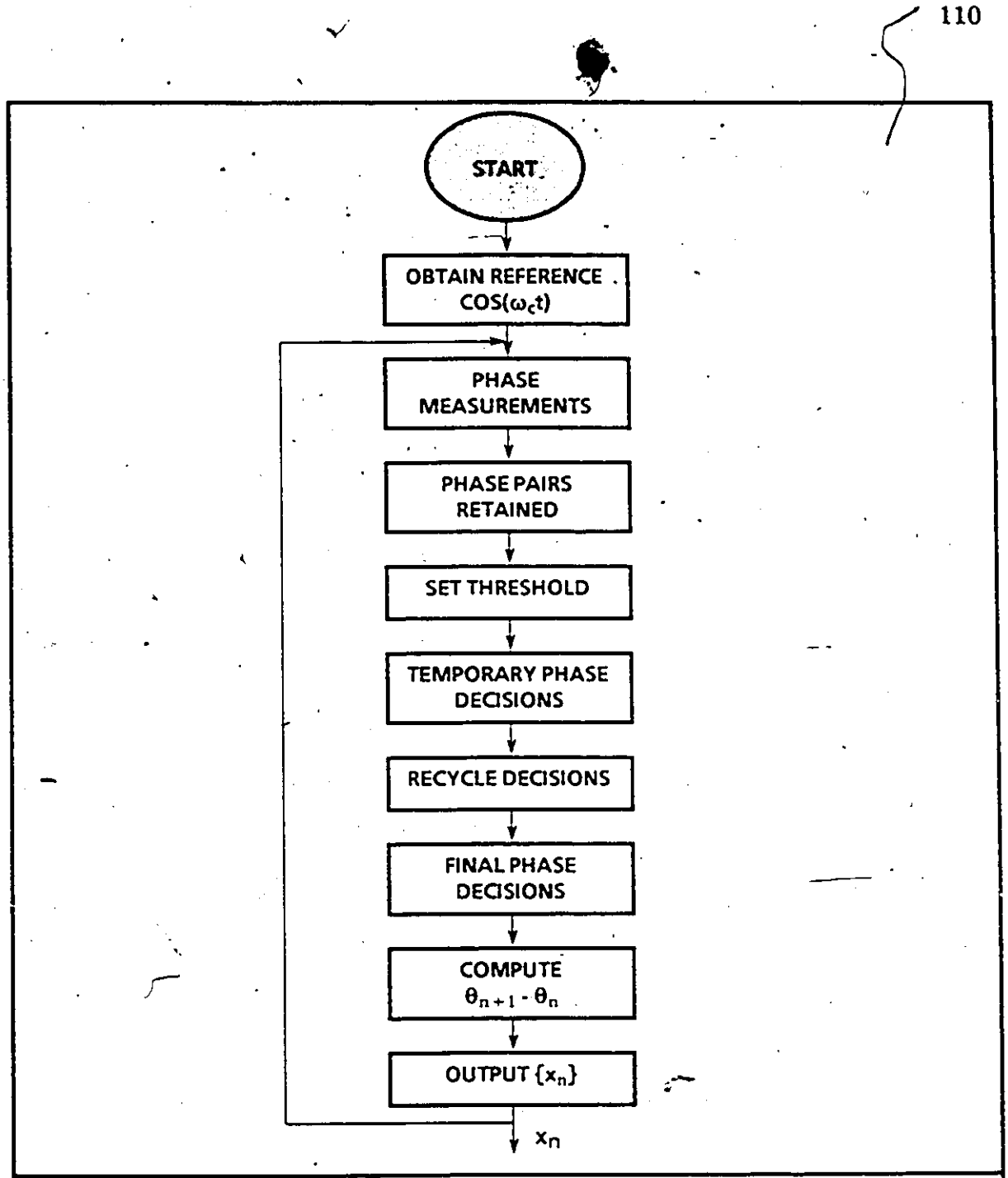

Figure 5.5 FLOW CHART OF THE ALGORITHM USED TO DEMODULATE THE CPFSK SIGNAL

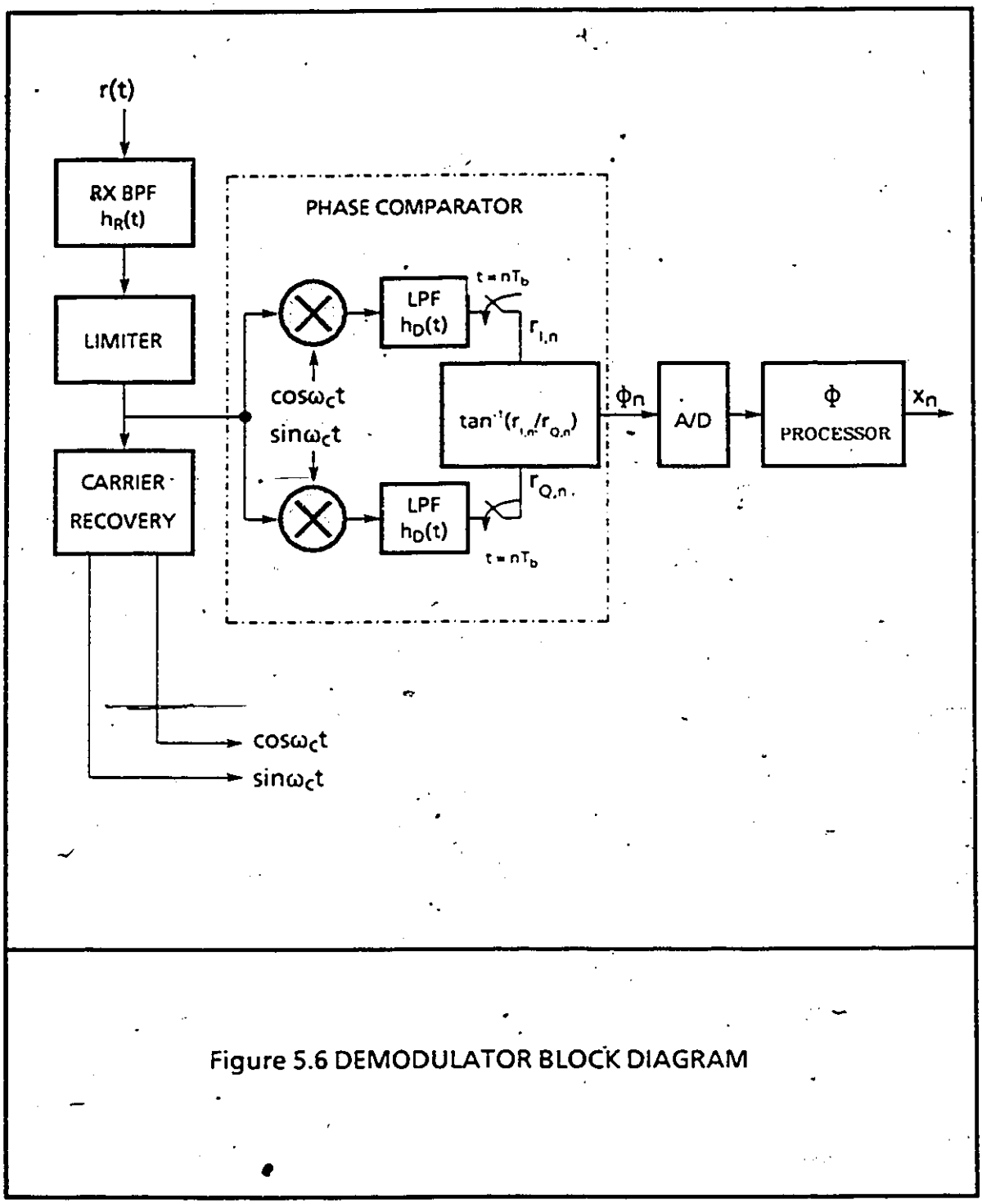

Figure 5.6 DEMODULATOR BLOCK DIAGRAM

signal is fed into the carrier recovery circuit, where a PLL is locked to the received signal to establish the coherent reference. The symbol timing clock is also extracted. The phases ϕ_n are quantized by the A/D into the phase regions shown in figure 5.2. The digital words from the A/D are passed on to the phase differential computer where the difference (5.1) is computed, and the demodulated binary data stream $\{x_n\}$ is obtained.

5.3 ERROR PROBABILITY OF THE CPFSK RECEIVER

Figure 5.7 shows the CPFSK baseband equivalent system, derived from the bandpass system in figures 3.4 and 5.6. In the baseband model the signals are replaced by their complex envelopes and the filters by their baseband equivalent filters, all referred to the receiver center frequency, f_c. The output of the decoder filter ($h_D(t)$) is given by

$$r(t) = y(t) + n(t) \tag{5.8}$$

$$\text{where } y(t) = s(t) * h_T(t) * h_C(t) * h_R(t) * h_D(t) \tag{5.9}$$

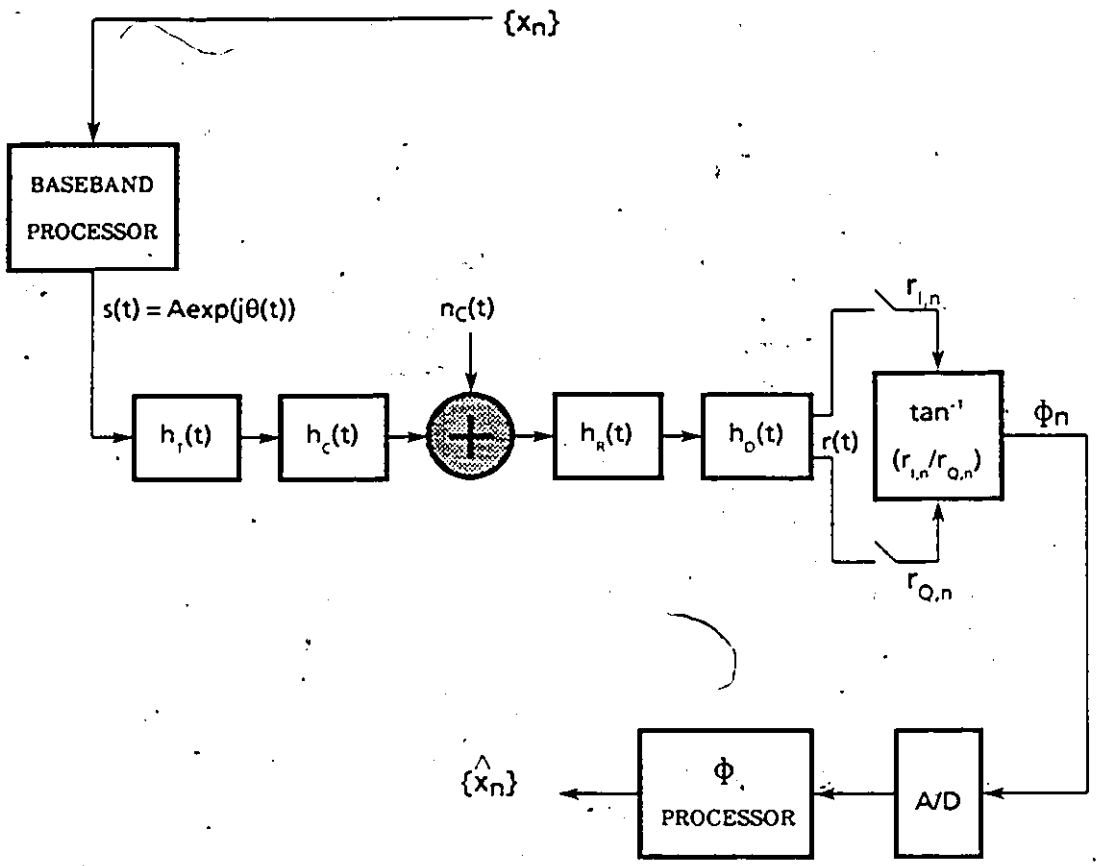

Figure 5.7 EQUIVALENT BASEBAND MODEL OF CPFSK SYSTEM

and $n(t) = n_C(t) * h_R(t) * h_D(t)$ (5.10)

In (5.9) and (5.10), $s(t) = A\exp(j\theta(t))$ is the transmitted complex envelope; $h_T(t)$, $h_C(t)$, $h_R(t)$, and $h_D(t)$ are, respectively, the impulse responses of the transmitter filter, channel filter, receiver filter, and detector filter, and $n_C(t)$ is the baseband equivalent additive white Gaussian noise (AWGN) introduced by the channel. Let $r_I(t)$ ($y_I(t)$, $n_I(t)$) be the real part and $r_Q(t)$ ($y_Q(t)$, $n_Q(t)$) be the imaginary part of $r(t)$ ($y(t)$, $n(t)$). Thus

$$r_I(t) = y_I(t) + n_I(t), \text{ and } r_Q(t) = y_Q(t) + n_Q(t) \quad (5.11)$$

The sampled values of the $r_I(t)$ and $r_Q(t)$, at times $t = nT_b$, are

$$r_{I,n} = y_{I,n} + n_{I,n}, \text{ and } r_{Q,n} = y_{Q,n} + n_{Q,n} \quad (5.12)$$

$$\text{where, } y_{I,n} = y_I(nT_b),\ y_{Q,n} = y_Q(nT_b), \quad (5.13)$$

$$\text{and } n_{I,n} = n_I(nT_b),\ n_{Q,n} = n_Q(nT_b) \quad (5.14)$$

In (5.12), $n_{I,n}$, and $n_{Q,n}$ are zero mean, independent Gaussian random variables with the same variance

$$\sigma^2_n = N_0/2 \int_{-\infty}^{\infty} |H_R(f)H_D(f)|^2 df = N_0 B_{RD} \qquad (5.15)$$

where, $N_0/2$ is the power spectral density of the noise, and B_{RD} is the noise bandwidth of $H_R(f)H_D(f)$. The phase of r(t) at time $t = nT_b$ is

$$\phi_n = \phi(nT_b) = \tan^{-1}((y_{I,n} + n_{I,n})/(y_{Q,n} + n_{Q,n})) \qquad (5.16)$$

Let $\beta_n = \beta(nT_b)$ be the phase of $(\exp(j\beta_n) = \exp(j(\phi_n - \theta_n)))$. The decision regarding the value of $\theta_n = \theta(nT_b)$ is based on $\phi_n = \phi(nT_b)$, so that if $|\phi_n - \theta_n| \leq \pi h$ (5.17)

there is no error. Thus the error probability of making an incorrect decision on θ_n is

$$P_\theta(e) = Pr(|\beta_n| \geq \pi h) \qquad (5.18)$$

Substituting the probability distribution function of the phase of the complex Gaussian random variable $(\exp(j\beta_n))$, which, for a specific signal to noise ratio $(\rho_s = 0.5A_y^2/\sigma^2_n)$, is given in [52] as

$$F(\beta) = (-\text{sgn}(\beta)/2\pi) \int_{-\pi/2}^{\pi/2-|\beta|} \exp(-\rho_s \sin^2(\beta)\sec^2 v)dv \quad \text{for } |\beta| \leq \pi \qquad (5.19)$$

where A_y is the amplitude of y(t) at $t=nT_b$; and using the following result

$$\Pr\{\beta_1<\beta<\beta_2\}=\begin{cases}F(\beta_2)-F(\beta_1)+1, & \beta_1<0<\beta_2\\ F(\beta_2)-F(\beta_1), & \beta_1>0 \text{ or } \beta_2<0\end{cases} \tag{5.20}$$

the phase error probability $P_\theta(e)$ of (5.18) reduces to

$$P_\theta(e)=2(F(\pi)-F(\pi/b))=1/\pi\int_{-\pi/2}^{\pi/2-|\pi/b|}\exp(-\rho_s\sin^2(\pi/b)\sec^2 v)dv \tag{5.21}$$

To evaluate the error probability of the proposed detection method, we first notice that an error can occur if either θ_{n+1} or θ_n is in error. Assuming that β_n and β_{n+1} are independent [10], the probability of this event (event #1) is

$$P_1=2P_\theta(e)-P^2_\theta(e) \tag{5.22}$$

However, if θ_{n+1} and θ_n are both shifted from their respective correct values by $2k\pi/b$, $k=1,2,\ldots,b-1$, then the nth data symbol is still decoded correctly, since $\theta_{n+1}-\theta_n$ is independent of this shift. The probability of this event (event #2) is

$$P_2=\sum_{k=1}^{b-1}(\Pr\{(2k-1)\pi/b\le\beta(nT_b)\le(2k+1)\pi/b\})^2 \tag{5.23}$$

Similarly, if only θ_{n+1} (θ_n) is shifted from the correct value by less than $2\pi-2k\pi/b$, $k=1,2,...,b-1$, such that the phase difference $\theta_{n+1} - \theta_n \bmod 2\pi$ is still positive (negative) for $x_n=+1$ and negative (positive) for $x_n=-1$, then the nth data symbol is again decoded correctly. The probability of this event (event #3) is

$$P_3=(1-P_\theta(e))\sum_{k=1}^{b/2-1}\Pr\{\pi/b\le\beta(nT_b)\le\pi-(2k-1)\pi/b\} \quad \text{for } b>2 \qquad (5.24)$$

Figure 5.8 illustrates how events #1, 2, and 3, described above, can occur for $h=1/4$. The probability of making an incorrect decision on the symbol data is therefore,

$$P_{x_n}(e)=P1 - P2 - P3 \qquad (5.25)$$

We now compute the error probability of binary CPFSK for the case where $h_D(t)$ is an integrate and dump circuit as in PSK (figure 5.3).

CASE I, $h_D(t)$=integrate and dump circuit: In this case, we assume that the transmitted signal is unfiltered, and that the channel bandwidth is infinite. Moreover, $h_R(t)$ is assumed to be wide enough not to distort the signal. The detector filter output

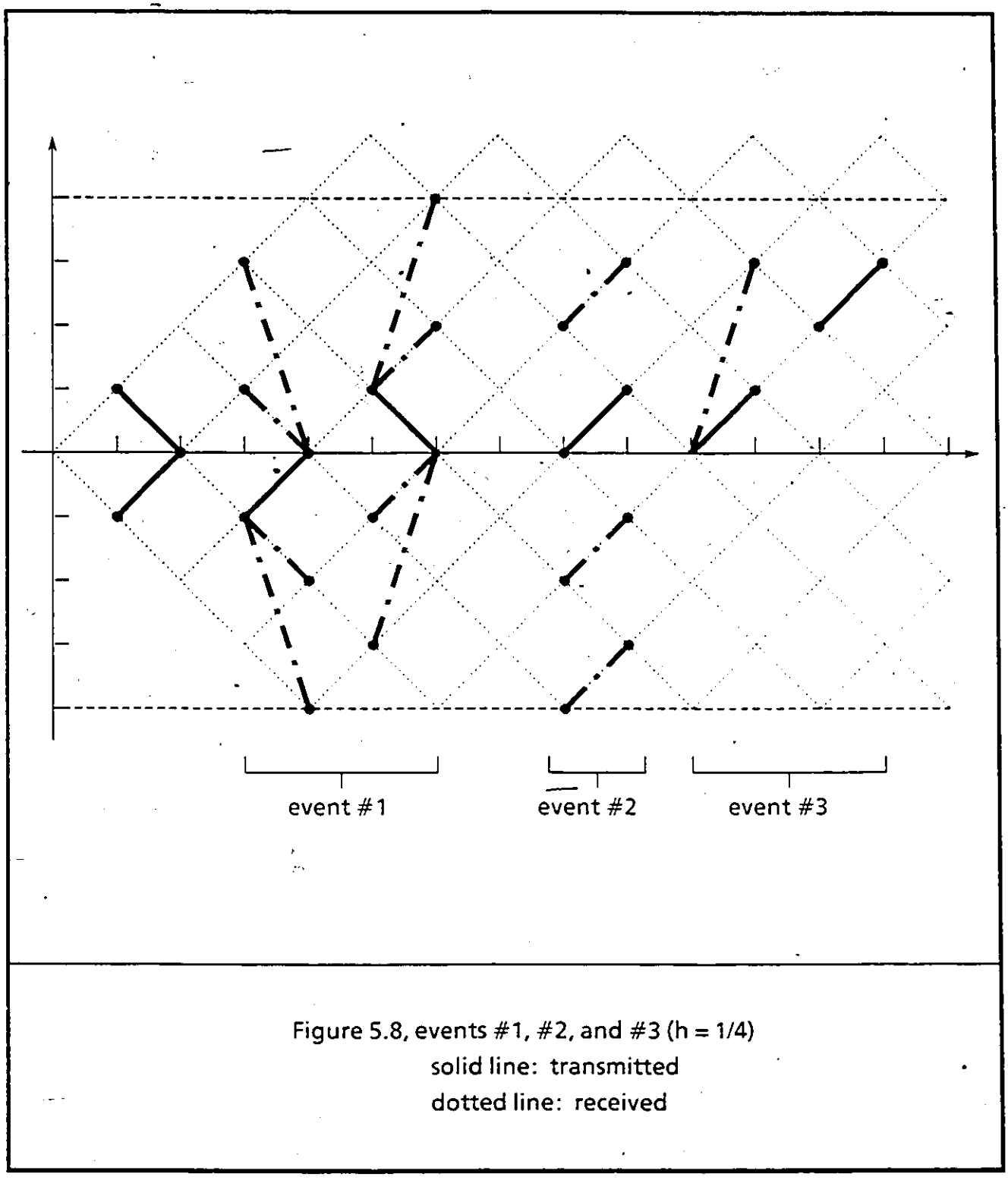

Figure 5.8, events #1, #2, and #3 (h = 1/4)
solid line: transmitted
dotted line: received

is expressed as

$$y(t) = \int_0^{T_b} A\exp(j\theta(t))dt \qquad (5.26)$$

Performing the integration, the amplitude of y(t) at the sampling instants $t = nT_b$, is found to be

$$A_y = (2AT_b/\pi h)(\sin(\pi h/2)) \qquad (5.27)$$

that is, $A_y = \varepsilon AT_b \qquad (5.28)$

where $\varepsilon = 0.90$, 0.97, and 0.99 for $h = 1/2$, 1/4, and 1/8. Notice that as h decreases, A_y approaches AT_b. The signal to noise ratio at the detector output is thus

$$\rho_s = 0.5A^2_y/\sigma^2_n = \varepsilon^2 0.5A^2T^2_b/N_0T_b = \varepsilon^2 E_b/N_0 \qquad (5.29)$$

where $\varepsilon^2 = 0.81$, 0.94, and 0.99 for $h = 1/2$, 1/4, and 1/8. The probability of error in (5.25) for two values of h (1/2, and 1/4) is plotted in figures 5.9, and 5.10 along with the coherent (b-ary CPSK) and differentially encoded and coherent b-ary PSK (DE-b-ary PSK). Notice that $(P_1 - P_2)$ is also the error probability of b-ary CPFSK with modulation index 1/b (event #3 does not occur

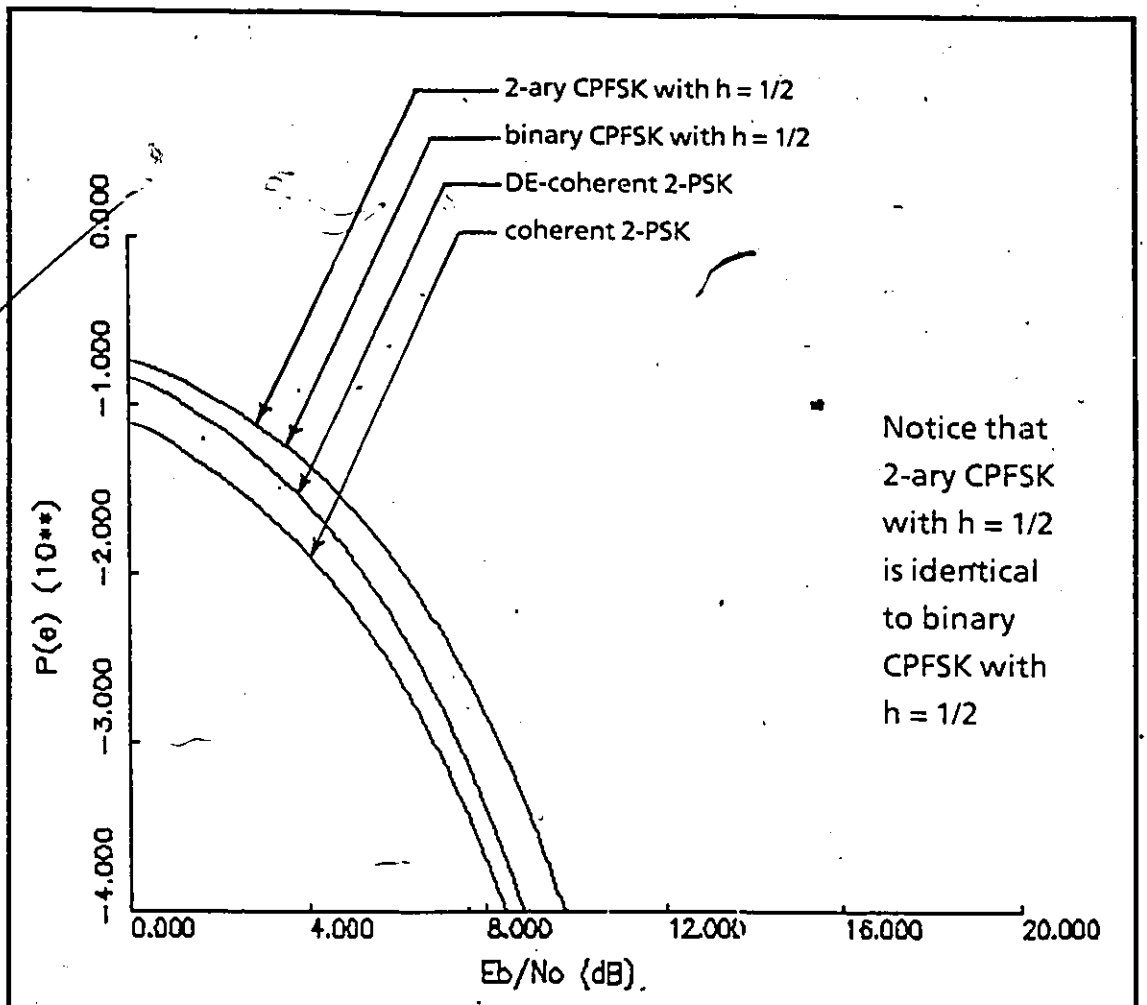

Figure 5.9 P(e) performance of CPFSK with h = 1/2, coherent BPSK and coherent detection of differentially encoded BPSK

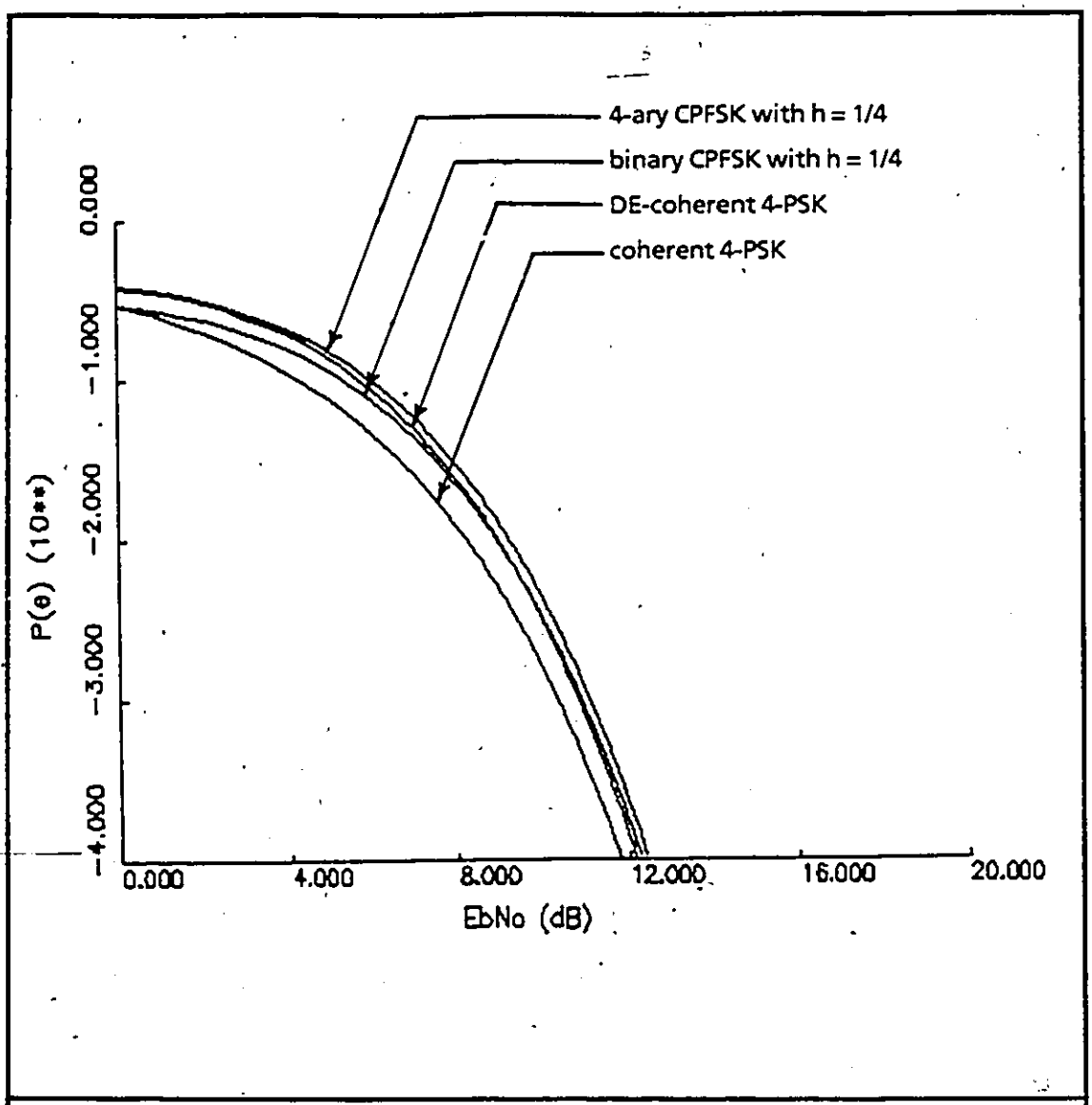

Figure 5.10 P(e) performance of CPFSK with h = 1/4,coherent 4-ary PSK (QPSK) and coherent detection of differentially encoded 4-ary PSK (DE-QPSK)

in b-ary CPFSK; since all phases are equally likely to occur, any shift in the value of a phase value yields an error). In figure 5.10, it can be noted that for high SNR, as the error probabilities are small, the error performance of binary CPFSK approaches that of b-ary CPFSK with $h = 1/b$. In this case (high SNR), (5.25) reduces to

$$P_{x_n}(e) \approx 2P_0(e) \tag{5.26}$$

That is to say that the error probability of binary and b-ary CPFSK with $h = 1/b$, is essentially double the error probability of θ_n at large SNR ($P_3 \approx P_2 \approx 0$). At low SNR, binary CPFSK is better than b-ary CPFSK DE-b-ary PSK. Note that for $P_{x_n}(e) = 10^{-4}$, $h = 1/4$ binary CPFSK is better than b-ary CPFSK by 0.15 dB, and only worse by 0.1 dB in E_b/N_o, as differentially encoded QPSK and MSK. The main lobe of $h = 1/4$ CPFSK is however, almost half that of MSK. In the case of $h = 1/2$, for the same $P_{x_n}(e) = 10^{-4}$, binary CPFSK is worse than differentially encoded BPSK by only 0.95 dB. Since the detection method is similar to the one used in DE-PSK systems, the complexity involved in practical realizations of this receiver are no more complex than that of PSK.

5.4 DEMODULATION OF THE h = 1/2 CPFSK SIGNAL USING THE MSK DEMODULATOR STRUCTURE

For the h = 1/2 CPFSK signal, generated in the manner shown earlier in chapter three, the MSK quadrature demodulator with slight modification, can still be used. In this case, the parallel to serial (P/S) converter is replaced by a NAND gate (see appendix B). The block diagram of such a demodulator is shown in figure 5.11.

5.5 SUMMARY

A new coherent technique for demodulating binary CPFSK has been presented. The binary data is recovered through a comparison of detected phase values. A hardware block diagram of the decoder was proposed. The probability of error of CPFSK signals was calculated and was found to be comparable to that of M-ary PSK (M = b). The case of h = 1/4 is of interest as it is worse than DE-MSK in E_b/N_0 performance, by only 0.95 dB at a P(e) of 10^{-4}, yet with almost half the bandwidth. Finally, it was shown that MSK signals generated in the manner shown in chapter three can be demodulated using the usual MSK demodulator (shown in figure 2.2.b) with a slight modification.

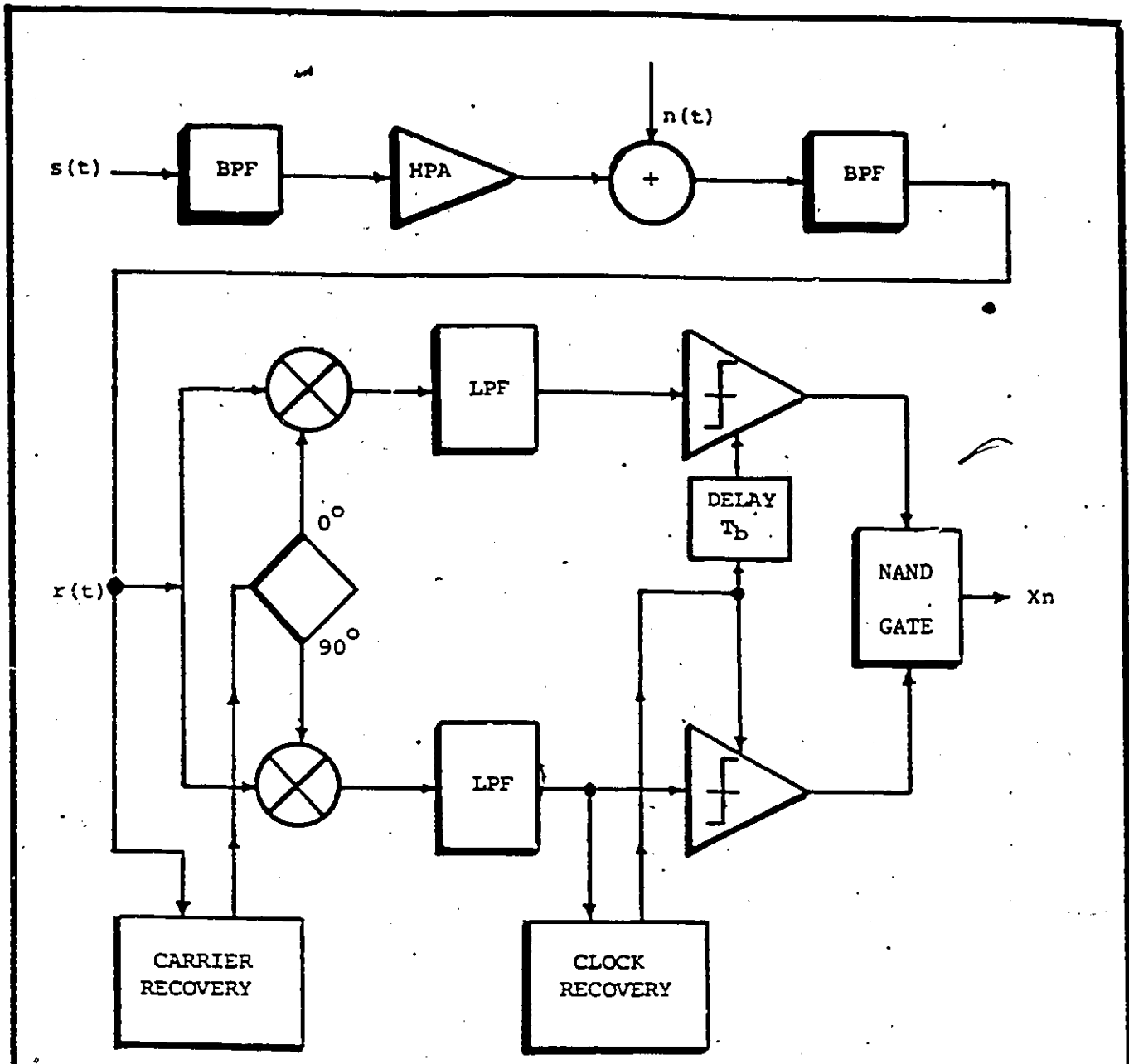

Figure 5.11 block diagram of h = 1/2 CPFSK demodulator using the MSK demodulator. (the channel path is also included)

CHAPTER SIX

CONCLUSIONS AND SUGGESTIONS FOR FURTHER RESEARCH

6.1 CONCLUSIONS

In the previous chapters, a new method for generating h = 1/b, bandwidth efficient binary CPFSK signals with one single circuit, was presented and studied.

The h = 1/b binary CPFSK signal was first represented by its preenvelope r(t). A baseband processor generated the real (I-channel) and the imaginary (Q-channel) parts of r(t). The two baseband signals were first filtered using raised cosine ($\alpha = 0.5$) low pass filters and then combined with a quadrature phase modulation scheme (QPSK modulator). The baseband processor was implemented for two values of h. Experimental results showed that the CPFSK preenvelope r(t) had constant amplitude and was free of amplitude variations. The eye diagrams for the I and Q channels were also shown to be very good.

An N-state (N = 4b) Markov chain model was developed and used

to derive the PSD function of CPFSK modulated signals. The PSD of h = 1/4 CPFSK was shown to be more compact than that of h = 1/2 CPFSK. Moreover, the main lobe was almost half that of h = 1/2 CPFSK. The N low pass equivalent state waveforms implemented in chapter three were shown for several values of h. In the last part of the thesis, a new coherent technique based on successive phase changes were used to estimate the transmitted binary data sequence. A possible hardware block diagram of the phase decoder was proposed. The probability of error of h = 1/b CPFSK signals was computed and was found to be comparable to that of DE-M-ary PSK where M = b. The case of h = 1/4 is of interest as it is was found to be marginally worse than DE-MSK in term of SNR (0.95 dB at a P(e) of 10^{-4}). Finally, the usual MSK demodulator (quadrature method) can be used with slight modification to demodulate h = 1/2 CPFSK as generated in the manner shown in chapter three.

6.2 SUGGESTIONS FOR FUTURE RESEARCH

For good power efficiency, a constant envelope modulation technique may be preferable, and this leads to the use of

frequency modulations. In FM schemes, to narrow the power spectrum, the modulation index can be decreased. The case of h = 1/4 CPFSK satisfies both points and ought to be investigated further. Since there are undoubtedly other interesting aspects which were not covered, suggestions for future research are made in following subsections.

6.2.1 DUO-BINARY h = 1/4 CPFSK

In order to improve further the spectral properties of the h = 1/4 CPFSK signal, the duo-binary h = 1/4 CPFSK technique (where h = 1/4 baseband signal processing is combined with the duo-binary (1 + D; class I) and modified duo-binary (1 - 2D) techniques) is suggested. The h = 1/4 duo-binary CPFSK should provide lower out-of-band energy and a faster spectral roll-off, compared to that of the conventional h = 1/4 CPFSK.

6.2.2 EFFECTS OF MULTIPATH FADING

Multipath fading in microwave digital radio systems can be a

major source of outage, especially for wideband, high capacity transmission. The investigation of its effect on the p(e) performance of h = 1/4 CPFSK modem and equalization techniques for performance improvement, is an interesting topic.

6.2.3 EFFECTS OF ACI AND CCI

The effect of adjacent channel interference (ACI) and/or co-channel interference (CCI) on the BER performance is another interesting topic to be investigated.

A further study of all these parameters and their effects on the BER performance could lead to additional valuable results.

APPENDIX A

DERIVATION OF CPFSK PHASE FUNCTION

In this appendix, the phase expression

$$\theta_n(t)=(\pi h/T_b)x_n(t-nT_b)+\pi h\sum_{k=1}^{n} x_k;\quad \text{for } t/T_b \in [n,n+1) \qquad \text{A.1}$$

of the full response binary CPFSK, is derived.

The derivation of (A.1) is based on the phase continuity condition. During the first interval $[0,T_b)$, the CPFSK phase is given by

$$\theta_1(t)=(\pi h/T_b)x_1 t=(\pi h/T_b)x_1(t-T_b)+\pi h\sum_{k=1}^{1}x_k. \qquad \text{A.2}$$

During the second interval $[T_b,2T_b)$, the phase must be continuous at the transition instant T_b, that is,

$$\theta_2(T_b)=\theta_1(T_b);\ \text{thus}\ \theta_2(t)=(\pi h/T_b)x_2(t-T_b)+\theta_1(T_b) \qquad \text{A.3}$$

which can also be expressed as

$$\theta_2(t)=(\pi h/T_b)x_2(t-2T_b)+\pi h\sum_{k=1}^{2}x_k. \qquad \text{A.4}$$

Similarly, the CPFSK signal's phase of the third interval is,

$$\theta_3(t)=(\pi h/T_b)x_3(t-3T_b)+\pi h\sum_{k=1}^{3}x_k. \qquad A.5$$

More generally, for $t \in [nT_b,(n+1)T_b)$, $\theta_n(t)$ can be represented as

$$\theta_n(t)=(\pi h/T_b)x_n(t-nT_b)+\pi h\sum_{k=1}^{n}x_k;\ \text{ for } t/T_b \in [n,n+1) \qquad A.1$$

consequently, the recursive relationship of the CPFSK signal's phase $\theta_n(t)$ has thus been established.

APPENDIX B

DEMODULATION OF CPFSK WITH h = 1/2 USING A QUADRATURE DEMODULATOR

When the MSK signal is generated as the sum of two waveforms in quadrature (see figure 2.2.a), the modulated signal can be written as

$$s(t) = x_{2n}\cos(\pi t/2T_b)\cos(\omega_c t) + x_{2n+1}\sin(\pi t/2T_b)\sin(\omega_c t) \qquad B1$$

where x_{2n} and x_{2n+1} are the even and odd bits. Therefore, the input binary data stream $\{x_n\}$ is correctly recovered when an MSK demodulator (similar to the one in figure 2.2.b) is used. To obtain the sequence $\{x_n\}$, the separately recovered even and odd bits are fed to a parallel to serial converter (P/S), as shown in figure 2.2.b. As CPFSK, the MSK signal can be represented by [22]

$$s(t) = \cos\{\omega_c t + x_n \pi t/2T_b + d_n\} \qquad B2$$

where d_n is a phase constant which is valid over the nth binary

data interval and is determined by the requirement that the phase of the waveform be continuous at the bit transition instants. The sequence $\{d_n\}$ can be represented as [22]

$$d_n = d_{n-1} + (x_{n-1} - x_n)n\pi/2. \qquad B3$$

The MSK representation of (B2), can be rewritten as [22]

$$s(t) = \cos(d_n)\cos(\pi t/2T_b)\cos(\omega_c t) - x_n\cos(d_n)\sin(\pi t/2T_b)\sin(\omega_c t). \quad B4$$

In this representation, x_n appears as encoded in both the I and Q channels as $\{\cos(d_n)\}$ and $\{-x_n\cos(d_n)\}$ respectively. It is clear that these signals are not identical to the even and odd bits. Thus, if a quadrature demodulator is used, the output of the P/S converter is not $\{x_n\}$. To accomodate such representation, the quadrature demodulator can be modified as follows:

1. Demodulate $\cos(d_n)$ and $-x_n\cos(d_n)$ using the quadrature demodulator (figure 2.2.b)

2. Rather than using a P/S converter, pass the signals through a NAND gate, whose output is the recovered input binary data stream.

LIST OF REFERENCES

1. W.R.Bennet and J.R.Davey, Data Transmission, McGraw-Hill Book Company, New York, 1965.

2. W.R.Lucky, J. Salz, and E.J.Weldon Jr., Principles of Data Communications, McGraw-Hill Book Company, New York, 1968.

3. H.Taub and D.Schilling, Principles of Communications Systems, McGraw-Hill Book Company, New York, 1971.

4. K.Feher, Digital Communications: Microwave Applications, Englewood Cliffs, N.J., Prentice-Hall Inc., 1981.

5. J.J.Spilker, Digital Communications by Satellite, Englewood, N.J., Prentice-Hall Inc., 1977.

6. H.Yazdani, K.Feher, and W.Steenaart, Constant Envelope band-limited BPSK Signal, IEEE Trans. on Comm., Vol.COM-28, pp. 889-897, June 1980.

7. F.Amoroso and J.A.Kivett, Simplified MSK Signaling Technique, IEEE Trans on Comm., Vol COM- , pp. 433-441, April 1977.

8. J.D.Oetting, A Comparison of Modulation Techniques for Digital Radio, IEEE Trans on Comm., Vol.COM-27, pp 1752-1762, Dec 1979.

9. W.M.Tey and T.T.Tjhung, Characteristics of Manchester-Coded FSK, IEEE Trans on Comm., Vol. COM-27, pp 209-216, Jan.1979.

10. W.C.Lindsay & M.K.Simon, Telecommunication Network Concepts, Englewood Cliffs, N.J., Prentice Hall Inc., 1973.

11. R.deBuda, Fast FSK Signals and their Demodulations, Can.Elec. J., Vol 1, No. 1, 1976.

12. T.Le-Ngoc, K.Feher, and H.P.Van, New Modulation Techniques for low-cost Power and Bandwidth efficient Satellite Earth Station, IEEE Trans on Comm., Vol.COM-30, No.1, January 1982.

13. M.C.Austin and M.U.Chang, Quadrature Overlapped Raised-Cosine Modulation, IEEE Trans on Comm., Vol. COM-29, No.3, Mar 1981.

14. H.E.Rowe & V.K.Prabhu, Power Spectrum of a Digital Frequency Modulation Signal, BSTJ VOL-54, No.6, Jul-Aug 1975.

15. D.Mulwijk, Correlative Phase Shift Keying-A class of Constant Envelope Modulation Techniques, IEEE Trans on Comm., Vol.COM-29, No.3, March 1981.

16. F.deJager and C.B.Dekker, Tamed Frequency Modulation: A novel Method to ahieve Spectrum Economy in Digital Transmission, IEEE Trans on Comm., Vol.COM-26, No.5, May 1978.

17. D.Muilwijk, Tamed Frequency Modulation: Bandwidth Saving Digital Modulation Method Suited For Mobile Radio, Philips Telecommunications Review, Vol 37, No.1, March 1979.

18. S.G.Wilson & R.C.Gaus, Power Spectra of Multi h Phase Codes, IEEE Trans on Comm., Vol.VOM-29, No.3, March 1981.

19. V.K.Prabhu, Spectral Occupancy of Digital Angle Modulation Signals, BSTJ Vol.55, No.4, April 1976.

20. R.deBuda, Coherent Demodulation of Frequency Shift Keying With Low Deviation Ratio, IEEE Trans on Comm., Vol. COM-2 , pp 429-435, June 1972.

21. F.Amoroso, The Bandwidth of Digital Data Signals, IEEE Communications Magazine, pp 13-24, Nov. 1980.

22. S.A.Gronemeyer & A.L.McBride, MSK & Offset QPSK Modulation IEEE Trans on Comm, Vol.COM-24, No.8, pp 809-819, Aug 1976.

23. P.Galko and S.Pasupathy, The Mean Power Spectral Density of Markov Chain Driven Signals, IEEE Trans on Information theory, Vol.IT-27, No.6, pp 746-754, Nov 1981.

24. D.M.Brady, FM-CPSK: Narrowband Digital FM with Coherent Phase Detection,

25. R.C.Davis, An Experimental 4-ary CPFSK Modem for Line of Sight Microwave Digital Data Transmission, EASCON 78, pp 674-682.

26. H.Miyakawa, H.Harashima, N.Tatsui & Y.Tanaka, Digital Phase Modulation Scheme Using Phase Continuous Waveform, Electron & Comm. in Japan, V01.58-A, No.12, 1975.

27. W.P.Osborne & M.B.Luntz, Coherent and Noncoherent detection of CPFSK, IEEE Trans on Comm., Vol.COM-22, pp 1023-1026, Aug 1974..

28. T.Aulin, C.E.Sundberg, Continuous Phase Modulation-Part I: Full Response Signaling, IEEE Trans on Comm., Vol.COM-29, pp 196-209, Mar 1981.

29. T.Aulin, N.Rydbeck, and C.E.Sundberg, Continuous phase Modulation-Part II: Partial Response Signaling, IEEE Trans on Comm., Vol.VOM-29, pp 210-225, Mar 1981.

30. H.Miyakawa, H.Harashima,, Y.Tanaska, A New Digital Modulation Scheme-Multimode Binary CPFSK, third Int. Conf. on Dig. Sat. Comm., pp 105-112, Kyoto Japan, Nov. 1975.

31. J.G.Anderson and D.P.Taylor, A Bandwidth Efficient Class of Signal Space Codes, IEEE Trans. Inf. Theory, Vol.1, IT-24, pp 703-712, Nov 1978.

32. T.Aulin & C.E.Sundberg, Binary CPFSK-Type of Signalling with Input Data Symbol Pulse Shaping-Error Probability & Spectrum, NTC 78, pp 6.5.1-6.5.5, Dec 1978.

33. T.Aulin, N.Rydbeck, C.E.Sundberg, Bandwidth Efficient Constant Envelope Digital Signalling with Phase Tree Demodulation, Electronic Letters, Vol.14, pp 487-489, Jul 1978.

34. T.Aulin, N.Rydbeck, C.E.Sundberg, Further Results on Digital FM with Coherent Phase Tree Demodulation Minimum Distance and Spectrum, Technical Report TR-119, University of Lund, Nov 1978.

35. P.Galko, S.Pasupathy, On a Class of Generalised MSK, ICC 81 Denver, pp 14-18, Jun 1981

36. G.S.Desphande, and P.H.Wittke, The Spectrum of Correlative Encoded FSK, ICC 78, pp 51.1/1-7, Dec 1980.

37. S.Pasupathy, Minimum Shift Keying: A Spectrally Efficient Modulation, IEEE Comm. Magazine, pp 14-22, Jul 1979.

38. F.Amoroso, Pulse and spectrum manipulation in the minimum shift keying (MSK) format, IEEE Trans. on Comm., Vol.COM-24, pp 381-384, Mar. 1976.

39. K.Feher, Digital communications: Satellite/Earth Station Engineering, Prentice-Hall Inc., Englewood Cliffs, N.J., Dec 1982.

40. H.R.Mathwich, J.F.Balcewicz, and M.Hecht, The effect of tandem band and amplitude limiting on the Eb/No performance of Minimum Shift Keying (MSK), IEEE Trans. Comm. Vol.COM-22, pp 1525-1540, Oct 1974.

41. J.G.Proakis, Digital communications. New York: McGraw-Hill, 1983.

42. M.Rabzel & S.Pasupathy, Spectral shaping in MSK-type-signals IEEE Trans. Commun. vol. COM-26, pp 189-195, Jan. 1978.

43. B. Bazin, A class of MSK baseband pulse formats with sharp spectral roll-off, IEEE trans. on commun., Vol. COM-27, May 1979.

44. R.E.Ziemer, and C.R.Ryan, Minimum shift keyed modem implementation for high data rate, IEEE Commun. Magazine, pp 28-37, Oct 1983.

45. M.K.Simon, A generalization of minimum shift keying (MSK) type signaling based upon input data symbol-pulse shaping, IEEE Trans. Commun., vol. COM-24, pp 845-856, Aug 1976.

46. H.P.Van, and K.Feher, A class of Two-Symbol-Interval Modems for Nonlinear Radio Systems, IEEE Trans. Commun., vol.COM-31, pp 433-441, Mar 1983.

47. S.Kato and K.Feher, XPSK: A new cross-correlated phase-shift keying modulation technique, IEEE Trans. Commun., vol.COM-31, pp 701-707, May 1983.

48 K. S. Shanmugam, Digital and analog communication systems. John Wiley & Sons, Inc. 1979.

49 J.C.Bellamy, Digital telephony. John Wiley & Sons, Inc. 1982.

50 M.K.Simon and .C.C.Wang, Two-bit Differential Detection of MSK, GLOBCOM 84, pp 740-745.

51 I.Korn, Digital Communications, Van Nostrand Reinhold Company, New York, 1985.

52 R.F.Pawla;S O.Rice, and J.H.Roberts, Distribution of the phase angle between two vectors perturbed by Gaussian Noise, IEEE Trans. on Comm., Vol. COM-30, August 1982, pp 1828-1841.

53 R.Gagliardi, Introduction to Communications Engineering. John Wiley & Sons, Inc. 1978.